



EASY FLUX[®] DL

EASYFLUX DL CR6OP or CR1KXOP
For CR6 or CR1000X and Open-Path
Eddy-Covariance Systems

Table of contents

1. Introduction	1
2. Precautions	3
3. Installation	3
3.1 Wiring	3
3.1.1 IRGA and sonic anemometer	4
3.1.2 VOLT 116 module	4
3.1.3 GPS receiver	5
3.1.4 Fine-wire thermocouple	5
3.1.5 Temperature and relative humidity probe	6
3.1.6 Radiation measurements, Option 1	7
3.1.7 Radiation measurements, Option 2	8
3.1.8 Precipitation gage	11
3.1.9 Soil temperature	11
3.1.10 Soil water content reflectometers	12
3.1.11 Soil heat flux plates	13
3.1.12 Self-calibrating soil heat flux plates	14
4. Operation	15
4.1 Set constants in CRBasic Editor and load program	16
4.2 Enter site-specific variables with data logger keypad or LoggerNet	19
4.3 Data retrieval	35
4.4 Output tables	35
4.5 Program sequence of measurement and corrections	75
5. References	76
Appendix A. Vapor pressure and dew point temperature	79
A.1 Equations to calculate dew point temperature from water vapor density	79
A.2 Approach to approximation of Td for the enhancement factor	81
A.3 Dew point temperature equation	81
A.4 Online flux program	82
A.5 Reference	82

Appendix B. Coordinate rotations: Double rotation method	83
B.1 Matrix transformation of instrument to flow coordinate system	83
B.2 Natural wind coordinate system	84
B.2.1 Covariance of momentum variables after coordinate rotation	86
B.2.2 Covariance of a scalar variable and momentum variable after second coordinate rotation	87
B.3 Extended equations	87
B.4 References	88
Appendix C. Coordinate rotations: Planar fit method	89
C.1 Planar fit	89
C.2 Algorithm	91
C.2.1 Variables and model	91
C.2.2 Covariance of momentum variables after two coordinate rotations	93
C.2.3 Covariance of a scalar variable with momentum variable after planar fit coordinate rotation	94
C.3 Extended equations	94
C.4 References	95
Appendix D. Frequency corrections	96
D.1 Introduction	96
D.2 Frequency loss	96
D.2.1 High frequency loss	96
D.2.2 Low frequency loss	97
D.3 Model for frequency loss corrections	97
D.4 Covariance variables requiring frequency corrections	99
D.4.1 Momentum covariance	99
D.4.2 Sonic temperature related covariance	99
D.4.3 Air temperature related covariance	99
D.4.4 CO ₂ and H ₂ O related covariances	100
D.5 Sensor configuration and separation variables	100
D.5.1 Path length variables	100
D.5.2 Separation variables	100
D.5.3 Fine-wire thermocouple	102
D.6 Surface layer atmospheric stability	103
D.6.1 Aerodynamic height	103
D.6.2 Monin-Obukhov length (L)	105

D.7 Cospectra	106
D.7.1 Cospectra for $z/L > 0$ (stable surface layer)	106
D.7.2 Cospectra for $z/L \leq 0$ (neutral to unstable surface layer)	107
D.8 Sub-transfer functions	108
D.8.1 Finite time block averaging	108
D.8.2 Line averaging	109
D.8.3 Volume averaging	111
D.8.4 FIR filtering	112
D.8.5 Time constant	112
D.8.6 Spatial separation	113
D.8.7 Total transfer function	114
D.9 Working model	115
D.10 Programmatic approach to computations for correction factors	115
D.11 References	117
Appendix E. WPL corrections	120
E.1 Basic considerations	120
E.2 Governing constraint and mean vertical velocity	122
E.3 Eddy-covariance measurements	123
E.3.1 CO ₂	123
E.3.2 H ₂ O	124
E.4 References	124
Appendix F. Data quality grading	125
F.1 Relative non-stationarity (RNcov) for steady state	126
F.2 Turbulence conditions	127
F.3 Wind direction in the sonic instrument coordinate system (wnd_dir_sonic)	130
F.4 Overall quality grade system	131
F.5 Programmatic procedure to grade data quality	131
F.6 References	132
Appendix G. Footprint	134
G.1 Kljun et al. (2004) analytical footprint equations	135
G.1.1 Models and parameters	135
G.1.2 Application of analytical footprint	137
G.1.3 Programmatic approach to determining footprint characteristics	140
G.2 Derivation of equations for upwind locations at inflection points of footprint in Kljun et al. (2004) (KCRS)	144

G.2.1 KCRS footprint model	144
G.2.2 Upwind location of maximum footprint	145
G.2.3 Upwind locations of inflection points	146
G.3 Kormann and Meixner (2001) (KM) analytical footprint equations	147
G.3.1 KM footprint model	147
G.3.2 Programmatic approach	148
G.3.3 Application of analytical footprint	149
G.3.4 Programmable algorithms	152
G.4 Derivation of analytical footprint in Kormann and Meixner (2001)	154
G.4.1 Model derivation	154
G.4.2 Analytical expression: Vertical profile of eddy diffusivity	155
G.4.3 Analytical expression: Crosswind integrated scalar concentration distribution	156
G.5 Upwind locations at inflection points of footprint in Kormann and Meixner (2001)	164
G.5.1 KM footprint model	164
G.5.2 Upwind location of maximum footprint	165
G.5.3 Upwind location of inflection points in footprint curve	165
G.6 References	166
Appendix H. Surface energy flux	168
Appendix I. EasyFlux DL CR6OP or CR1KXOP process flow diagram	171
I.1 Sequence of program functions	171
I.1.1 Every SCAN_INTERVAL (default 100 ms)	171
I.1.2 Every SLOWSEQUENCE_SCAN_INTERVAL (default 5 sec)	172
I.1.3 Every 5 min	172
I.1.4 Every AVERAGING_INTERVAL (default 30 min)	172

1. Introduction

EasyFlux[®] *DL CR6OP* or *CR1KXOP* is a CRBasic program that enables a CR6 or CR1000X data logger to collect fully corrected fluxes of CO₂, latent heat (H₂O), sensible heat, ground surface heat flux (optional), and momentum from a Campbell Scientific open-path eddy-covariance system with optional GPS and energy balance sensors. The program processes eddy-covariance data using commonly used corrections in scientific literature. Because the number of analog channels on the CR6 or CR1000X is limited, the program also supports the addition of a VOLT 116 analog input module, which allows expansion to include a full suite of energy balance sensors, thus enabling the program to calculate the ground surface heat flux and energy closure. Specifically, the program supports data collection and processing from the following sensors:

Gas analyzer and sonic anemometer (qty 1)

- EC150 with CSAT3A or CSAT3AH
- IRGASON

GPS receiver (optional, qty 0 to 1)

- GPS16X-HVS

Fine-wire thermocouple (optional, qty 0 to 1)

- FW05
- FW1
- FW3

Biometeorology (biomet) and energy balance sensors (optional)

- Air temperature/relative humidity (RH) probe (qty 0 to 1)
 - HMP155A
 - EE181
 - HygroVUE™10

- Radiation measurement instrument
 - Option 1
 - CS301 or CS320 pyranometer (qty 0 to 1)
 - CS310 quantum sensor (qty 0 to 1)
 - SI-111 infrared radiometer (qty 0 to 1)
 - Option 2
 - SN500SS or NR01 or CNR4 4-component net radiometers (qty 0 to 1; if using CNR4, the CNF4 ventilation and heater unit is also supported)
 - CS310 quantum sensor (qty 0 to 1)
- TE525MM rain gage (qty 0 to 1)
- TCAV averaging soil thermocouple probe (qty 0 to 3)
- Soil water content reflectometer (qty 0 to 3)
 - CS650
 - CS655
- Soil heat flux plate
 - Option 1: HFP01 soil heat flux plate (qty 0 to 3)
 - Option 2: HFP01SC self-calibrating soil heat flux plate (qty 0 to 3)

NOTE:

It may be possible to customize the program for other sensors or quantities in configurations not described here. Contact Campbell Scientific for more information.

NOTE:

In this manual, "IRGA" refers to either the EC150 or the IRGASON infrared gas analyzer; "sonic anemometer" refers to either the CSAT3A/CSAT3AH or IRGASON sonic anemometer; and "FW" refers to a FW05, FW1, or FW3 fine-wire thermocouple.

2. Precautions

- *EasyFlux DL CR6OP* or *CR1KXOP* requires the CR6 to have operating system (OS) version 11.01 or newer, the CR1000X to have OS 5.01 or newer, and the EC100 to have OS 8.02 or newer. Use of a VOLT 116 requires OS 6.01 or newer.
- The program applies the most common open-path eddy-covariance corrections to fluxes; however, it is the user's responsibility to determine the appropriateness of these corrections for their site.
- Campbell Scientific always recommends saving time-series data in the event raw data reprocessing is warranted. Further, it is the user's responsibility to determine the quality and fitness of all data for publication, regardless of whether said data was processed by *EasyFlux DL CR6OP* or *CR1KXOP* or another tool.
- As *EasyFlux DL CR6OP* or *CR1KXOP* is not encrypted, the user can view and edit the code; however, Campbell Scientific does not guarantee the function of an altered program.

3. Installation

3.1 Wiring

The user should install sensors and system components according to the respective product manuals. For standard program usability, when wiring the sensors to the data logger or to a VOLT 116, the user should follow the default wiring schemes, along with the type and quantity of instruments supported by *EasyFlux DL CR6OP* or *CR1KXOP*. [Table 3-1](#) (p. 4) through [Table 3-13](#) (p. 14) present the wiring schemes.

An IRGA with an associated sonic anemometer are the only required sensors for the program; additional sensors described in the following tables are optional. Many of the optional sensors are wired to a VOLT 116 analog channel expansion module, since the CR6 and CR1000X typically lack enough terminals on their own for a full energy balance sensor suite. If one or more of the optional sensors are not used, the data logger terminals assigned to those sensor wires should be left unwired.

NOTE:

If the standard data logger program is modified, the wiring presented in [Table 3-1](#) (p. 4) may no longer apply. In these cases, refer directly to the program code to determine proper wiring.

3.1.1 IRGA and sonic anemometer

An open-path IRGA and sonic anemometer must be connected to the EC100 electronics, and the EC100 must be wired to a CR6 or CR1000X data logger for *EasyFlux DL CR6OP* or *CR1KXOP* to be functional. [Table 3-1](#) (p. 4) shows the default wiring for these sensors.

Sensor	Quantity	Wire description	Color	CR6 terminal	CR1000X terminal
IRGASON or EC150/CSAT3A or CSAT3AH (from EC100)	1	SDM data	Green	U9	C5
		SDM clock	White	U10	C6
		SDM enable	Red/brown	U11	C7
		Signal ground	Black	G (power ground)	G (power ground)
		Shield	Clear	AG \perp (analog ground)	AG \perp (analog ground)
Heating controller ^{1/} with CSAT3AH	1	RS-485 A-	Brown	C1	C1/C3 ^{2/}
		RS-485 B+	White	C2	C2/C4 ^{2/}
		Signal ground	Black	RG	RG

^{1/}Heater temp/RH probe cable to controller **Temp/RH** port, CSAT3H heater cable to controller **Heater** port, and CSAT3AH chassis temperature cable to controller **Chassis** port.

^{2/}C1 and C2 are used if GPS is not an option; C3 and C4 are used if any SDI sensor is an option. If both GPS and SDI sensors are options, an MD485 is needed for communication between the heating controller and data logger using a **CS I/O** port. For more information, please contact Campbell Scientific.

3.1.2 VOLT 116 module

Due to the limitations on channel count of the CR6 or CR1000X, a VOLT 116 module is required when using a fine-wire thermocouple, any of the radiation sensors except the SN500 and CS320, or any of the soil sensors. If using a VOLT 116, prepare the instrument as follows:

1. Connect the module to a 10-32 VDC power source.
2. Launch the Campbell Scientific *Device Configuration Utility* software (v2.12 or newer) and select **VOLT 100 Series** among the list of **GRANITE** devices. If this is the first time connecting, follow the instructions on the main screen to download the USB driver to the computer.
3. Select the appropriate COM port and click **Connect**.
4. Once connected, a list of settings is shown. Navigate to the bottom setting, **CPI Address**. Change this value to **1**. Click **Apply** and exit the software.
5. Use a CAT5e or CAT6 Ethernet cable (included with the VOLT 116) to connect the **CPI** port on the module to the CR6 or CR1000X **CPI** port.

3.1.3 GPS receiver

A GPS receiver such as the GPS16X-HVS is optional but will keep the data logger clock synchronized to GPS time. If the CR6 or CR1000X clock differs by one millisecond or more, *EasyFlux DL CR6OP* or *CR1KXOP* will resynchronize the data logger clock to match the GPS. The GPS receiver also calculates solar position. [Table 3-2](#) (p. 5) shows the default wiring for the GPS16X-HVS.

Sensor	Quantity	Wire description	Color	CR6 terminal	CR1000X terminal
GPS16X-HVS	0 or 1	PPS	Grey	U1	C1
		TXD	White	U2	C2
		Power enable ground	Yellow	G	G
		Rx data	Blue	G	G
		Shield	Clear	AG \perp	AG \perp
		12V	Red	12V	12V
		Power ground	Black	G	G

3.1.4 Fine-wire thermocouple

Several models of fine-wire thermocouple sensors are available that can be integrated with the IRGA and sonic anemometer for direct measurements of sensible heat flux. *EasyFlux DL CR6OP* or *CR1KXOP* can support from zero to one fine-wire thermocouple with the IRGA and sonic anemometer. [Table 3-3](#) (p. 6) shows the available types and default wiring for adding a fine-wire thermocouple.

Table 3-3: Default wiring for fine-wire thermocouple

Sensor	Quantity	Wire description	Color	VOLT 116 terminal
FW05, FW1, or FW3	0 or 1	Signal	Purple	Diff 15H
		Signal reference	Red	Diff 15L
		Shield	Clear	AG \perp

3.1.5 Temperature and relative humidity probe

EasyFlux DL CR6OP or *CR1KXOP* can support from zero to one temperature and relative humidity probe with the IRGA and sonic anemometer. The default wiring for the HMP155A, EE181, and HygroVUE™10 is shown in [Table 3-4](#) (p. 6).

NOTE:

The three options for a temperature and relative humidity probe are the HMP155A, EE181, and HygroVUE™10. For details and specifications of these probes, visit www.campbellsci.com . The physical wiring to the CR6 or CR1000X data logger is the same for HMP155A and EE181; however, the colors of the wires may differ, so EE181 sensor wire colors are noted by italic text in [Table 3-4](#) (p. 6).

Table 3-4: Default wiring for temperature and relative humidity probe

Probe	Quantity	Wire description	Color	CR6 terminal	CR1000X terminal
HMP155A/ EE181	0 or 1 (cannot be used with HygroVUE™10)	Temp signal	Yellow/ <i>yellow</i>	U7	7H
		RH signal	Blue/ <i>blue</i>	U8	7L
		Temp/RH signal reference	White/ <i>black</i>	G ^{1/}	G ^{1/}
		Shield	Clear/ <i>clear</i>	AG \perp	AG \perp
		Power	Red/ <i>red</i>	+12 V	+12 V
		Power ground	Black/ <i>black</i>	G	G

Table 3-4: Default wiring for temperature and relative humidity probe

Probe	Quantity	Wire description	Color	CR6 terminal	CR1000X terminal
HygroVUE™10	0 or 1 (cannot be used with HMP155A or EE181)	Temp/RH signals	White	U7	C3
		Temp/RH reference	Clear	AG \perp	AG \perp
		Power	Brown	12 V	12 V
		Power ground	Black	G	G

¹/Due to terminal constraints, the temp/RH probe is a single-ended (SE) voltage measurement. As an SE measurement from a sensor that is powered continuously, the signal reference and power ground leads should both be wired to ground (G).

3.1.6 Radiation measurements, Option 1

Two options are available for making radiation measurements with *EasyFlux DL CR6OP* or *CR1KXOP*. The program can support any combination of the four sensors described in [Table 3-5](#) (p. 7). Alternatively, it can support one of the three types of 4-component radiometers described in [Table 3-6](#) (p. 9). [Table 3-5](#) (p. 7) gives the default wiring for Option 1. [Table 3-6](#) (p. 9) shows the details of the default wiring for Option 2.

Table 3-5: Default wiring for radiation measurements, Option 1

Sensor	Quantity	Wire description	Color	VOLT 116 terminal (unless otherwise indicated)
CS301 pyranometer	0 or 1	Signal	White	Diff 10H
		Signal reference	Black	Diff 10L
		Shield	Clear	AG \perp
CS320 digital thermopile pyranometer	0 or 1	SDI-12 signal	White	CR6 or CR1000X C3
		Signal reference	Blue	CR6 or CR1000X AG \perp
		Shield	Clear	CR6 or CR1000X AG \perp
		Power	Red	CR6 or CR1000X 12V
		Power ground	Black	CR6 or CR1000X G

Sensor	Quantity	Wire description	Color	VOLT 116 terminal (unless otherwise indicated)
CS310 quantum sensor	0 or 1	Signal	White	Diff 8H
		Signal reference	Black	Diff 8L
		Shield	Clear	AG \perp
SI-111 infrared radiometer	0 or 1	Target temp signal	Red	Diff 11H
		Target temp reference	Black	Diff 11L
		Shield	Clear	AG \perp
		Sensor temp signal	Green	Diff 12H
		Sensor temp reference	Blue	AG \perp
		Voltage excitation	White	X3

3.1.7 Radiation measurements, Option 2

Three models of 4-component net radiometers are compatible with the *EasyFlux DL CR6OP* or *CR1KXOP* program: SN500SS, NR01, and CNR4. However, due to limitations in channel numbers and computation procedures, only one model can be used at a time. The default wiring for each of the 4-component net radiometers is shown in [Table 3-6](#) (p. 9), [Table 3-9](#) (p. 11) and [Table 3-10](#) (p. 12) give information on adding an optional CNF4 ventilation and heater unit to the CNR4 4-component net radiometer.

A CNF4 ventilation and heater unit may be used with the CNR4 4-component net radiometer for more accurate radiation measurements. The CNF4 requires a solid-state relay to control the ventilator and heater. An A21REL-12 4-channel relay driver must be ordered (sold separately) and installed in the system enclosure just below the VOLT 116 module. [Table 3-7](#) (p. 10) lists the wiring connections needed to power and control the A21REL-12. [Table 3-8](#) (p. 11) lists the wiring for the CNF4.

A CABLE3CBL-1 or similar 3-conductor 22 AWG cable is recommended for connections from the A21REL-12 to the VOLT 116, and a CABLEPCBL-1 or similar 2-conductor 16 AWG power cable is recommended for power connections from the A21REL-12 to the DIN rail terminal block.

Table 3-6: Default wiring for radiation measurements, Option 2

Sensor	Quantity	Wire description	Color	VOLT 116 terminal (unless otherwise indicated)
SN500SS 4-component net radiometer	0 or 1	SDI-12	White	CR6 or CR1000X C3
		Shield	Clear	CR6 or CR1000X AG \perp
		Power	Red	CR6 or CR1000X 12V
		Power ground	Black	CR6 or CR1000X G
NR01 4-component net radiometer	0 or 1	Pyranometer up signal	Red (cbl 1)	Diff 9H
		Pyranometer up reference	Blue (cbl 1)	Diff 9L
		Pyranometer down signal	White (cbl 1)	Diff 10H
		Pyranometer down reference	Green (cbl 1)	Diff 10L Jump to 9L
		Pyrgeometer up signal	Brown (cbl 1)	Diff 11H
		Pyrgeometer up reference	Yellow (cbl 1)	Diff 11L Jump to 10L
		Pyrgeometer down signal	Purple (cbl 1)	Diff 12H
		Pyrgeometer down reference	Grey (cbl 1)	Diff 12L Jump to 11L
		PT100 signal	White (cbl 2)	Diff 4H
		PT100 reference	Green (cbl 2)	Diff 4L
		Current excite	Red (cbl 2)	X1
		Current return	Blue (cbl 2)	AG \perp
		Shields	Clear	AG \perp
		Heater power	Brown	SW12-1 ^{1/}
		Heater ground	Yellow	G
		Ground	Purple/pink	G
Shield	Grey	AG \perp		

Table 3-6: Default wiring for radiation measurements, Option 2

Sensor	Quantity	Wire description	Color	VOLT 116 terminal (unless otherwise indicated)
CNR4 4-component net radiometer	0 or 1	Pyranometer up signal	Red	Diff 9H
		Pyranometer up reference	Blue	Diff 9L
		Pyranometer down signal	White	Diff 10H
		Pyranometer down reference	Black	Diff 10L Jump to 9L
		Pyrgeometer up signal	Grey	Diff 11H
		Pyrgeometer up reference	Yellow	Diff 11L Jump to 10L
		Pyrgeometer down signal	Brown	Diff 12H
		Pyrgeometer down reference	Green	Diff 12L Jump to 11L
		Thermistor signal	White	Diff 4H
		Thermistor V excite	Red	X1
		Thermistor reference	Black	AG \perp
		Shields	Clear	AG \perp

¹Use CR6 or CR1000X SW12-1 and G if self-calibrated soil heat flux plate is used.

Table 3-7: A21REL-12 wiring with CNF4

A21REL-12 terminal	Connecting terminal	Cable	Color
+12V	DIN rail terminal block: 12V	CABLEPCBL-1	Red
Ground	DIN rail terminal block: GND	CABLEPCBL-1	Black
CTRL 1	VOLT 116 SW5V #1	CABLE3CBL-1	Red
CTRL 2	VOLT 116 SW5V #2	CABLE3CBL-1	Black
CTRL 3	VOLT 116 SW5V #3	CABLE3CBL-1	White

Table 3-8: Default wiring for CNF4

Sensor	Quantity	Wire description	Color	Wiring
CNF4	0 or 1 (only if a CNR4 is used)	Tachometer output	Green	CR6 U7 CR1000X P2
		Tachometer reference	Grey	CR6 or CR1000X AG ⚡
		Ventilator power	Yellow	A21REL-12 REL 1 NO
		Ventilator ground	Brown	A21REL-12 REL G
		Heater #1 power	White	A21REL-12 REL 2 NO
		Heater #1 ground	Red	A21REL-12 REL G
		Heater #2 power	Black	A21REL-12 REL 3 NO
		Heater #2 ground	Blue	A21REL-12 REL G

3.1.8 Precipitation gage

EasyFlux DL CR6OP or *CR1KXOP* can support a from zero to one TE525MM tipping-bucket rain gage or similar precipitation gage. The default wiring for a precipitation gage is shown in [Table 3-9](#) (p. 11).

Table 3-9: Default wiring for precipitation gage

Sensor	Quantity	Wire description	Color	CR6 terminal	CR1000X terminal
TE525MM tipping-bucket rain gage	0 or 1	Pulse output	Black	U6	P1
		Signal ground	White	AG ⚡	AG ⚡
		Shield	Clear	AG ⚡	AG ⚡

3.1.9 Soil temperature

The TCAV is an averaging soil thermocouple probe used for measuring soil temperature.

EasyFlux DL CR6OP or *CR1KXOP* can support up to three TCAV probes. The order of wiring, however, is important. If only one TCAV probe is used, it must be wired as described for TCAV #1 in [Table 3-10](#) (p. 12). An additional TCAV probe would be wired according to TCAV #2 in [Table 3-10](#) (p. 12).

CAUTION:

If one or two TCAV probes are used and are wired to terminals **2H** and **2L** as a starting measurement channel (leaving terminals **1H** and **1L** empty), the data logger will automatically assign TCAV measurements according to the number of TCAV probes.

Table 3-10: Default wiring for soil thermocouple

Sensor	Quantity	Wire description	Color	VOLT 116 terminal
TCAV #1	0 to 3	Signal	Purple	Diff 1H/2H
		Signal reference	Red	Diff 1L/2L
		Shield	Clear	AG \perp
TCAV #2		Signal	Purple	Diff 2H/3H
		Signal reference	Red	Diff 2L/3L
		Shield	Clear	AG \perp
TCAV #3		Signal	Purple	Diff 3H
		Signal reference	Red	Diff 3L
		Shield	Clear	AG \perp

NOTE:

The CS650 or CS655 sensors also measure soil temperature. If the CS650 or CS655 sensors are used but no TCAV probes are used, *EasyFlux DL CR6OP* or *CR1KXOP* will use soil temperature from the CS650 or CS655 to compute ground-surface heat flux. If available, soil temperature data from the TCAV probe is preferred because it provides a better spatial average. See wiring details for these sensors in [Table 3-11](#) (p. 13).

3.1.10 Soil water content reflectometers

EasyFlux DL CR6OP or *CR1KXOP* supports zero or one of two models of soil water content reflectometers: CS650 or CS655, and up to three of the one selected model are supported. The default wiring for each is shown in [Table 3-11](#) (p. 13).

CAUTION:

If only one soil water content reflectometer is being used, the user should wire it according to the first sensor as described in [Table 3-11](#) (p. 13). If only one sensor is being used but is wired according to the second or third sensor, *EasyFlux DL CR6OP* or *CR1KXOP* will record no soil water content measurements.

Sensor	Quantity	Wire description	Color	CR6 terminal	CR1000X terminal
CS650/ CS655 #1	0 to 3	SDI-12 data	Green	U3	C3
		SDI-12 power	Red	+12 V	+12 V
		SDI-12 reference	Black	G	G
		Shield	Clear	G	G
		Not used	Orange	AG \perp	AG \perp
CS650/ CS655 #2		SDI-12 data	Green	U3	C3
		SDI-12 power	Red	+12 V	+12 V
		SDI-12 reference	Black	G	G
		Shield	Clear	AG \perp	AG \perp
		Not used	Orange	G	G
CS650/ CS655 #3		SDI-12 data	Green	U3	C3
		SDI-12 power	Red	+12 V	+12 V
		SDI-12 reference	Black	G	G
		Shield	Clear	AG \perp	AG \perp
		Not used	Orange	G	G

3.1.11 Soil heat flux plates

EasyFlux DL CR6OP or *CR1KXOP* can support from zero to three standard (non-self-calibrating) soil heat flux plates. The default wiring for the standard soil heat flux plates is shown in [Table 3-12](#) (p. 14).

Sensor	Quantity	Wire description	Color	VOLT 116 terminal
HFP01 #1	0 to 3	Signal	White	Diff 5H
		Signal reference	Green	Diff 5L
		Shield	Clear	AG \perp
HFP01 #2		Signal	White	Diff 6H
		Signal reference	Green	Diff 6L
		Shield	Clear	AG \perp
HFP01 #3		Signal	White	Diff 7H
		Signal reference	Green	Diff 7L
		Shield	Clear	AG \perp

3.1.12 Self-calibrating soil heat flux plates

EasyFlux DL CR6OP or *CR1KXOP* can also support from zero to three self-calibrating soil heat flux plates. The default wiring for the self-calibrating soil heat flux plates is shown in [Table 3-13](#) (p. 14).

Sensor	Quantity	Wire description	Color	VOLT 116 terminal
HFP01SC #1		Signal	White	Diff 5H
		Signal reference	Green	Diff 5L
		Shield	Clear	AG \perp
		Heater signal	Yellow	Diff 13H
		Heater reference	Purple	Diff 13L
		Shield	Clear	AG \perp
		Heater power	Red	SW12-1 ^{1/}
		Power reference	Black	G

Table 3-13: Default wiring for self-calibrating soil heat flux plates

Sensor	Quantity	Wire description	Color	VOLT 116 terminal
HFP01SC #2	0 to 3	Signal	White	Diff 6H
		Signal reference	Green	Diff 6L
		Shield	Clear	AG \perp
		Heater signal	Yellow	Diff 14H
		Heater reference	Purple	Diff 14L
		Shield	Clear	AG \perp
		Heater power	Red	SW12-1 ^{1/}
		Power reference	Black	G
HFP01SC #3		Signal	White	7H
		Signal reference	Green	7L
		Shield	Clear	AG \perp
		Heater signal	Yellow	Diff 16H
		Heater reference	Purple	Diff 16L
		Shield	Clear	AG \perp
	Heater power	Red	SW12-2 ^{1/}	
	Power reference	Black	G	

^{1/}The SW12 ports on the VOLT 116 are limited to 200 mA output, so no more than two HFP01SC sensors may be connected to each port. The user should connect heater power wires from HFP01SC #1 and #2 to SW12-1 and connect heater wires from HFP01SC #3 to SW12-2.

4. Operation

Operating *EasyFlux DL CR6OP* or *CR1KXOP* requires the user to enter or edit certain constants and input variables unique to the program or site. Constants are typically edited only once upon initializing the program. Site-specific variables are edited upon initial deployment and also periodically as site conditions change (for example, canopy height adjustments throughout a growing season). [Set constants in CRBasic Editor and load program](#) (p. 16) gives details on editing constants; [Enter site-specific variables with data logger keypad or LoggerNet](#) (p. 19) gives details on editing variables.

Typical operation also includes periodic zeroing and spanning of the IRGASON or EC150 gas analyzer.

4.1 Set constants in *CRBasic Editor* and load program

Before operating the station, values for configuration constants should be verified in the program code.

Once the program is open in *CRBasic Editor*, find the section entitled *USER-DEFINED CONFIGURATION CONSTANTS*, followed by the heading *Start of Constants Customization Section* (see [Figure 4-1](#) [p. 18]). Review the constants in this section and modify as needed. If locating the correct lines of code is difficult, search the program for the word “unique”, which will locate all lines of code containing constants that need to be verified. Look for the text comments on the right side of each line of code for more explanation of the constant. Generally, the constants fall into four categories:

1. Program function constants

These constants determine the timing of code execution, frequency of writing to output tables, memory allocation, and more. In most cases, the default constants for these values can be maintained.

Of specific note, if the program function constant `ONE_FULL_TABLE` is set to `TRUE`, all the intermediate and auxiliary measurements will be included as data fields in the main `FLUX_CSFormat` output table, rather than being in a separate output table called `FLUX_NOTES`. For more information, see [Output tables](#) (p. 35).

2. Sensor selection constants

All sensor selection constants begin with the prefix *SENSOR*. The value is set to `TRUE` in the constant table if the system includes the sensor. For example, if a system has a fine-wire thermocouple, the constant `SENSOR_FW` should be set to `TRUE`. When set to `TRUE`, the wiring in [Table 3-13](#) (p. 14) will apply to the sensor, and the data from that sensor will be included in the data output tables.

If a sensor is not used, ensure the constant is set to `FALSE`.

3. Sensor quantity constants

The value for these constants indicates the number of each type of sensor in the system. For example, if three soil heat flux (SHF) plates are being used, the constant `NMBR_SHF` would be set to 3.

4. Sensor calibration constants

Some sensors have unique parameters for their measurement working equations (for example, multipliers and/or offsets for linear working equations) that are used to convert raw measurements of voltage into the values applicable in analysis. Typically, these parameter values are found on the calibration sheet from the original manufacturer of the sensor. For example, if a CS301 pyranometer is being used, a unique multiplier is set in the following line of code: **Constant PYRAN_MULT = 5**. The comments in the code explain that the value entered is the sensor multiplier provided in the CS301 calibration sheet.

NOTE:

Constants relating to a particular sensor have been grouped together with the sensor selection constant at the beginning, such that if the sensor selection constant is set to **FALSE**, then the other constants for that sensor may be ignored. For example, all constants dealing with the temp/RH probe are grouped together with the **SENSOR_T_RH** constant at the top. If a temp/RH probe is not being used, **SENSOR_T_RH** should be set to **FALSE**, thereby conditionally excluding the next four constants dealing with multipliers and offsets in the program.

After all constants are verified, the user should save the program under a new or modified file name to keep track of different program versions. Finally, send the program to the CR6 or CR1000X using *LoggerNet* or *PC400* user interface software.

```

File Edit View Search Compile Template Instruction Goto Window Tools Help
[Icons]
1 'Start of Constants Customization Section
2 ConstTable (Const_Table)
3
4 '* PROGRAM FUNCTION CONSTANTS
5 Const SCN_INTV           = 50           'Unique: measurement rate (ms): 40 ms (25 Hz), 50 :
6 Const SLW_SCN_INTV      = 5000        'Unique: slow sequence measurement rate (ms) >3000
7 Const OUTPUT_INTV       = 30           'Unique: online flux data output interval (minutes
8 Const DAY_FLUX_CRD      = 30           'Unique: number of days of Flux_AmeriFluxFormat, F
9 Const DAY_TSR5_CRD      = 1            'Unique: number of days of Time_Series table data
10 Const NTCH_FRQ_SLW As Long = 50        'Unique: slowsequence analog measurement integrati
11 Const ONE_FL_TABLE As Boolean = FALSE   'Unique: whether or not all half-hourly or hourly
12
13 '* GAS ANALYZER AND SONIC ANEMOMETER
14 Const IRGASON           As Boolean = FALSE 'Unique: IRGASON. TRUE as default. If TRUE, CSAT3A
15 Const CSAT3A_EC150 As Boolean = TRUE      'Unique: CSAT3A + EC150. FALSE as default. If TRUE
16 Const SDM_CLK_SPD As Long = 30           'Unique: default SDM clock speed (uS). May need to
17 Const EC100SDM_ADR As Long = 1           'Unique: SDM address for EC100 (1 as default).
18 Const BANDWIDTH        = 10            'Unique: in Hz. For spectral analysis, set to 1/2
19 #If (CSAT3A_EC150) Then
20 Const CSAT_TYP_3AH As Boolean = TRUE      'Unique: CSAT3AH (heated sonic anemometer). If TRU
21 #EndIf
22
23 '* GPS
24 Const SENSOR_GPS As Boolean = TRUE        'Unique: GPS16X-HVS GPS receiver with integrated a
25 Const UTC_OFST    = -7                   'Unique: The local standard time, in hours, from U
26
27 '* PERIPHERAL
28 Const CDM_VOLT_116 As Boolean = TRUE      'Unique: A CDM-A/VOLT116 is being used with the CR
29 #If (CDM_VOLT_116) Then
30 Const SN_CDM_VOLT As Long = 1025         'Unique: CDM-A/VOLT116 serial number.
31 Const MODEL_CDMVLT = VOLT116            'Unique: CDM-A/VOLT Model.
32 Const CPI_CDM_VOLT As Long = 1          'Unique: CPI address for CDM-A/VOLT116.
33 Const CPI_DEVICE As String = "VOLT116"  'Unique: CDM-A/VOLT116 module name or identifier.
34 #EndIf
35
36 '* FINE WIRE THERMOCOUPLE
37 Const SENSOR_FW As Boolean = TRUE        'Unique: FW05, FW1, FW3, or other fine wire thermo
38
39 '* TEMP/RH PROBE
40 Const SENSOR_HYGRO As Boolean = FALSE    'Unique: HygroVUE10 temperature and relative humid
41 Const SENSOR_T_RH As Boolean = TRUE      'Unique: HMP155A or EE08: temperature and relative
42 '.....
43 '.....
44
45 EndConstTable
46 'End of Constants Customization Section

```

Figure 4-1. Example screen from *CRBasic Editor* showing user-defined configuration constants.

4.2 Enter site-specific variables with data logger keypad or *LoggerNet*

After the eddy-covariance station is installed and the data logger is running the program, connect a CR1000KD keyboard/display to the CR6 or CR1000X CS I/O port to view a custom menu of station-specific variables (Figure 4-2 [p. 20]). Use this menu to enter, view, and modify these variables. Use the up and down arrow buttons to navigate to different variables. Press **Enter** to select a variable or to set a new value after typing it. Press **Esc** to return to the previous menu.

Figure 4-2 (p. 20) depicts the structure of the custom menu. Bypass the custom menu to interact directly with the data logger through the data logger default menus. To bypass the custom menus, select **System Menu**. If no CR1000KD is available, these variables may be viewed and edited using the *LoggerNet* connect screen numeric display of variables from the Public table.

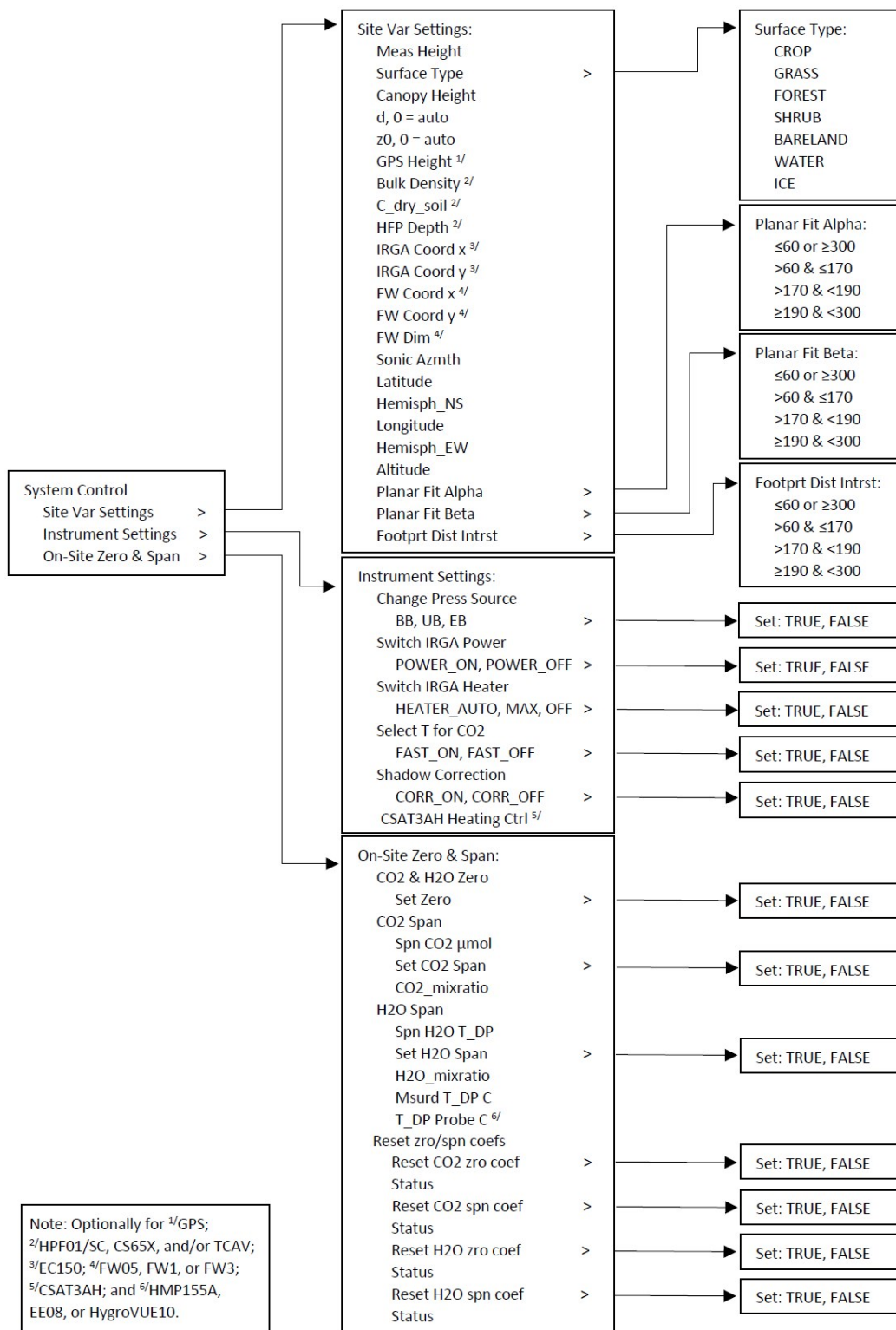


Figure 4-2. Custom keypad menu; arrows indicate submenus.

Before fluxes are processed correctly, the user must go through each station variable and set or confirm the assigned value. [Table 4-1](#) (p. 21) gives short descriptions of each station variable.

Table 4-1: Station variables with descriptions				
Station variable	Units	Default	Description	Name of variable in Public table (if no CR1000KD is available)
Meas Height	m	2	Height of the center of the eddy-covariance sensor measurement volumes above ground.	height_measurement
Surf Type	adimensional	GRASS	Type of surface at the measurement site; used to estimate displacement height (see Aerodynamic height [p. 103]) and roughness length (see Programmatic approach to determining footprint characteristics [p. 140]).	surface_type 1 = CROP 2 = GRASS 3 = FOREST 4 = SHRUB 5 = BARELAND 6 = WATER 7 = ICE
Canopy Height	m	0.5	Average height of the canopy.	height_canopy
d	m	0 (Auto)	Displacement height; set to 0 for program to auto-calculate. See Aerodynamic height (p. 103).	displacement_user
z_0	m	0 (Auto)	Roughness length; set to 0 for program to auto-calculate. See Programmatic approach to determining footprint characteristics (p. 140).	roughness_user

Table 4-1: Station variables with descriptions

Station variable	Units	Default	Description	Name of variable in Public table (if no CR1000KD is available)
GPS Height	m	1	Height of the GPS receiver above the ground surface; variable is omitted if GPS is not used.	height_GPS16X
Bulk Density	kg·m ⁻³	1300	Average bulk density of soil; variable is omitted if soil heat flux sensors are not used.	soil_bulk_density
C_dry_soil	J·kg ⁻¹ ·K ⁻¹	870	Specific heat of dry mineral soil; variable is omitted if soil heat flux sensors are not used.	cds
HFP Depth	m	0.08	Depth of the soil heat flux plates; variable is omitted if soil heat flux plates are not used.	thick_abv_HFP
IRGA Coord x	m	0 for IRGASON; 0.04066 for EC150	Distance along the sonic x-axis between the sonic sampling volume and the gas analyzer sampling volume. If an IRGASON is used, this is default to 0; if an EC150 with CSAT3A is used, this defaults to 0.04066, which corresponds to the EC150 mounting position closest to the CSAT3A sonic measurement volume.	separation_x_IRGA

Table 4-1: Station variables with descriptions

Station variable	Units	Default	Description	Name of variable in Public table (if no CR1000KD is available)
IRGA Coord y	m	0 for IRGASON; 0.02905 for EC150	Distance along the sonic y-axis between the sonic sampling volume and the gas analyzer sampling volume. If an IRGASON is used, this is default to 0; if an EC150 with CSAT3A is used, this defaults to 0.02905, which corresponds to the EC150 mounting position closest to the CSAT3A sonic measurement volume.	separation_y_IRGA
FW Coord x	m	0.005870	Distance along the sonic x-axis between the sonic sampling volume and fine-wire thermocouple; variable is omitted if no fine-wire thermocouple is used.	separation_x_FW
FW Coord y	m	0.03259	Distance along the sonic y-axis between the sonic sampling volume and fine-wire thermocouple; variable is omitted if no fine-wire thermocouple is used.	separation_y_FW

Table 4-1: Station variables with descriptions

Station variable	Units	Default	Description	Name of variable in Public table (if no CR1000KD is available)
FW Dim	m	FW05_DIA	User selects which fine-wire thermocouple is being used to load the appropriate diameter: 1.27×10^{-5} m for FW05_DIA, 2.54×10^{-5} m for FW1_DIA, and 7.62×10^{-5} m for FW3_DIA; variable is omitted if no fine-wire thermocouple is used.	FW_diameter
Sonic Azmth	decimal degrees	0	Compass direction in which the sonic head (or sonic negative x-axis) points.	sonic_azimuth
Latitude	decimal degrees	41.766	Site latitude in degrees north or south.	Latitude
Hemisph_NS	adimensional	NORTH	Site latitudinal hemisphere; options are NORTH or SOUTH.	hemisphere_NS 1 = North -1 = South
Longitude	decimal degrees	111.855	Site longitude in degrees east or west.	Longitude
Hemisph_EW	adimensional	WEST	Site longitudinal hemisphere; options are EAST or WEST.	hemisphere_EW 1 = East -1 = West
Altitude	m	1356	Site altitude.	altitude

Table 4-1: Station variables with descriptions

Station variable		Units	Default	Description	Name of variable in Public table (if no CR1000KD is available)
Planar Fit Alpha	≤60 or ≥300	decimal degrees	0	Alpha angle used to rotate the wind when the mean horizontal wind is blowing from the sector of 0 to 60° and 300 to 360° in the sonic coordinate system (that is, wind blowing into sonic head). ^{1/}	alpha_PF_60_300
Planar Fit Alpha	>60 & ≤170	decimal degrees	0	Alpha angle used to rotate the wind when the mean horizontal wind is blowing from the sector of 60 to 170° in the sonic coordinate system (that is, wind blowing from left and behind sonic head). ^{1/}	alpha_PF_60_170
Planar Fit Alpha	>170 & <190	decimal degrees	0	Alpha angle used to rotate the wind when the mean horizontal wind is blowing from the sector of 170 to 190° in the sonic coordinate system (that is, wind blowing from behind sonic head). ^{1/}	alpha_PF_170_190

Table 4-1: Station variables with descriptions

Station variable		Units	Default	Description	Name of variable in Public table (if no CR1000KD is available)
Planar Fit Alpha	≥ 190 & < 300	decimal degrees	0	Alpha angle used to rotate the wind when the mean horizontal wind is blowing from the sector of 190 to 300° in the sonic coordinate system (that is, wind blowing from right and behind sonic head). ^{1/}	alpha_PF_190_300
Planar Fit Beta	≤ 60 or ≥ 300	decimal degrees	0	Beta angle used to rotate the wind when the mean horizontal wind is blowing from the sector of 0 to 60° and 300 to 360° in the sonic coordinate system (that is, wind blowing into sonic head). ^{1/}	beta_PF_60_300
Planar Fit Beta	> 60 & ≤ 170	decimal degrees	0	Beta angle used to rotate the wind when the mean horizontal wind is blowing from the sector of 60 to 170° in the sonic coordinate system (that is, wind blowing from left and behind sonic head). ^{1/}	beta_PF_60_170

Table 4-1: Station variables with descriptions

Station variable		Units	Default	Description	Name of variable in Public table (if no CR1000KD is available)
Planar Fit Beta	>170 & <190	decimal degrees	0	Beta angle used to rotate the wind when the mean horizontal wind is blowing from the sector of 170 to 190° in the sonic coordinate system (that is, wind blowing from behind sonic head). ^{1/}	beta_PF_170_190
Planar Fit Beta	≥190 & <300	decimal degrees	0	Beta angle used to rotate the wind when the mean horizontal wind is blowing from the sector of 190 to 300° in the sonic coordinate system (that is, wind blowing from right and behind sonic head). ^{1/}	beta_PF_190_300

Table 4-1: Station variables with descriptions

Station variable		Units	Default	Description	Name of variable in Public table (if no CR1000KD is available)
Footprint Dist of Interest	≤60 or ≥300	m	100z	<p>Upwind distance of interest from the station when the mean horizontal wind is blowing from the sector of 0 to 60° and 300 to 360° in the sonic coordinate system (that is, wind blowing into sonic head).</p> <p>Note: Program will report the percentage of cumulative footprint from within this distance. Default value is 100× the aerodynamic height (z); z is the difference between measurement height and displacement height.</p>	dist_intrst_60_300
Footprint Dist of Interest	>60 & ≤170	m	100z	<p>Upwind distance of interest from the station when the mean horizontal wind is blowing from the sector of 60 to 170° in the sonic coordinate system (that is, wind blowing from left and behind sonic head).</p>	dist_intrst_60_170

Table 4-1: Station variables with descriptions

Station variable		Units	Default	Description	Name of variable in Public table (if no CR1000KD is available)
Footprint Dist of Interest	>170 & <190	m	100z	Upwind distance of interest from the station when the mean horizontal wind is blowing from the sector of 170 to 190° in the sonic coordinate system (that is, wind blowing from behind sonic head).	dist_intrst_170_190
Footprint Dist of Interest	≥190 & <300	m	100z	Upwind distance of interest from the station when the mean horizontal wind is blowing from the sector of 190 to 300° in the sonic coordinate system (that is, wind blowing from right and behind sonic head).	dist_intrst_190_300

¹Leave **all** planar fit alpha and beta angles set to 0 to use Tanner and Thurtell (1969) method of double coordinate rotations.

Table 4-2: Instrument settings with descriptions

Station variable		Default	Description	Name of variable in Public table (if no CR1000KD is available)
Change Pressure Source	Select Source	EB	Used to select the barometer to use for measurements of ambient pressure. BB – EC100 on-board basic barometer. UB – User-selected barometer. (The multiplier and offset for this user-selected barometer must be input through <i>ECMon</i> .) EB – Enhanced barometer.	press_source 0 = BB 1 = UB 2 = EB
	Set Source	FALSE	If the variable Select Source has been changed, this variable must be set to TRUE to enable the change. The program will return Set Source to FALSE once the change has been applied.	set_press_source_flg -1 = True 0 = False
Switch IRGA Power	IRGA ON/OFF	POWER_ON	Used to power down or power on the gas analyzer head. The EC100 electronics and sonic anemometer will continue to be powered. Options are POWER_ON or POWER_OFF .	IRGA_power 0 = Power On 1 = Power Off
	Set IRGA Pwr	FALSE	If the variable IRGA ON/OFF has been changed, this variable must be set to TRUE to enable the change. The program will return Set IRGA Pwr to FALSE once the change has been applied.	set_IRGA_power_flg -1 = True 0 = False

Table 4-2: Instrument settings with descriptions

Station variable		Default	Description	Name of variable in Public table (if no CR1000KD is available)
Select IRGA Heater	Select Heater	HEATER_AUTO	Used to enable the automatic window heater control by selecting HEATER_AUTO or HEATER_MAX , or to disable the window heaters by selecting HEATER_OFF .	heater 0 = Max -1 = Off -2 = Auto
	Set Selected	FALSE	If the variable Select Heater has been changed, this variable must be set to TRUE to enable the change. The program will return Set Selected to FALSE once the change has been applied.	set_heater_flg -1 = True 0 = False
Spectroscopic correction	Select T for CO2	FAST_ON	Used to enable the use of CO ₂ corrected for spectroscopic effect from air temperature measured by fast response sensors. Use is enabled by selecting FAST_ON or disabled by selecting FAST_OFF .	select_CO2_fast_tmpr -1 = FAST_ON 0 = FAST_OFF
	Set Selected	FALSE	If the variable Select T for CO2 has been changed, this variable must be set to TRUE to enable the change. The program will return Set Selected to FALSE once the change has been applied.	set_CO2_fast_tmpr_flg -1 = True 0 = False

Table 4-2: Instrument settings with descriptions

Station variable		Default	Description	Name of variable in Public table (if no CR1000KD is available)
Shadow Correction	Select Correction	CORR_OFF	Used to enable the Kaimal sonic transducer wind shadowing correction as described in the CSAT3B manual. CORR_ON enables the correction, while CORR_OFF disables it.	shadow_corr -1 = CORR_ON 0 = CORR_OFF
	Set Selected	FALSE	If the variable Select Correction has been changed, this variable must be set to TRUE to enable the change. The program will return Set Selected to FALSE once the change has been applied.	set_shadow_corr_flg -1 = True 0 = False
CSAT3AH Heating Ctrl (if CSAT3AH is an option)	User Ctrl On	TRUE	The variable User Ctrl On will turn off if this variable is changed to FALSE .	CSAT3H_user_ctrl_flg -1 = True 0 = False

Table 4-3: On-site zero and span variables

On-site zero and span variable	Units	Default	Description	Name of variable in Public table (if no CR1000KD is available)
Set Zero	adimensional	FALSE	Set to TRUE after flowing zero gas through the zero/span shroud and reaching equilibrium.	set_zero_flg -1 = True 0 = False

Table 4-3: On-site zero and span variables

On-site zero and span variable		Units	Default	Description	Name of variable in Public table (if no CR1000KD is available)
Span Concentrations	CO2	ppm	0	Concentration of span gas flowing through the zero/span shroud. It should be on a basis of dry air.	CO2_span_gas
	T_DP	deg C	0	Dew point temperature of the H ₂ O span gas generated from a dew point generator. It should match the dew point temperature setting on the generator.	T_DP_span_gas
Set CO2 Span		adimensional	FALSE	Set this to TRUE after flowing CO ₂ span gas through the zero/span shroud and reaching equilibrium.	set_CO2_span_flg -1 = True 0 = False
Set H2O Span		adimensional	FALSE	Set this to TRUE after flowing H ₂ O span gas through the zero/span shroud and reaching equilibrium.	set_H2O_span_flg -1 = True 0 = False
CO2_mixratio		ppm	–	Real-time measurement of CO ₂ molar mixing ratio (dry basis) as measured by the gas analyzer. This can be monitored to know when equilibrium is reached.	CO2_mixratio

Table 4-3: On-site zero and span variables

On-site zero and span variable	Units	Default	Description	Name of variable in Public table (if no CR1000KD is available)
H2O_mixratio	ppth	–	Real-time measurement of H ₂ O molar mixing ratio (dry basis) as measured by the gas analyzer. This can be monitored to know when equilibrium is reached.	H2O_mixratio
Td	deg C	–	Real-time measurement of dew point temperature as measured by the gas analyzer.	T_DP
Td_probe	deg C	–	Real-time measurement of dew point temperature derived from measurements by the temp/RH probe. It is omitted if no temp/RH probe is used. This value could potentially be input for dew point temperature (<i>Td</i> , above) if a dew point generator is unavailable and performing a rough H ₂ O span is helpful (such as, during troubleshooting).	T_DP_Probe

4.3 Data retrieval

The program stores a very limited amount of data to the internal CPU of the data logger, so a microSD Flash card should be used with the CR6 or CR1000X. [Table 4-4](#) (p. 35) shows the number of days of data a 2 GB, 8 GB, and 16 GB card will typically hold before the memory is full and data starts to be overwritten. In cases where real-time remote monitoring is desired, various telemetry options (such as cellular or radio) are available to transmit the processed flux data. Certain conditions may also allow remote transmittal of time series data. Contact Campbell Scientific for more details.

microSD flash card size	Fill time with gas analyzer and sonic only	Fill time with gas analyzer, sonic, FW, and biomet/energy balance sensors ^{1/}
2 GB	~29 days	~23 days
8 GB	~121 days	~92 days
16 GB	~242 days	~184 days

^{1/}Biomet and energy balance sensors used for this fill time estimate include the following: HMP155A, CS301, CS310, SI-111, TE525MM, TCAV (qty 3), CS655 (qty 3), and HFP01 (qty 3).

NOTE:

The microSD flash cards from various manufacturers may have slightly different memory sizes on their 2 GB, 8 GB, and 16 GB cards, respectively. Also, as a card ages, some of its sectors may become unusable, decreasing the available memory. Fill time estimates given in [Table 4-4](#) (p. 35) are approximations for new cards.

CAUTION:

Campbell Scientific recommends and supports only the use of microSD cards obtained from Campbell Scientific. These cards are industrial grade and have passed Campbell Scientific hardware quality testing. Use of consumer grade cards substantially increases the risk of data loss.

4.4 Output tables

Besides the standard **Public**, **Status**, and **TableInfo** tables that every data logger reports, the program has six output tables. [Table 4-5](#) (p. 36) gives the names of these output tables, along with a short description, the frequency at which a record is written to the table, and the amount of memory allocated from the CPU and microSD card for each table.

NOTE:

Variable naming conventions used by AmeriFlux and other flux networks have been adopted in the *EasyFlux DL CR6OP* or *CR1KXOP*. Additionally, an EasyFlux output table called **Flux_AmeriFluxFormat** reports the data variables in the order and format prescribed by AmeriFlux (see <http://ameriflux.lbl.gov/data/aboutdata/data-variables/> )

The **Flux_CSFormat** and **Flux_Notes** tables have the same content as they did in prior versions of *EasyFlux DL CR6OP* for CR3000 (v1.0), although variable names have been updated to conform to AmeriFlux convention. If the user would prefer to have the data fields contained in the **Flux_Notes** table appended to the end of the **Flux_CSFormat** table, rather than being placed in a separate output table, then the user should change the constant **ONE_FULL_TABLE** from **FALSE** to **TRUE**. See [Set constants in CRBasic Editor and load program](#) (p. 16).

Table 4-5: Data output tables

Table name	Description	Recording interval	Memory on CR6 or CR1000X CPU	Memory on microSD card
Time_Series	Time series data, aligned to account for electronic delays	SCAN_INTERVAL (default 100 ms)	Auto-Allocate (typically less than 1 hour)	Broken up into 1-day files; see Table 4-4 (p. 35)
Diagnostic	Most recent diagnostic flags from gas analyzer and sonic anemometer	SCAN_INTERVAL (default 100 ms)	1 record (most recent scan)	0 records
Config_Setting_Notes	Settings for the gas analyzer and sonic anemometer	When settings are changed or system is power cycled	1 record	300 records
Flux_AmeriFluxFormat	Processed flux and statistical data following AmeriFlux reporting conventions and order	OUTPUT_INTERVAL (default 30 min)	NUM_DAY_CPU (default 7 days)	Broken up into 30-day files; see Table 4-4 (p. 35)

Table name	Description	Recording interval	Memory on CR6 or CR1000X CPU	Memory on microSD card
Flux_CSFormat	Processed flux and statistical data	OUTPUT_INTERVAL (default 30 min)	NUM_DAY_CPU (default 7 days)	Broken up into 30-day files; see Table 4-4 (p. 35)
Flux_Notes	Intermediate variables, station constants, and correction variables used to generate flux results	OUTPUT_INTERVAL (default 30 min)	NUM_DAY_CPU (default 7 days)	Broken up into 30-day files; see Table 4-4 (p. 35)

[Table 4-5](#) (p. 36) through [Table 4-11](#) (p. 56) give a description of all data fields found in each data output table and when each data field is included in the table.

NOTE:

Prior to coordinate rotations, the orthogonal wind components from the sonic anemometer are denoted as U_x , U_y , and U_z . Following coordinate rotations, the common denotation of u , v , and w is used, respectively.

NOTE:

Variables with $_R$ denote that the value was computed after coordinate rotations were done. Variables with $_F$ denote that the value was calculated after frequency corrections were applied. Similarly, $_SND$ and $_WPL$ refer to variables that have had the SND correction or the WPL correction applied, respectively.

Data field name	Units	Description	Data field included
U_x	$m \cdot s^{-1}$	Wind speed along sonic x-axis	Always
U_y	$m \cdot s^{-1}$	Wind speed along sonic y-axis	Always
U_z	$m \cdot s^{-1}$	Wind speed along sonic z-axis	Always
T_SONIC	deg C	Sonic temperature	Always
diag_sonic	adimensional	Raw sonic diagnostic value (0 indicates no diagnostic flags set)	Always

Data field name	Units	Description	Data field included
CO2_density	mg·m ⁻³	CO ₂ density	Always
CO2_density_fast_tmpr	mg·m ⁻³	CO ₂ density with spectroscopy correction using fast response temperature	Always
H2O_density	g·m ⁻³	Water vapor density	Always
diag_irga	adimensional	Raw gas analyzer diagnostic value (0 indicates no diagnostic flags set)	Always
T_SONIC_corr	deg C	Air temperature derived from sonic temperature corrected for humidity and pressure	If IRGASON is used
TA_1_1_1	deg C	Air temperature measured by EC100 temperature probe	Always
PA	kPa	Ambient pressure	Always
CO2_sig_strgth	adimensional	CO ₂ signal strength	Always
H2O_sig_strgth	adimensional	H ₂ O signal strength	Always
FW	deg C	Air temperature measured by fine-wire thermocouple	If FW05, FW1, or FW3 is used

Data field name	Description	Data field included
sonic_amp_l_f	Amplitude low diagnostic flag	Always
sonic_amp_h_f	Amplitude high diagnostic flag	Always
sonic_sig_lck_f	Signal lock diagnostic flag	Always
sonic_del_T_f_f	Delta temperature diagnostic flag	Always
sonic_aq_sig_f	Acquiring signal diagnostic flag	Always
sonic_cal_err_f	Calibration error diagnostic flag	Always
CSAT3H_user_ctrl_flg	CSAT3AH heating control start	If CSAT3AH

Table 4-7: Data fields in the Diagnostic output table

Data field name	Description	Data field included
CSAT3H_ctrl_on	CSAT3AH heating controller active	If CSAT3AH
T_trnsd_uppr	Upper transducer temperature (°C)	If CSAT3AH
T_trnsd_lwr	Lower transducer temperature (°C)	If CSAT3AH
pwr_trnsds	Power heating transducers (W)	If CSAT3AH
trnsd_heater_on	Transducer heater is on if TRUE	If CSAT3AH
trnsd_heater_fail	Transducer heater failed if TRUE	If CSAT3AH
T_arm_uppr	Upper arm temperature (°C)	If CSAT3AH
T_arm_lwr	Lower arm temperature (°C)	If CSAT3AH
pwr_arms	Power heating arms (WH)	If CSAT3AH
arm_heater_on	Arm heater is on if TRUE	If CSAT3AH
arm_heater_fail	Arm heater failed if TRUE	If CSAT3AH
pwr_trnsds_arms	Power heating transducers and arms (W)	If CSAT3AH
diag_sonic_slwintv	Aggregated diagnosis code within the last slow scan interval	If CSAT3AH
trnsd_ice_wet_lck	Seconds that transducers were locked due to ice and/or wet	If CSAT3AH
heating_inaplcbl_f	Heating would be inapplicable to improve the current measurements	If CSAT3AH
com_rslt_get	Number of failures for CR6 or CR1000X to get data from heating controller	If CSAT3AH
com_rslt_snt	Number of failures for CR6 or CR1000X to send data to heating controller	If CSAT3AH
T_amb_ctrl	Ambient air temperature (°C) measured by the temp/RH probe of heating controller	If CSAT3AH
RH_amb_ctrl	Ambient relative humidity (%) measured by the temp/RH probe of heating controller	If CSAT3AH
T_DP_amb_ctrl	Ambient dew point temperature (°C) measured by the temp/RH probe of heating controller	If CSAT3AH

Table 4-7: Data fields in the Diagnostic output table

Data field name	Description	Data field included
irga_bad_data_f	Any gas analyzer diagnostic flag is set	Always
irga_gen_fault_f	General system fault diagnostic flag	Always
irga_startup_f	Startup diagnostic flag	Always
irga_motor_spd_f	Motor speed diagnostic flag	Always
irga_tec_tmpr_f	Thermoelectric cooler (TEC) temperature diagnostic flag	Always
irga_src_pwr_f	Source power diagnostic flag	Always
irga_src_tmpr_f	Source temperature diagnostic flag	Always
irga_src_curr_f	Source current diagnostic flag	Always
irga_off_f	Gas head power down diagnostic flag	Always
irga_sync_f	Synchronization diagnostic flag	Always
irga_amb_tmpr_f	Ambient temperature probe diagnostic flag	Always
irga_amb_press_f	Ambient pressure diagnostic flag	Always
irga_CO2_I_f	CO ₂ I signal diagnostic flag	Always
irga_CO2_lo_f	CO ₂ I/O signal diagnostic flag	Always
irga_H2O_I_f	H ₂ O I signal diagnostic flag	Always
irga_H2O_lo_f	H ₂ O I/O signal diagnostic flag	Always
irga_CO2_lo_var_f	CO ₂ I/O variation diagnostic flag	Always
irga_H2O_lo_var_f	H ₂ O I/O variation diagnostic flag	Always
irga_CO2_sig_strgth_f	CO ₂ signal strength diagnostic flag	Always
irga_H2O_sig_strgth_f	H ₂ O signal strength diagnostic flag	Always
irga_cal_err_f	Calibration file read error flag	Always
irga_htr_ctrl_off_f	Heater control off diagnostic flag	Always
CO2_zero_coeff	CO ₂ zero coefficient	Always
CO2_span_coeff	CO ₂ span coefficient	Always

Data field name	Description	Data field included
H2O_zero_coeff	H ₂ O zero coefficient	Always
H2O_span_coeff	H ₂ O span coefficient	Always
shfp_cal_fail_1_1_1	Self-calibration of soil heat flux plate #1 failed if TRUE	If HFP01SC
shfp_cal_fail_1_1_2	Self-calibration of soil heat flux plate #2 failed if TRUE	If HFP01SC
shfp_cal_fail_1_1_3	Self-calibration of soil heat flux plate #3 failed if TRUE	If HFP01SC

Data field name	Units	Description	Data field included
config_type	dimensional	Configuration type	Always
Status	dimensional	Configuration status	Always
bandwidth_freq	Hz	EC100 bandwidth (5, 10, 12.5, or 20 for 5 Hz, 10 Hz, 12.5 Hz, or 20 Hz, respectively)	Always
press_source	adimensional	Sensor used by EC100 for ambient pressure (0 for EC100 basic barometer, 1 for user/custom barometer, 2 for EC100 enhanced barometer)	Always
tmpr_source	adimensional	Sensor used by EC100 for ambient temperature (0 for EC100 temperature probe, no other values valid)	Always
CO ₂ _zero_coeff	adimensional	CO ₂ zero coefficient set from last CO ₂ zero	Always
CO ₂ _span_coeff	adimensional	CO ₂ span coefficient set from last CO ₂ span	Always

Data field name	Units	Description	Data field included
H2O_zero_coeff	adimensional	H ₂ O zero coefficient set from last H ₂ O zero	Always
H2O_span_coeff	adimensional	H ₂ O span coefficient set from last H ₂ O span	Always
CO2_span_mixra	ppm	CO ₂ mixing ratio of span gas	Always
H2O_span_T_DP	deg C	Dew point temperature of span gas	Always
Heat_control	adimensional	Heater control setting (-1 for Disabled, -2 for Auto Control)	Always
IRGA_power	adimensional	Gas head power state (0 for On, 1 for Off)	Always
CO2_fast_tmpr	adimensional	If TRUE, CO ₂ with spectroscopy correction using fast air temperature is used for flux calculation; if FALSE, conventional CO ₂ is used	Always
Shadow_corr	adimensional	Application of transducer shadowing correction (0 for Off, 1 for On)	Always
CSAT3AH_user_ctrl_on	adimensional	CSAT3AH heating set by a user (TRUE for On, FALSE for Off)	If CSAT3AH

Data field name	Units	Description	Data field included
TIMESTAMP_START	YYYYMMDDHHMM	Start time of the averaging period	Always
TIMESTAMP_END	YYYYMMDDHHMM	End time of the averaging period	Always
CO2	μmol·mol ⁻¹	CO ₂ mole fraction	Always

Data field name	Units	Description	Data field included
CO2_SIGMA	$\mu\text{mol}\cdot\text{mol}^{-1}$	Standard deviation of CO ₂	Always
H2O	$\text{mmol}\cdot\text{mol}^{-1}$	Average H ₂ O molar mixing ratio (dry basis)	Always
H2O_SIGMA	$\text{mmol}\cdot\text{mol}^{-1}$	Standard deviation of H ₂ O	Always
FC	$\mu\text{mol}\cdot\text{m}^{-2}\cdot\text{s}^{-1}$	CO ₂ flux after corrections	Always
FC_SSITC_TEST	adimensional	Result of steady state and integral turbulence characteristics for FC according to Foken et al. (2004)	Always
LE	$\text{W}\cdot\text{m}^{-2}$	Latent heat flux after corrections	Always
LE_SSITC_TEST	adimensional	Result of steady state and integral turbulence characteristics for LE according to Foken et al. (2004)	Always
ET	$\text{mm}\cdot\text{hour}^{-1}$	Evapotranspiration	Always
ET_SSITC_TEST	adimensional	Result of steady state and integral turbulence characteristics for ET according to Foken et al. (2004)	Always
H	$\text{W}\cdot\text{m}^{-2}$	Sensible heat flux after corrections	Always

Table 4-9: Data fields in the Flux_AmeriFluxFormat output table

Data field name	Units	Description	Data field included
H_SSITC_TEST	adimensional	Result of steady state and integral turbulence characteristics for H according to Foken et al. (2004)	Always
G	$W \cdot m^{-2}$	Calculated heat flux at the ground surface	If energy balance sensors are used
SG	$W \cdot m^{-2}$	Change in heat storage in the soil above the soil heat flux plates during the averaging interval	If energy balance sensors are used
FETCH_MAX	m	Distance upwind where the maximum contribution to the footprint is found	Always
FETCH_90	m	Upwind distance that contains 90% of cumulative footprint; if NAN is returned, integration of the model never reached 90% within the allowable distance of integration (see Footprint [p. 134])	Always
FETCH_55	m	Upwind distance that contains 55% of footprint	Always
FETCH_40	m	Upwind distance that contains 40% of footprint	Always
WD	decimal degrees	Average wind direction	Always
WS	$m \cdot s^{-1}$	Average wind speed	Always
WS_MAX	$m \cdot s^{-1}$	Maximum wind speed	Always

Table 4-9: Data fields in the Flux_AmeriFluxFormat output table

Data field name	Units	Description	Data field included
USTAR	$\text{m}\cdot\text{s}^{-1}$	Friction velocity	Always
ZL	adimensional	Stability	Always
TAU	$\text{kg}\cdot\text{m}^{-1}\cdot\text{s}^{-2}$	Momentum flux	Always
TAU_SSITC_TEST	adimensional	Result of steady state and integral turbulence characteristics for TAU according to Foken et al. (2004)	Always
MO_LENGTH	m	Monin-Obukhov length	Always
U	$\text{m}\cdot\text{s}^{-1}$	Average streamwise wind	Always
U_SIGMA	$\text{m}\cdot\text{s}^{-1}$	Standard deviation of streamwise wind	Always
V	$\text{m}\cdot\text{s}^{-1}$	Average crosswind	Always
V_SIGMA	$\text{m}\cdot\text{s}^{-1}$	Standard deviation of crosswind	Always
W	$\text{m}\cdot\text{s}^{-1}$	Average vertical wind	Always
W_SIGMA	$\text{m}\cdot\text{s}^{-1}$	Standard deviation of vertical wind	Always
PA	kPa	Average atmospheric pressure	Always
TA_1_1_1	deg C	Average air temperature from EC100 temperature probe	Always
RH_1_1_1	%	Average relative humidity calculated from EC100 temperature probe, H ₂ O (from analyzer), and pressure	Always

Table 4-9: Data fields in the Flux_AmeriFluxFormat output table

Data field name	Units	Description	Data field included
T_DP_1_1_1	deg C	Average dew point temperature calculated from EC100 temperature probe, H ₂ O (from analyzer), and pressure	Always
TA_1_1_2	deg C	Average air temperature calculated from sonic temperature, H ₂ O, and pressure	If IRGASON
RH_1_1_2	%	Average relative humidity calculated from sonic temperature, H ₂ O, and pressure	If IRGASON
T_DP_1_1_2	deg C	Average dew point temperature calculated from sonic temperature, H ₂ O, and pressure	If IRGASON
TA_1_1_3	deg C	Average air temperature from temp/RH probe	If temp/RH probe is used
RH_1_1_3	%	Average relative humidity from temp/RH probe	If temp/RH probe is used
T_DP_1_1_3	deg C	Average dew point temperature from temp/RH probe	If temp/RH probe is used
VPD	hPa	Vapor pressure deficit	If temp/RH probe is used
T_SONIC	deg C	Average sonic temperature	Always
T_SONIC_SIGMA	deg C	Standard deviation of sonic temperature	Always
PBLH	m	Estimated planetary boundary layer height	Always

Table 4-9: Data fields in the Flux_AmeriFluxFormat output table

Data field name	Units	Description	Data field included
TS_1_1_x	deg C	Average soil temperature; x of 1 to 3 is an index for the number of soil temperature measurements made	If TCAV or CS65X is used (if both, TCAV temperature is used)
SWC_1_1_x	%	Soil water content; x of 1 to 3 is an index for the number of soil sensors	If CS65X is used
ALB	adimensional	Albedo	If SN500SS, NR01, or CNR4 is used
NETRAD	W·m ⁻²	Net radiation	If SN500SS, NR01, or CNR4 is used
PPFD_IN	μmol·m ⁻² ·s ⁻¹	Photosynthetic photon density	If CS310 is used
SW_IN	W·m ⁻²	Incoming short-wave radiation	If SN500SS, NR01, CNR4, CS301, or CS320 is used
SW_OUT	W·m ⁻²	Outgoing short-wave radiation	If SN500SS, NR01, or CNR4 is used
LW_IN	W·m ⁻²	Incoming long-wave radiation	If SN500SS, NR01, or CNR4 is used
LW_OUT	W·m ⁻²	Outgoing long-wave radiation	If SN500SS, NR01, or CNR4 is used
P	mm	Precipitation in output interval	If TE525 is used
T_CANOPY	deg C	Canopy temperature	If SI-111 is used

Data field name	Units	Description	Data field included
FC_mass	$\text{mg}\cdot\text{m}^{-2}\cdot\text{s}^{-1}$	Final corrected CO ₂ flux	Always
FC_QC	grade	Overall quality grade for Fc_molar and Fc_mass following Foken et al. (2012)	Always
FC_samples	count	Total number of time series samples used in calculation of Fc	Always
LE	$\text{W}\cdot\text{m}^{-2}$	Final corrected latent heat flux	Always
LE_QC	grade	Overall quality grade for LE following Foken et al. (2012)	Always
LE_samples	count	Total number of time series samples used in calculation of LE	Always
H	$\text{W}\cdot\text{m}^{-2}$	Final corrected sensible heat flux derived from sonic sensible heat flux	Always
H_QC	grade	Overall quality grade for H following Foken et al. (2012)	Always
H_samples	count	Total number of time series samples used in calculation of H	Always
H_FW	$\text{W}\cdot\text{m}^{-2}$	Final corrected sensible heat flux derived from fine-wire thermocouple measurements	If FW05, FW1, or FW3 is used
H_FW_samples	count	Total number of time series samples used in calculation of H_FW	If FW05, FW1, or FW3 is used
NETRAD	$\text{W}\cdot\text{m}^{-2}$	Average net radiation (corrected for wind)	If SN500SS, NR01, or CNR4 is used
G	$\text{W}\cdot\text{m}^{-2}$	Heat flux at the ground surface	If soil heat flux sensors are used

Table 4-10: Data fields in the Flux_CSFormat output table

Data field name	Units	Description	Data field included
SG	$W \cdot m^{-2}$	Change in heat storage in the soil above the soil heat flux plates during the averaging interval	If soil heat flux sensors are used
energy_closure	fraction	Ratio of sensible and latent heat fluxes over surface heat flux plus net radiation	If energy balance sensors are used
poor_engr_clsur	adimensional	If TRUE, energy closure is poor likely due to an instrument issue; check zero and span of analyzer	If energy balance sensors and TE525 are used
Bowen_ratio	fraction	Ratio of final sensible heat flux over final latent heat flux	Always
TAU	$kg \cdot m^{-1} \cdot s^{-2}$	Final corrected momentum flux	Always
TAU_QC	grade	Overall quality grade for TAU following Foken et al. (2012)	Always
USTAR	$m \cdot s^{-1}$	Friction velocity after coordinate rotations and frequency corrections	Always
TSTAR	deg C	Scaling temperature after coordinate rotations, frequency corrections, and SND correction	Always
TKE	$m^2 \cdot s^{-2}$	Specific turbulence kinetic energy after coordinate rotations	Always
TA_1_1_1	deg C	Average ambient temperature from EC100 temperature probe	Always

Table 4-10: Data fields in the Flux_CSFormat output table

Data field name	Units	Description	Data field included
RH_1_1_1	deg C	Relative humidity calculated from TA_1_1_1 (EC100 temperature probe), water vapor density, and pressure	Always
T_DP_1_1_1	deg C	Average dew point temperature calculated using temperature from the EC100 temperature probe	Always
e_amb	kPa	Average water vapor pressure calculated using temperature from the EC100 temperature probe	Always
e_sat_amb	kPa	Average saturated water vapor pressure calculated using temperature from the EC100 temperature probe	Always
TA_1_2	deg C	Average ambient temperature calculated from sonic temperature, water vapor density, and pressure	If IRGASON
RH_1_1_2	deg C	Average relative humidity calculated using sonic temperature, water vapor density, and pressure	If IRGASON
T_DP_1_1_2	deg C	Average dew point temperature calculated using sonic temperature, water vapor density, and pressure	If IRGASON
e	kPa	Average water vapor pressure calculated from sonic temperature	If IRGASON

Table 4-10: Data fields in the Flux_CSFormat output table

Data field name	Units	Description	Data field included
e_sat	kPa	Average saturated water vapor pressure calculated from sonic temperature	If IRGASON
TA_1_1_3	deg C	Average air temperature from temp/RH probe	If temp/RH probe is used
RH_1_1_3	%	Average relative humidity from temp/RH probe	If temp/RH probe is used
T_DP_1_1_3	deg C	Average dew point temperature from temp/RH probe	If temp/RH probe is used
e_probe	kPa	Average water vapor pressure derived from temp/RH probe	If temp/RH probe is used
e_sat_probe	kPa	Average saturated water vapor pressure derived from temp/RH probe	If temp/RH probe used
H2O_probe		Average water vapor density derived from temp/RH probe measurements	If temp/RH probe used
PA	kPa	Average atmospheric pressure	Always
VPD	kPa	Vapor pressure deficit	Always
Ux	m·s ⁻¹	Wind speed along x-axis of sonic anemometer (U _x)	Always
Ux_SIGMA	m·s ⁻¹	Standard deviation of U _x	Always
Uy	m·s ⁻¹	Wind speed along y-axis of sonic anemometer (U _y)	Always
Uy_SIGMA	m·s ⁻¹	Standard deviation of U _y	Always
Uz	m·s ⁻¹	Wind speed along z-axis of sonic anemometer (U _z)	Always
Uz_SIGMA	m·s ⁻¹	Standard deviation of U _z	Always

Table 4-10: Data fields in the Flux_CSFormat output table

Data field name	Units	Description	Data field included
T_SONIC	deg C	Sonic temperature	Always
T_SONIC_SIGMA	deg C	Standard deviation of sonic temperature	Always
sonic_azimuth	decimal degrees	Compass direction in which the sonic negative x-axis points	Always
WS	m·s ⁻¹	Wind speed	Always
WS_RSLT	m·s ⁻¹	Resultant horizontal wind speed	Always
WD_SONIC	decimal degrees	Average wind direction in the sonic coordinate system	Always
WD_SIGMA	decimal degrees	Standard deviation of wind direction in the sonic coordinate system	Always
WD	decimal degrees	Compass wind direction	Always
WS_MAX	m·s ⁻¹	Maximum wind speed	Always
CO2_density	mg·m ⁻³	CO ₂ mass density	Always
CO2_density_SIGMA	mg·m ⁻³	Standard deviation of CO ₂ mass density	Always
H2O_density	mmol·mol ⁻¹	Water vapor mass density	Always
H2O_density_SIGMA	mmol·mol ⁻¹	Standard deviation of water vapor mass density	Always
CO2_sig_strgth_Min	adimensional	Minimum CO ₂ signal strength	Always
H2O_sig_strgth_Min	adimensional	Minimum H ₂ O signal strength	Always
FW	deg C	Fine-wire thermocouple temperature	If FW05, FW1, or FW3 is used
FW_SIGMA	deg C	Standard deviation of fine-wire thermocouple temperature	If FW05, FW1, or FW3 is used

Table 4-10: Data fields in the Flux_CSFormat output table

Data field name	Units	Description	Data field included
P	mm	Total precipitation	If TE525 is used
ALB	adimensional	Albedo	If SN500SS, CNR4, or NR01 is used
SW_IN	W·m ⁻²	Incoming short-wave radiation	If SN500SS, CNR4, CS301, CS320, or NR01 is used
SW_OUT	W·m ⁻²	Outgoing short-wave radiation	If SN500SS, CNR4, or NR01 is used
LW_IN	W·m ⁻²	Incoming long-wave radiation	If SN500SS, CNR4, or NR01 is used
LW_OUT	W·m ⁻²	Outgoing long-wave radiation	If SN500SS, CNR4, or NR01 is used
T_nr	Klvin	Sensor body temperature	If CNR4 or NR01 is used
T_nr_in	Klvin	Face-up sensor body temperature	If SN500SS is used
T_nr_out	Klvin	Face-down sensor body temperature	If SN500SS is used
R_LW_in_meas	W·m ⁻²	Raw incoming long-wave radiation	If CNR4 or NR01 is used
R_LW_out_meas	W·m ⁻²	Raw outgoing long-wave radiation	If CNR4 or NR01 is used
PPFD_IN	μmol·s ⁻¹ ·m ⁻²	Density of photosynthetic active radiation	If CS310 is used
sun_azimuth	decimal degrees	Solar azimuth	Always
sun_elevation	decimal degrees	Solar elevation	Always
hour_angle	decimal degrees	Solar hour angle	Always

Table 4-10: Data fields in the Flux_CSFormat output table

Data field name	Units	Description	Data field included
sun_declination	decimal degrees	Solar declination	Always
air_mass_coeff	adimensional	Air mass coefficient; ratio of the path length between the current solar position to solar noon	Always
daytime	fraction	Day time in fraction of an output interval	Always
T_CANOPY	deg C	Temperature of targeted object	If SI-111 is used
T_SI111_body	deg C	Temperature of sensor body	If SI-111 is used
TS_1_1_x	deg C	Soil temperature for each TCAV sensor; x of 1 to 3 is an index for the number of TCAV sensors	If TCAV is used
SWC_1_1_x	m ³ ·m ⁻³	Volumetric soil water content for each CS650 or CS655; x of 1 to 3 is an index for the number of sensors	If CS650 or CS655 is used
TS_CS65X_1_1_x	deg C	Soil temperature for each CS650 or CS655; x of 1 to 3 is an index for the number of sensors	If CS650 or CS655 is used
CS65x_ec_1_1_x	dS·m ⁻¹	Electrical conductivity for each CS650 or CS655 sensor; x of 1 to 3 is an index for the number of sensors	If CS650 or CS655 is used
G_plate_1_1_x	W·m ⁻²	Heat flux through sensor plate; x of 1 to 3 is an index for the number of HFP01 or HFP01SC sensors	If HFP01 or HFP01SC is used

Table 4-10: Data fields in the Flux_CSFormat output table

Data field name	Units	Description	Data field included
G_1_1_x	W·m ⁻²	Heat flux across the ground surface (summation of heat flux through plate and heat storage above plate); x of 1 to 3 is an index for the number of replications for soil heat flux measurements	If HFP01 or HFP01SC, TCAV, and/or CS650/CS655 are used
SG_1_1_x	W·m ⁻²	Heat flux found from heat storage in soil layer above sensor plate; x of 1 to 3 is an index for the number of replications for soil heat flux measurements	If HFP01 or HFP01SC, TCAV, and/or CS650/CS655 are used
FETCH_MAX	m	Distance upwind where the maximum contribution to the footprint is found	Always
FETCH_90	m	Upwind distance that contains 90% of cumulative footprint; if NAN is returned, integration of the model never reached 90% within the allowable distance of integration (see Footprint [p. 134])	Always
FETCH_55	m	Upwind distance that contains 55% of footprint	Always
FETCH_40	m	Upwind distance that contains 40% of footprint	Always
UPWND_DIST_INTRST	m	Upwind distance of interest for the average wind direction	Always

Table 4-10: Data fields in the Flux_CSFormat output table

Data field name	Units	Description	Data field included
FP_DIST_INTRST	%	Percentage of footprint from within the upwind range of interest	Always
FP_EQUATION	text	Returns either Kljun or KormannMeixner; the model of Kljun et al. (2004) is used for applicable atmospheric conditions; otherwise, the model of Kormann & Meixner (2001) is used	Always

Table 4-11: Data fields in the Flux_Notes output table

Data field name	Units	Description	Data field included
UxUy_cov	$m^2 \cdot s^{-2}$	Covariance of U_x and U_y	Always
UxUz_cov	$m^2 \cdot s^{-2}$	Covariance of U_x and U_z	Always
UyUz_cov	$m^2 \cdot s^{-2}$	Covariance of U_y and U_z	Always
TsUx_cov	$deg \cdot C \cdot m \cdot s^{-1}$	Covariance of T_s and U_x	Always
TsUy_cov	$deg \cdot C \cdot m \cdot s^{-1}$	Covariance of T_s and U_y	Always
TsUz_cov	$deg \cdot C \cdot m \cdot s^{-1}$	Covariance of T_s and U_z	Always
USTAR_R	$m \cdot s^{-1}$	Friction velocity after coordinate rotations	Always
U	$m \cdot s^{-1}$	Streamwise wind speed after coordinate rotations	Always
U_SIGMA	$m \cdot s^{-1}$	Standard deviation of streamwise wind after coordinate rotations	Always
V	$m \cdot s^{-1}$	Crosswind speed after coordinate rotations	Always

Table 4-11: Data fields in the Flux_Notes output table

Data field name	Units	Description	Data field included
V_SIGMA	$m \cdot s^{-1}$	Standard deviation of crosswind after coordinate rotations	Always
W	$m \cdot s^{-1}$	Vertical wind speed after coordinate rotations	Always
W_SIGMA	$m \cdot s^{-1}$	Standard deviation of vertical wind after coordinate rotations	Always
UV_cov	$m \cdot s^{-1}$	Covariance of streamwise wind and crosswind after coordinate rotations	Always
UW_cov	$m \cdot s^{-1}$	Covariance of streamwise wind and vertical wind after coordinate rotations	Always
VW_cov	$m \cdot s^{-1}$	Covariance of crosswind and vertical wind after coordinate rotations	Always
UT_SONIC_Cov	$m \cdot \text{deg} \cdot C \cdot s^{-1}$	Covariance of streamwise wind and sonic temperature after coordinate rotations	Always
VT_SONIC_Cov	$m \cdot \text{deg} \cdot C \cdot s^{-1}$	Covariance of crosswind and sonic temperature after coordinate rotations	Always
WT_SONIC_Cov	$m \cdot \text{deg} \cdot C \cdot s^{-1}$	Covariance of vertical wind and sonic temperature after coordinate rotations	Always
UW_Cov_fc	$m^2 \cdot s^{-2}$	Covariance of streamwise wind and vertical wind after coordinate rotations and frequency corrections	Always

Table 4-11: Data fields in the Flux_Notes output table

Data field name	Units	Description	Data field included
VW_Cov_fc	$m^2 \cdot s^{-2}$	Covariance of crosswind and vertical wind after coordinate rotations and frequency corrections	Always
WT_SONIC_Cov_fc	$m \cdot \text{deg} \cdot C \cdot s^{-1}$	Covariance of vertical wind and sonic temperature after coordinate rotations and frequency corrections	Always
WT_SONIC_Cov__fc_SND	$m \cdot \text{deg} \cdot C \cdot s^{-1}$	Covariance of vertical wind and sonic temperature after coordinate rotations, frequency corrections, and SND correction	Always
sonic_samples	count	Number of raw sonic samples in averaging period without diagnostic flags	Always
diag_sonic_aggregate	adimensional	Aggregated diagnosis code	Always
no_sonic_head_Tot	count	Number of sonic samples where no sonic head was detected	Always
no_new_sonic_data_Tot	count	Number of scans where no sonic data was received	Always
sonic_amp_l_f_Tot	count	Number of sonic samples with amplitude low diagnostic flag	Always
sonic_amp_h_f_Tot	count	Number of sonic samples with amplitude high diagnostic flag	Always
sonic_sig_lck_f_Tot	count	Number of sonic samples with signal lock diagnostic flag	Always

Table 4-11: Data fields in the Flux_Notes output table

Data field name	Units	Description	Data field included
sonic_del_T_f_Tot	count	Number of sonic samples with delta temperature diagnostic flag	Always
sonic_aq_sig_f_Tot	count	Number of sonic samples with acquiring signal diagnostic flag	Always
sonic_cal_err_f_Tot	count	Number of sonic samples with calibration error diagnostic flag	Always
CSAT3H_user_ctrl_on_Tot	count	Number of slow scan intervals over an averaging interval for CSAT3H heating on, allowed by a user	If CSAT3AH
CSAT3H_ctrl_on_Tot	count	Number of slow scan intervals over an averaging interval for CSAT3H heating on, controlled by the controller itself	If CSAT3AH
T_trnsd_uppr	deg C	Upper transducer temperature	If CSAT3AH
T_trnsd_uppr_Min	deg C	Minimum upper transducer temperature	If CSAT3AH
T_trnsd_lwr	deg C	Lower transducer temperature	If CSAT3AH
T_trnsd_lwr_Min	deg C	Minimum lower transducer temperature	If CSAT3AH
pwr_trnsd_Max	WH	Maximum transducer heating power	If CSAT3AH
trnsd_heater_secs	s	Transducer heating time length	If CSAT3AH

Table 4-11: Data fields in the Flux_Notes output table

Data field name	Units	Description	Data field included
trnsd_heater_fail_Tot	count	Number of transducer heater failures	If CSAT3AH
T_arm_uppr	deg C	Upper arm temperature	If CSAT3AH
T_arm_uppr_Min	deg C	Minimum upper arm temperature	If CSAT3AH
T_arm_lwr	deg C	Lower arm temperature	If CSAT3AH
T_arm_lwr_Min	deg C	Minimum lower arm temperature	If CSAT3AH
pwr_arms_Max	WH	Maximum arm heating power	If CSAT3AH
arm_heater_secs	s	Arm heating time length	If CSAT3AH
arm_heater_fail_Tot	count	Number of arm heater failures	If CSAT3AH
pwr_hr_trnsds_arms	WH	Power used to heat transducers and arms	If CSAT3AH
trnsd_ice_wet_lck	count	Number of times sonic transducers were locked due to ice and wet	If CSAT3AH
heating_inaplcbl_f_Tot	count	Number of times heating would be inapplicable to improve measurement problems	If CSAT3AH
T_amb_ctrl	deg C	Ambient air temperature measured by the heating controller temp/RH probe	If CSAT3AH
T_amb_ctrl_Min	deg C	Minimum ambient air temperature measured by the heating controller temp/RH probe	If CSAT3AH

Table 4-11: Data fields in the Flux_Notes output table

Data field name	Units	Description	Data field included
RH_amb_ctrl_Max	%	Maximum relative humidity measured by the heating controller temp/RH probe	If CSAT3AH
T_DP_amb_ctrl_Max	deg C	Maximum dew point temperature computed from the measurements from the heating controller temp/RH probe	If CSAT3AH
com_rslt_get_Tot	count	Number of successes in getting data from the heating controller	If CSAT3AH
com_rslt_snt_Tot	count	Number of successes in sending data to the heating controller	If CSAT3AH
UxCO2_Cov	mg·m ⁻² ·s ⁻¹	Covariance of U _x and CO ₂ density	Always
UyCO2_Cov	mg·m ⁻² ·s ⁻¹	Covariance of U _y and CO ₂ density	Always
UzCO2_Cov	mg·m ⁻² ·s ⁻¹	Covariance of U _z and CO ₂ density	Always
UxH2O_Cov	g·m ⁻² ·s ⁻¹	Covariance of U _x and H ₂ O density	Always
UyH2O_Cov	g·m ⁻² ·s ⁻¹	Covariance of U _y and H ₂ O density	Always
UzH2O_Cov	g·m ⁻² ·s ⁻¹	Covariance of U _z and H ₂ O density	Always
UCO2_Cov	mg·m ⁻² ·s ⁻¹	Covariance of streamwise wind and CO ₂ density after coordinate rotations	Always

Table 4-11: Data fields in the Flux_Notes output table

Data field name	Units	Description	Data field included
VCO2_Cov	$\text{mg}\cdot\text{m}^{-2}\cdot\text{s}^{-1}$	Covariance of crosswind and CO ₂ density after coordinate rotations	Always
WCO2_Cov	$\text{mg}\cdot\text{m}^{-2}\cdot\text{s}^{-1}$	Covariance of vertical wind and CO ₂ density after coordinate rotations	Always
UH2O_Cov	$\text{g}\cdot\text{m}^{-2}\cdot\text{s}^{-1}$	Covariance of streamwise wind and H ₂ O density after coordinate rotations	Always
VH2O_Cov	$\text{g}\cdot\text{m}^{-2}\cdot\text{s}^{-1}$	Covariance of crosswind and H ₂ O density after coordinate rotations	Always
WH2O_Cov	$\text{g}\cdot\text{m}^{-2}\cdot\text{s}^{-1}$	Covariance of vertical wind and H ₂ O density after coordinate rotations	Always
WCO2_Cov_fc	$\text{mg}\cdot\text{m}^{-2}\cdot\text{s}^{-1}$	Covariance of vertical wind and CO ₂ density after coordinate rotations and frequency corrections	Always
WH2O_Cov_fc	$\text{g}\cdot\text{m}^{-2}\cdot\text{s}^{-1}$	Covariance of vertical wind and H ₂ O density after coordinate rotations and frequency corrections	Always
CO2_E_WPL_fc	$\text{mg}\cdot\text{m}^{-2}\cdot\text{s}^{-1}$	CO ₂ flux WPL correction term due to water vapor flux after coordinate rotations and frequency corrections	Always
CO2_T_WPL_fc	$\text{mg}\cdot\text{m}^{-2}\cdot\text{s}^{-1}$	CO ₂ flux WPL correction term due to sensible heat flux after coordinate rotations and frequency corrections	Always

Table 4-11: Data fields in the Flux_Notes output table

Data field name	Units	Description	Data field included
H2O_E_WPL_fc	$\text{g}\cdot\text{m}^{-2}\cdot\text{s}^{-1}$	H ₂ O flux WPL correction term due to water vapor flux after coordinate rotations and frequency corrections	Always
H2O_T_WPL_fc	$\text{g}\cdot\text{m}^{-2}\cdot\text{s}^{-1}$	H ₂ O flux WPL correction term due to sensible heat flux after coordinate rotations and frequency corrections	Always
CO2_samples	count	Number of CO ₂ samples without diagnostic flags and within thresholds for CO ₂ signal strength, set in code to default 0.7 (see Set constants in CRBasic Editor and load program [p. 16]) and the factory calibrated CO ₂ measurement range (0 to 1000 $\mu\text{mol}/\text{mol}$)	Always
H2O_samples	count	Number of H ₂ O samples without diagnostic flags and within thresholds for H ₂ O signal strength, set in code to default 0.7 (see Set constants in CRBasic Editor and load program [p. 16]) and the factory calibrated H ₂ O measurement range (0 to 72 mmol/mol)	Always
no_irga_head_Tot	count	Number of samples where no gas analyzer head was detected	Always

Table 4-11: Data fields in the Flux_Notes output table

Data field name	Units	Description	Data field included
no_new_irga_data_Tot	count	Number of scans where no gas analyzer data was received	Always
irga_bad_data_f_Tot	count	Number of gas analyzer samples with any diagnostic flag set high	Always
irga_gen_fault_f_Tot	count	Number of gas analyzer samples with general system fault diagnostic flag	Always
irga_startup_f_Tot	count	Number of gas analyzer samples with startup diagnostic flag	Always
irga_motor_spd_f_Tot	count	Number of gas analyzer samples with motor speed diagnostic flag	Always
irga_tec_tmpr_f_Tot	count	Number of gas analyzer samples with TEC temperature diagnostic flag	Always
irga_src_pwr_f_Tot	count	Number of gas analyzer samples with source power diagnostic flag	Always
irga_src_tmpr_f_Tot	count	Number of gas analyzer samples with source temperature diagnostic flag	Always
irga_src_curr_f_Tot	count	Number of gas analyzer samples with source current diagnostic flag	Always
irga_off_f_Tot	count	Number of gas analyzer samples with gas head power down diagnostic flag	Always

Table 4-11: Data fields in the Flux_Notes output table

Data field name	Units	Description	Data field included
irga_sync_f_Tot	count	Number of gas analyzer samples with synchronization diagnostic flag	Always
irga_amb_tmpr_f_Tot	count	Number of gas analyzer samples with ambient temperature probe diagnostic flag	Always
irga_amb_press_f_Tot	count	Number of gas analyzer samples with ambient pressure diagnostic flag	Always
irga_CO2_I_f_Tot	count	Number of gas analyzer samples with CO ₂ I signal diagnostic flag	Always
irga_CO2_lo_f_Tot	count	Number of gas analyzer samples with CO ₂ I/O signal diagnostic flag	Always
irga_H2O_I_f_Tot	count	Number of gas analyzer samples with H ₂ O I signal diagnostic flag	Always
irga_H2O_lo_f_Tot	count	Number of gas analyzer samples with H ₂ O I/O signal diagnostic flag	Always
irga_CO2_lo_var_f_Tot	count	Number of gas analyzer samples with CO ₂ I/O variation diagnostic flag	Always
irga_H2O_lo_var_f_Tot	count	Number of gas analyzer samples with H ₂ O I/O variation diagnostic flag	Always
irga_CO2_sig_strgth_f_Tot	count	Number of gas analyzer samples with CO ₂ signal strength diagnostic flag	Always

Table 4-11: Data fields in the Flux_Notes output table

Data field name	Units	Description	Data field included
irga_H2O_sig_strgth_f_Tot	count	Number of gas analyzer samples with H ₂ O signal strength diagnostic flag	Always
irga_cal_err_f_Tot	count	Number of gas analyzer samples with calibration file read error flag	Always
irga_htr_ctrl_off_f_Tot	count	Number of gas analyzer samples with heater control off diagnostic flag	Always
UxFW_cov	deg C·m·s ⁻¹	Covariance of U _x and fine-wire thermocouple temperature	If FW05, FW1, or FW3 is used
UyFW_cov	deg C·m·s ⁻¹	Covariance of U _y and fine-wire thermocouple temperature	If FW05, FW1, or FW3 is used
UzFW_cov	deg C·m·s ⁻¹	Covariance of U _z and fine-wire thermocouple temperature	If FW05, FW1, or FW3 is used
UFW_cov	deg C·m·s ⁻¹	Covariance of streamwise wind and fine-wire thermocouple temperature after coordinate rotations	If FW05, FW1, or FW3 is used
VFW_cov	deg C·m·s ⁻¹	Covariance of crosswind and fine-wire thermocouple temperature after coordinate rotations	If FW05, FW1, or FW3 is used
WFW_cov	deg C·m·s ⁻¹	Covariance of vertical wind and fine-wire thermocouple temperature after coordinate rotations	If FW05, FW1, or FW3 is used

Table 4-11: Data fields in the Flux_Notes output table

Data field name	Units	Description	Data field included
WFW_cov_fc	deg C·m·s ⁻¹	Covariance of vertical wind and fine-wire thermocouple temperature after coordinate rotations and frequency corrections	If FW05, FW1, or FW3 is used
FW_samples	count	Number of valid fine-wire thermocouple measurements in the averaging period from which covariances may be calculated	If FW05, FW1, or FW3 is used
alpha	decimal degrees	Alpha angle used for coordinate rotations (regardless of planar fit or double rotation method; angle convention of Wilczak, Oncley, and Stage [2001] used)	Always
beta	decimal degrees	Beta angle used for coordinate rotations (regardless of planar fit or double rotation method; angle convention of Wilczak, Oncley, and Stage [2001] used)	Always
gamma	decimal degrees	Gamma angle used for coordinate rotations (regardless of planar fit or double rotation method; angle convention of Wilczak, Oncley, and Stage [2001] used)	Always

Table 4-11: Data fields in the Flux_Notes output table

Data field name	Units	Description	Data field included
height_measurement	m	User-entered measurement height of eddy-covariance sensors	Always
height_canopy	m	User-entered canopy height	Always
surface_type_text	text	User-entered surface type	Always
displacement_user	m	User-entered displacement height; 0 for auto calculation	Always
d	m	Displacement height used in calculation, which will be equal to displacement_user if user entered a non-0 value; if displacement_user is 0, program will auto calculate	Always
roughness_user	m	User-entered roughness length; 0 for calculation	Always
z0	m	Roughness length used in calculations, which will be equal to roughness_user if user entered a non-0 value; if roughness_user is 0, program will auto calculate	Always
z	m	Aerodynamic height (for example, height_measurement – d)	Always
MO_LENGTH	m	Monin-Obukhov length	Always
ZL	m·m ⁻¹	Atmospheric surface layer stability	Always
iteration_FreqFactor	count	Number of iterations for recalculating Monin-Obukhov length and frequency factors	Always

Table 4-11: Data fields in the Flux_Notes output table

Data field name	Units	Description	Data field included
latitude	decimal degrees	Latitude; positive for northern hemisphere, negative for southern hemisphere	Always
longitude	decimal degrees	Longitude; positive for eastern hemisphere, negative for western hemisphere	Always
altitude	m	Number of meters above sea level at the site	Always
UTC_OFFSET	Hr	Time offset in hours between the site local standard time and UTC/GMT	Always
separation_x_irga	m	Separation between sonic anemometer and gas analyzer with respect to sonic x-axis	Always
separation_y_irga	m	Separation between sonic anemometer and gas analyzer with respect to sonic y-axis	Always
separation_lat_dist_irga	m	Separation distance between sonic anemometer and gas analyzer along the axis perpendicular to oncoming wind	Always
separation_lag_dist_irga	m	Separation distance between sonic anemometer and gas analyzer along the axis parallel to oncoming wind	Always

Table 4-11: Data fields in the Flux_Notes output table

Data field name	Units	Description	Data field included
separation_lag_scan_irga	scans	Number of scans to lag gas analyzer data relative to sonic anemometer data to account for separation along the axis of oncoming wind and wind velocity	Always
separation_x_FW	m	Separation between sonic anemometer and fine-wire thermocouple with respect to sonic x-axis	If FW05, FW1, or FW3 is used
separation_y_FW	m	Separation between sonic anemometer and fine-wire thermocouple with respect to sonic anemometer y-axis	If FW05, FW1, or FW3 is used
FW_diameter	m	Effective diameter of fine-wire thermocouple junction	If FW05, FW1, or FW3 is used
separation_lat_dist_FW	m	Separation distance between sonic anemometer and fine-wire thermocouple along axis perpendicular to oncoming wind	If FW05, FW1, or FW3 is used
separation_lag_dist_FW	m	Separation distance between sonic anemometer and fine-wire thermocouple along axis parallel to oncoming wind	If FW05, FW1, or FW3 is used
separation_lag_scan_FW	scans	Number of scans to lag fine-wire thermocouple data relative to sonic anemometer data to account for separation along axis of oncoming wind and wind velocity	If FW05, FW1, or FW3 is used

Table 4-11: Data fields in the Flux_Notes output table

Data field name	Units	Description	Data field included
time_const_FW	m	Calculated time constant of fine-wire thermocouple	If FW05, FW1, or FW3 is used
MAX_LAG	scans	Maximum number of scans to lag gas analyzer or fine-wire thermocouple data with respect to sonic anemometer data when doing cross correlation for covariance maximization (for example, if MAX_LAG = 2, the program will consider lags of -2, -1, 0, +1, and +2; default value is 5)	Always
lag_irga	scans	Lag applied to gas analyzer data with respect to sonic anemometer data that maximizes covariance	Always
lag_FW	scans	Lag applied to fine-wire thermocouple data with respect to sonic anemometer data that maximizes covariance	Always
FreqFactor_UW_VW	number	Frequency correction factor applied to momentum fluxes	Always
FreqFactor_WT_SONIC	number	Frequency correction factor applied to WT_SONIC covariance	Always
FreqFactor_WCO2_WH2O	number	Frequency correction factor applied to WCO ₂ and WH ₂ O covariance values	Always
FreqFactor_WFW	number	Frequency correction factor applied to fine-wire thermocouple derived WFW covariance	Always

Table 4-11: Data fields in the Flux_Notes output table

Data field name	Units	Description	Data field included
rho_d_amb	g·m ⁻³	Average density of dry air using air temperature from 107 probe, H ₂ O density from gas analyzer, and atmospheric pressure from barometer	Always
rho_a_amb	kg·m ⁻³	Average density of ambient moist air using air temperature from 107 probe, H ₂ O density from gas analyzer, and pressure from barometer	Always
rho_d	g·m ⁻³	Average density of dry air using air temperature from sonic temperature, H ₂ O density from gas analyzer, and atmospheric pressure from barometer	Always
rho_a	kg·m ⁻³	Average density of ambient moist air using air temperature from sonic temperature, H ₂ O density from gas analyzer, and atmospheric pressure from barometer	Always
rho_d_probe	g·m ⁻³	Average density of dry air using air temperature and relative humidity from HMP probe and atmospheric pressure from barometer	If temp/RH probe is used

Table 4-11: Data fields in the Flux_Notes output table

Data field name	Units	Description	Data field included
rho_a_probe	kg·m ⁻³	Average density of ambient moist air using air temperature and relative humidity from HMP probe and atmospheric pressure from barometer	If temp/RH probe is used
Cp	J·kg ⁻¹ ·K ⁻¹	Specific heat of ambient moist air at constant pressure	Always
Lv	J·g ⁻¹	Latent heat of vaporization	Always
T_panel	deg C	Average temperature of the data logger wiring panel	Always
V_batt	volt	Average battery voltage supplying power to the data logger	Always
slowsequence_Tot	count	Number of slow sequences during the averaging interval (for example, the number of times biomet and energy balance sensors were measured)	Always
nr01_heater_secs	s	Number of seconds in the averaging interval that NR01 heater was enabled	If NR01 is used
cnr4_fan_secs	s	Number of seconds in the averaging interval that CNR4 fan was enabled	If CNR4 and CNF4 are used
cnr4_heater_1_secs	s	Number of seconds in the averaging interval that CNR4 heater #1 was enabled	If CNR4 and CNF4 are used
cnr4_heater_2_secs	s	Number of seconds in the averaging interval that CNR4 heater #2 was enabled	If CNR4 and CNF4 are used

Table 4-11: Data fields in the Flux_Notes output table

Data field name	Units	Description	Data field included
sn500_heater_secs	s	Number of seconds in the averaging interval that SN500SS heater was enabled	If SN500SS is used
V_CS320	mV	Output voltage from CS320	If CS320 is used
T_CS320	deg C	Temperature of CS320	If CS320 is used
x_incline	decimal degrees	Pyranometer incline relative to its x-axis	If CS320 is used
y_incline	decimal degrees	Pyranometer incline relative to its y-axis	If CS320 is used
z_incline	decimal degrees	Pyranometer incline relative to its z-axis	If CS320 is used
CS320_heater_secs	s	Number of seconds in the averaging interval that CS320 heater was enabled	If CS320 is used
shfp_cal_1_1_x	$W \cdot m^{-2} \cdot mV^{-1}$	Calibrated multiplier for heat flux plate; this value is 1000 divided by the sensitivity as reported in the calibration sheet, but for HFP01SC, this is determined from self-calibration after the OPEC system runs longer than calibration interval (x of 1 to 3 is an index for the number of sensors)	If HFP01 or HFP01SC is used

Data field name	Units	Description	Data field included
shfp_cal_fail_1_1_x	adimensional	Reads TRUE after self-calibration if any readings from HFP01SC were not valid (NAN) or if calibrated sensitivity was <80% or >105% of the nominal sensitivity reported on the sensor calibration sheet (x of 1 to 3 is an index for the number of sensors)	If HFP01SC is used
process_time_Avg	ms	Average processing time for each scan	Always
process_time_Max	ms	Maximum processing time for a scan	Always
buff_depth_Max	number	Maximum number of records stored in buffer	Always

4.5 Program sequence of measurement and corrections

The main correction procedures and algorithms implemented into the program are listed below. For more information on the sequence of measurements and corrections, refer to [EasyFlux DL CR6OP or CR1KXOP process flow diagram](#) (p. 171). The appendices of this manual will give additional information on each major correction and its implementation in the program.

1. Despike and filter 10 Hz data using sonic anemometer and gas analyzer diagnostic codes and signal strength and measurement output range thresholds.
2. Coordinate rotations with an option to use the double rotation method (Tanner and Thurtell 1969) or planar fit method (Wilczak, Oncley, and Stage 2001).
3. Lag CO₂ and H₂O measurements against sonic wind measurements for maximization of CO₂ and H₂O fluxes (Horst and Lenschow 2009; Foken et al. 2012), with additional constraints to ensure lags are physically possible.

4. Frequency corrections using commonly used cospectra (Moore 1986; van Dijk 2002a; Moncrieff et al. 1997) and transfer functions of block averaging (Kaimal, Clifford, and Lataitis 1989; Massman 2000), line/volume averaging (Moore 1986; Moncrieff et al. 1997; Foken et al. 2012; van Dijk 2002a), time constants (Montgomery 1947; Shapland et al. 2014; Geankoplis 1993, 114–131 and Appendix), and sensor separation (Horst and Lenschow 2009; Foken et al. 2012).
5. A modified SND correction (Schotanus, Nieuwstadt, and de Bruin 1983) to derive sensible heat flux from sonic sensible heat flux following the implementation as outlined in van Dijk (2002b). Additionally, fully corrected real sensible heat flux computed from fine-wire thermometry to be optionally provided.
6. Correction for air density changes using WPL equations (Webb, Pearman, and Leuning 1980).
7. Data quality qualifications based on steady state conditions, surface-layer turbulence characteristics, and wind directions following Foken et al. (2012) for Flux_CSFormat or Foken et al. (2004) for the Flux_AmeriFluxFormat output table.
8. If energy balance sensors are used, calculation of energy closure based on energy balance measurements and corrected sensible and latent heat fluxes.
9. Footprint characteristics computed using Kljun et al. (2004) as the first option and Kormann and Meixner (2001) as the second when Kljun et al. (2004) is not applicable.

5. References

- Foken, T., R. Leuning, S.R. Oncley, M. Mauder, and M. Aubinet. 2012. "Correction and Data Quality Control." In *Eddy Covariance: A Practical Guide to Measurement and Data Analysis*, edited by Aubinet, M., T. Vesala, and D. Papale, 85–131. New York: Springer.
- Foken, T., M. Göckede, M. Mauder, L. Mahrt, B. Amiro, and W. Munger. 2004. "Post-Field Data Quality Control." In *Handbook of Micrometeorology: A Guide for Surface Flux Measurement and Analysis*, edited by Lee, X., W. Massman, and B. Law, 181–208. Dordrecht: Kluwer Academic Publishers.
- Geankoplis, C.J. 1993. *Transportation Processes and Unit Operation, 3rd edition*. New Jersey: PTR Prentice Hall.
- Horst, T.W. and D.H. Lenschow. 2009. "Attenuation of scalar fluxes measured with spatially-displaced sensors." *Boundary-Layer Meteorology* 130: 275–300.

- Kaimal, J.C., S.F. Clifford, and R.J. Lataitis. 1989. "Effect of finite sampling on atmospheric spectra." *Boundary-Layer Meteorology* 7: 827–837.
- Kljun, N., P. Calanca, M.W. Rotach, and H.P. Schmid. 2004. "A simple parameterization for flux footprint predictions." *Advances in Water Resources* 23: 765–772.
- Kormann, R. and F.X. Meixner. 2001. "Analytical footprint model for non-neutral stratification." *Boundary-Layer Meteorology* 99: 207–224.
- Moncrieff, J.B., J.M. Massheder, H. de Bruin, J.A. Elbers, T. Friberg, B. Heusinkveld, P. Kabat, S. Scott, H. Soegaard, and A. Verhoef. 1997. "A system to measure surface fluxes of momentum, sensible heat, water vapour and carbon dioxide." *Journal of Hydrology* 188-189: 589–611.
- Massman, W.J. 2000. "A simple method for estimating frequency response corrections for eddy covariance systems." *Agricultural Forest Meteorology* 104: 185–198.
- Montgomery, R.B. 1947. "Viscosity and thermal conductivity of air and diffusivity of water vapor in air." *Journal of the Atmospheric Sciences* 4: 193–196.
- Moore, C.J. 1986. "Frequency response corrections for eddy correlation systems." *Boundary-Layer Meteorology* 37: 17–35.
- Schotanus, P.S., F.T.M. Nieuwstadt, and H.A.R. de Bruin. 1983. "Temperature measurement with a sonic anemometer and its application to heat and moisture flux." *Boundary-Layer Meteorology* 26: 81–93.
- Shapland, T.M., R.L. Snyder, K.T. Paw U, and A.J. McElrone. 2014. "Thermocouple frequency response compensation leads to convergence of the surface renewal alpha calibration." *Agricultural and Forest Meteorology* 189-190: 36–47.
- Tanner, C.B. and G.W. Thurtell. 1969. "Anemoclinometer measurements of Reynolds stress and heat transport in the atmospheric surface layer science lab." *US Army Electronics Command Atmospheric Sciences Laboratory TR ECOM 66-G22-F: R1–R10*.
- van Dijk, A. 2002a. "Extension of 3D of 'The effect of linear averaging on scalar flux measurements with a sonic anemometer near the surface' by Kristensen and Fitzjarrald." *Journal of Atmospheric and Oceanic Technology* 19: 80–82.
- van Dijk, A. 2002b. "The Principle of Surface Flux Physics." Research Group of the Royal Netherlands Meteorological Institute and Department of Meteorology and Air Quality with Agricultural University Wageningen.
- Webb, E.K., G.I. Pearman, and R. Leuning. 1980. "Correction of flux measurements for density effects due to heat and water transfer." *Quarterly Journal of the Royal Meteorological Society* 106: 85–100.

Wilczak, J.M., S.P. Oncley, and S.A. Stage. 2001. "Sonic anemometer tilt correction algorithm."
Boundary-Layer Meteorology 99: 127–150.

Appendix A. Vapor pressure and dew point temperature

Infrared gas analyzers (IRGAs) require an occasional span (in other words, field calibration) of water vapor. When doing a span, the humidity of the span gas must be known and entered using the **On Site Zero & Span** menu on the data logger keypad (alternatively, it should be entered into *ECMon*, the IRGA user interface software). Although this humidity may be expressed in various units, dew point temperature is used since the H₂O span gas is typically generated with a dew point generator. Because dew point temperature is used, it is sometimes desirable to convert the water vapor density measurements of the IRGA to dew point temperature, especially as it provides comparability with the span gas before and after the span. Accordingly, the program converts water vapor density to dew point temperature using the algorithms described in this appendix.

A.1 Equations to calculate dew point temperature from water vapor density

An eddy-covariance system measures and reports water vapor density (ρ_w in g·m⁻³), air temperature (T in °C), and total atmospheric pressure (P in kPa). Using the ideal gas equation, vapor pressure (e in kPa) can be calculated using:

$$e = \rho_w R_v (T + 273.15) \quad (1)$$

where:

R_v is the gas constant for water vapor (4.61495·10⁻⁴ kPa·m³·K⁻¹·g⁻¹).

In this equation, if e were saturation water vapor pressure (e_s in kPa), T would be dew point temperature (T_d). However, since the air is unlikely to be saturated, other equations are needed to estimate the dew point temperature.

Buck (1981) developed equations to relate saturation water vapor pressure to dew point temperature in moist air. The equations were designed to be easily implemented in a computer program for conversion of saturation water vapor pressure to dew point temperature, or vice versa. The general model of equations was:

$$e_s = f_w(T_d, P) e_{ws}(T_d) \quad (2)$$

where:

e_s is saturation vapor pressure, and $e_{ws}(T_d)$ is saturation vapor pressure of pure water at pressure of the sea level, given by:

$$e_{ws} = a \exp\left(\frac{bT_d}{T_d + c}\right) \quad (3)$$

where:

a , b , and c are parameters, and $f_w(T_d, P)$ is the enhancement factor that is the ratio of vapor pressure of moist air to that of pure water vapor, given by:

$$f_w(T_d, P) = \frac{e_s}{e_{ws}} = A + P[B + C(T_d + D + EP)^2] \quad (4)$$

where:

A , B , C , D , and E are parameters. In Buck (1981), Figure 1 and Table 2 show results for $e_{ws}(T_d)$ from Model 3, and Buck (1981) Figure 3 and Table 3 show results for $f_w(T_d, P)$ from Model 4. Combining the saturation water vapor pressure equation, which has an error of ± 0.05 percent in a temperature range of -40 to $+50$ °C and within a normal range of surface layer pressures, with the enhancement factor, which has an equivalent error of ± 0.05 percent in the same temperature range, generates the following water vapor pressure equation for moist air:

$$e_s(T_d, P) = \begin{cases} 0.61121 \exp\left(\frac{17.368T_d}{T_d + 238.88}\right) f_w(T_d, P) & T_d \geq 0 \\ 0.61121 \exp\left(\frac{17.966T_d}{T_d + 247.15}\right) f_w(T_d, P) & T_d < 0 \end{cases} \quad (5)$$

where:

$$f_w(T_d, P) = 1.00041 + P[3.48 \times 10^{-5} + 7.4 \times 10^{-9}(T_d + 30.6 - 0.38P)^2] \quad (6)$$

Given measured water vapor pressure and total pressure from an eddy-covariance system, the only unknown variable in Eq. (5) and Eq. (6) is dew point temperature. However, analytically solving the equations for T_d is not feasible, due to complications from the quadratic term in Eq. (6). Fortunately, the enhancement factor is a very weak function of T_d , which is why Buck (1981) recommended that "a rough approximation of T_d will serve nicely in calculating $f_w(T_d, P)$."

A question then emerges concerning what should be considered reasonable for a rough approximation. In the case that relative humidity is high, the air temperature measured by an eddy-covariance system may be close enough to be a rough estimation of T_d ; however, this may

be considered unreasonable in a numerical analysis sense because an error range is unknown. And when relative humidity is low, this approximation could differ from the true dew point temperature by more than 10 °C, making it even more unreasonable in terms of atmospheric physics. Thus, another approach was proposed by Buck (1981) for calculating a more accurate approximation of T_d , described below.

A.2 Approach to approximation of T_d for the enhancement factor

For general use, to calculate dew point temperature (T_{d_gu} where subscript gu indicates general use), Buck (1981) recommended the following equation:

$$e_s(T_{d_gu}, P) = 0.61121 \exp\left(\frac{17.502 T_{d_gu}}{T_{d_gu} + 240.97}\right) f_w(P) \quad (7)$$

where:

$$f_w(P) = 1.0007 + 3.46 \times 10^{-5} P \quad (8)$$

Unlike $f_w(T_d, P)$ in Eq. (5), $f_w(P)$ in Eq. (7) does not include a quadratic term of dew point temperature; rather, T_{d_gu} can be analytically expressed in terms of saturation water pressure and total pressure as:

$$T_{d_gu} = \frac{240.97 \{ \ln e_s - \ln [0.61121 f_w(P)] \}}{17.502 - \{ \ln e_s - \ln [0.61121 f_w(P)] \}} \quad (9)$$

Because in Eq. (7) the saturation water vapor equation for pure water has an error limit of ± 0.2 percent in a temperature range of -20 to $+50$ °C and a normal range of surface-layer pressures (Buck 1981, Figure 1 and Table 1), and because the enhancement factor also has an error limit of ± 0.2 percent in a temperature range of -40 to $+50$ °C (Buck 1981, Figure 3 and Table 3), the dew point temperature for general use (T_{d_gu}) as calculated using Eq. (9) has a known error limit and can be considered a relatively accurate approximation for T_d in Eq. (6).

A.3 Dew point temperature equation

Now that a good approximation for T_d is found, T_{d_gu} from Eq. (9) may be substituted for T_d into Eq. (6). The resulting enhancement factor can then be used along with measured water vapor pressure and total pressure to give a more accurate dew point temperature (T_d), given by:

$$T_d = \begin{cases} \frac{238.88 \left\{ \ln e_s - \ln [0.61121 f_w(T_{d_gu}, P)] \right\}}{17.368 - \left\{ \ln e_s - \ln [0.61121 f_w(T_{d_gu}, P)] \right\}} & T_{d_gu} \geq 0 \\ \frac{247.15 \left\{ \ln e_s - \ln [0.61121 f_w(T_{d_gu}, P)] \right\}}{17.966 - \left\{ \ln e_s - \ln [0.61121 f_w(T_{d_gu}, P)] \right\}} & T_{d_gu} < 0 \end{cases} \quad (10)$$

Note that in this equation, the variable T_{d_gu} , instead of T_d in Eq. (5), is used to judge the boundary for use of two sub-equations, although using either variable for the boundary should yield nearly the same result since T_d and T_{d_gu} should be within 0.1 °C of each other if the magnitude of dew point temperature is less than 50 °C (Buck 1981). Furthermore, the two sub-equations in Eq. (5) have the same accuracy around 0 °C dew point temperature for a range of -1 to +1 °C (Buck 1981, Figure 1) and are effectively interchangeable from -1 to +1 °C. Because the two sub-equations in Eq. (10) are simply rearrangements of the two sub-equations in Eq. (5), respectively, the two sub-equations in Eq. (10) must also be interchangeable from -1 to +1 °C.

A.4 Online flux program

The data logger program calculates T_d by first converting measured water vapor density to water vapor pressure (e) (Eq. [1]). Because dew point temperature is the temperature at which e becomes saturated vapor pressure (e_s), we use the value of e from the IRGA in place of e_s in Eq. (10).

A.5 Reference

Buck, A.L. 1981. "New equations for computing vapor pressure and enhancement factor." *Journal of Applied Meteorology* 20: 1527–1532.

Appendix B. Coordinate rotations: Double rotation method

The covariance of vertical wind with a scalar (for example, heat, water vapor, or CO₂) yields a scalar flux. The covariance of vertical wind with horizontal wind along with air density gives momentum flux. If the measured vertical wind is not truly normal to the surface of interest, the flux estimates are in error (Kaimal and Haugen 1969).

Flow velocities measured by a three-dimensional (3D) anemometer are defined in an instrument coordinate system. Although the instrument coordinate system is defined accurately in the manufacturing process by precision machining, and field mounting may be done carefully to align the sensor vertical axis (z_m -axis) to be perpendicular to the field surface, it is almost impossible for the z_m -axis to be aligned perfectly. Some degree of leveling errors will be present, and surface undulation may occur. Tilts of the order of a degree could cause errors in excess of 100 percent for momentum flux (Kraus 1968).

Kaimal and Haugen (1969) further confirmed that large errors can occur in the measurement of momentum flux unless the sensors are vertically aligned and horizontally leveled with great accuracy (at least $\pm 0.1^\circ$). The errors caused by tilt in estimates of flux can be corrected using the mathematical method of coordinate transformations based on the physical process of turbulent flows (that is, the mean vertical velocity of dry air is zero).

B.1 Matrix transformation of instrument to flow coordinate system

Let us define a 3D right-handed orthogonal instrument coordinate system where u_m , v_m , and w_m are the orthogonal components of the 3D wind vector reported by the sonic anemometer. Now suppose that it is more convenient to report the same vector but use components of another orthogonal coordinate system that we will call the flow coordinate system, where the u -axis is parallel to the mean wind vector over some period (namely, the streamwise vector), v is the mean crosswind component, and w is the vertical component. This is possible using the matrix transformation presented in Eq. (11).

This transformation performs the following functions: (1) the instrument coordinate system is rotated about the w_m -axis by a counterclockwise angle (γ) as viewed against the w_m direction to the first rotated coordinate system, and if components are reported at this intermediary stage, u_1 , v_1 , and w_1 are used, where subscript 1 indicates the value of variable after the first rotation; (2) the coordinate system is rotated about the v_1 -axis by a counterclockwise angle (α) as viewed down the v_1 -axis, which results in the second rotated system where u_2 , v_2 , and w_2 are the components of the wind vector after the second rotation; and (3) the second rotated system is rotated about the u_2 -axis by a counterclockwise angle (β) as viewed against the u_2 -axis, resulting in the final flow coordinate system (u , v , w).

NOTE:

The angle rotations from the instrument coordinate system to the natural flow coordinate system are used inconsistently in the literature. Tanner and Thurtell (1969) used counterclockwise rotations about vertical and streamwise axes and clockwise rotation about a lateral axis. Wilczak, Oncley, and Stage (2001) used clockwise rotations for all three axes. The online flux program uses the rotation convention of Wilczak, Oncley, and Stage (2001) regardless of whether the double rotation or the planar fit method is used.

$$\begin{aligned} \begin{pmatrix} u \\ v \\ w \end{pmatrix} &= \begin{pmatrix} 1 & 0 & 0 \\ 0 & \cos \beta & \sin \beta \\ 0 & -\sin \beta & \cos \beta \end{pmatrix} \begin{pmatrix} \cos \alpha & 0 & -\sin \alpha \\ 0 & 1 & 0 \\ \sin \alpha & 0 & \cos \alpha \end{pmatrix} \begin{pmatrix} \cos \gamma & \sin \gamma & 0 \\ -\sin \gamma & \cos \gamma & 0 \\ 0 & 0 & 1 \end{pmatrix} \begin{pmatrix} u_m \\ v_m \\ w_m \end{pmatrix} \\ &= \mathbf{U}(\beta)\mathbf{V}(\alpha)\mathbf{W}(\gamma) \begin{pmatrix} u_m \\ v_m \\ w_m \end{pmatrix} = \mathbf{U}(\beta)\mathbf{V}(\alpha) \begin{pmatrix} u_1 \\ v_1 \\ w_1 \end{pmatrix} = \mathbf{U}(\beta) \begin{pmatrix} u_2 \\ v_2 \\ w_2 \end{pmatrix} \end{aligned} \tag{11}$$

where $\mathbf{U}(\beta)$, $\mathbf{V}(\alpha)$, and $\mathbf{W}(\gamma)$ are the three 3×3 matrices shown in the first part of Eq. (11). The rotations are performed sequentially as shown in the second part of Eq. (11). The second and third rotation angles are defined with respect to the coordinates after the preceding rotation.

B.2 Natural wind coordinate system

A 3D right-handed natural wind coordinate system has the u -axis parallel to the mean or streamwise flow; thus, the mean wind components along v -axis (\overline{v}) and w -axis (\overline{w}) are zero, as shown in Figure B-1 (p. 85).

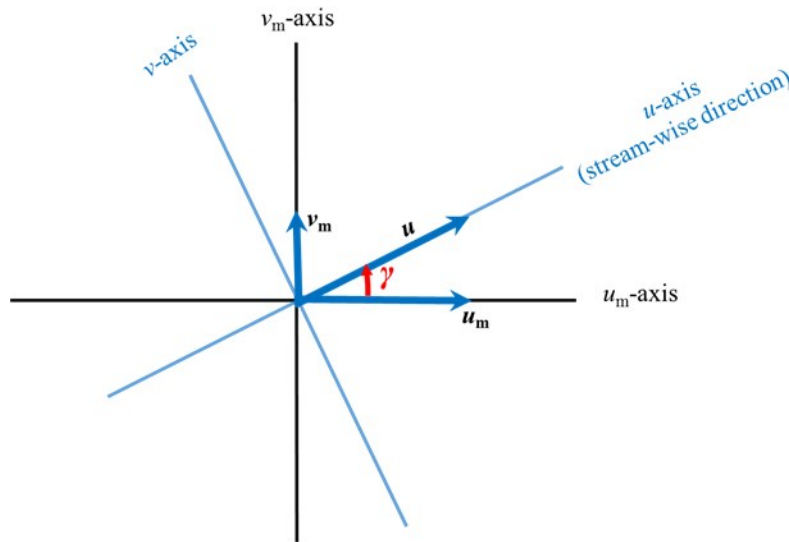


Figure B-1. As viewed down the z_m -axis and z -axis, and assuming the vertical wind component is zero, horizontal wind components v_m and u_m are measured in the instrument coordinate system and then rotated by angle γ , yielding the streamwise wind velocity vector (u). The u -axis and v -axis of the flow coordinate system are also shown.

Because velocity in the v direction (orthogonal to u direction) is zero and flow is horizontally homogenous, the tilt in the v direction causes less error than in the u direction. Additionally, the calculation of the third rotation angle assumes the following:

$$\overline{w_2' v_2'} = 0 \quad (12)$$

which may not necessarily be true in field conditions and introduces more uncertainties; therefore, the third rotation is not recommended (Wilczak, Oncley, and Stage 2001). The algorithm for the first two rotations is given as follows.

Angle γ in Figure B-1 (p. 85) can be approximated by:

$$\gamma = \arctan \left(\frac{\overline{v_m}}{\overline{u_m}} \right) \quad (13)$$

This angle is the mean wind direction of 0 to 360° that is output from the CRBasic instruction of **WindVector** used in the data logger. The counterclockwise angle α around the v_1 -axis is given by:

$$\alpha = -\arctan \frac{\overline{w_1}}{\overline{u_1}} = -\arctan \frac{\overline{w_m}}{\overline{u_m} \cos \gamma + \overline{v_m} \sin \gamma} \quad (14)$$

The CRBasic function [ATN2\(\)](#) is used to calculate Eq. (14) and return an angle in the range of $\pm 180^\circ$. The result, however, must be further constrained to the range of $\pm 90^\circ$ since, relative to γ , the range of this angle is narrower and should be within $\pm 90^\circ$.

According to Eq. (11), the first two rotations are expressed as:

$$\begin{bmatrix} u_2 \\ v_2 \\ w_2 \end{bmatrix} = \begin{bmatrix} \cos \alpha \cos \gamma & \cos \alpha \sin \gamma & -\sin \alpha \\ -\sin \gamma & \cos \gamma & 0 \\ \sin \alpha \cos \gamma & \sin \alpha \sin \gamma & \cos \alpha \end{bmatrix} \begin{bmatrix} u_m \\ v_m \\ w_m \end{bmatrix} = \mathbf{R}_2 \begin{bmatrix} u_m \\ v_m \\ w_m \end{bmatrix} \quad (15)$$

B.2.1 Covariance of momentum variables after coordinate rotation

Using matrix operations, the covariance of the momentum variables can be reasonably found via the process below.

From Eq. (15), the mean terms can be written as:

$$\begin{bmatrix} \bar{u}_2 \\ \bar{v}_2 \\ \bar{w}_2 \end{bmatrix} = \mathbf{R}_2 \begin{bmatrix} \bar{u}_m \\ \bar{v}_m \\ \bar{w}_m \end{bmatrix} = \begin{bmatrix} \cos \alpha (\bar{u}_m \cos \gamma + \bar{v}_m \sin \gamma) - \bar{w}_m \sin \alpha \\ 0 \\ \sin \alpha (\bar{u}_m \cos \gamma + \bar{v}_m \sin \gamma) + \bar{w}_m \cos \alpha \end{bmatrix} \quad (16)$$

and the fluctuation terms can be written as:

$$\begin{bmatrix} u'_2 \\ v'_2 \\ w'_2 \end{bmatrix} = \mathbf{R}_2 \begin{bmatrix} u'_m \\ v'_m \\ w'_m \end{bmatrix} \quad (17)$$

Self-multiplication generates:

$$\begin{bmatrix} u'_2 \\ v'_2 \\ w'_2 \end{bmatrix} \begin{bmatrix} u'_2 & v'_2 & w'_2 \end{bmatrix} = \mathbf{R}_2 \begin{bmatrix} u'_m \\ v'_m \\ w'_m \end{bmatrix} \begin{bmatrix} u'_m & v'_m & w'_m \end{bmatrix} \mathbf{R}_2^T \quad (18)$$

Applying Reynolds averaging yields:

$$\begin{bmatrix} \overline{u_2'^2} & \overline{u_2'v_2'} & \overline{u_2'w_2'} \\ \overline{u_2'v_2'} & \overline{v_2'^2} & \overline{v_2'w_2'} \\ \overline{u_2'w_2'} & \overline{v_2'w_2'} & \overline{w_2'^2} \end{bmatrix} = \mathbf{R}_2 \begin{bmatrix} \overline{u_m'^2} & \overline{u_m'v_m'} & \overline{u_m'w_m'} \\ \overline{u_m'v_m'} & \overline{v_m'^2} & \overline{v_m'w_m'} \\ \overline{u_m'w_m'} & \overline{v_m'w_m'} & \overline{w_m'^2} \end{bmatrix} \mathbf{R}_2^T \quad (19)$$

See [Extended equations](#) (p. 87) for the expansion of these matrix operations for CRBasic coding.

B.2.2 Covariance of a scalar variable and momentum variable after second coordinate rotation

The covariance of a scalar variable (Q) and each rotated wind variable is found by multiplying the fluctuation of the scalar (Q') to Eq. (17), to give Eq. (20):

$$Q' \begin{bmatrix} u_2' \\ v_2' \\ w_2' \end{bmatrix} = \mathbf{R}_2 Q' \begin{bmatrix} u_m' \\ v_m' \\ w_m' \end{bmatrix} \quad (20)$$

Then, by applying Reynolds averaging:

$$\begin{bmatrix} \overline{Q'u_2'} \\ \overline{Q'v_2'} \\ \overline{Q'w_2'} \end{bmatrix} = \mathbf{R}_2 \begin{bmatrix} \overline{Q'u_m'} \\ \overline{Q'v_m'} \\ \overline{Q'w_m'} \end{bmatrix} = \begin{bmatrix} \cos \alpha \left(\overline{Q'u_m'} \cos \gamma + \overline{Q'v_m'} \sin \gamma \right) - \overline{Q'w_m'} \sin \alpha \\ -\overline{Q'u_m'} \sin \gamma + \overline{Q'v_m'} \cos \gamma \\ \sin \alpha \left(\overline{Q'u_m'} \cos \gamma + \overline{Q'v_m'} \sin \gamma \right) + \overline{Q'w_m'} \cos \alpha \end{bmatrix} \quad (21)$$

B.3 Extended equations

The extended form of Eq. (19) is given by:

$$\begin{bmatrix} \overline{u_2'^2} & \overline{u_2'v_2'} & \overline{u_2'w_2'} \\ \overline{u_2'v_2'} & \overline{v_2'^2} & \overline{v_2'w_2'} \\ \overline{u_2'w_2'} & \overline{v_2'w_2'} & \overline{w_2'^2} \end{bmatrix} = \begin{bmatrix} \cos \alpha \cos \gamma & \cos \alpha \sin \gamma & -\sin \alpha \\ -\sin \gamma & \cos \gamma & 0 \\ \sin \alpha \cos \gamma & \sin \alpha \sin \gamma & \cos \alpha \end{bmatrix} \begin{bmatrix} \overline{u_m'^2} & \overline{u_m'v_m'} & \overline{u_m'w_m'} \\ \overline{u_m'v_m'} & \overline{v_m'^2} & \overline{v_m'w_m'} \\ \overline{u_m'w_m'} & \overline{v_m'w_m'} & \overline{w_m'^2} \end{bmatrix} \begin{bmatrix} \cos \alpha \cos \gamma & -\sin \gamma & \sin \alpha \cos \gamma \\ \cos \alpha \sin \gamma & \cos \gamma & \sin \alpha \sin \gamma \\ -\sin \alpha & 0 & \cos \alpha \end{bmatrix} \quad (22)$$

In Eq. (22), the extended forms of variance terms in the matrix on the left-hand side are expressed in terms of the matrices on the right-hand side:

$$\overline{u_2'^2} = \cos^2 \alpha \left(\overline{u_m'^2} \cos^2 \gamma + \overline{v_m'^2} \sin^2 \gamma \right) + \overline{w_m'^2} \sin^2 \alpha + \overline{u_m'v_m'} \cos^2 \alpha \sin 2\gamma - \sin 2\alpha \left(\overline{u_m'w_m'} \cos \gamma + \overline{v_m'w_m'} \sin \gamma \right)$$

$$\overline{v_2'^2} = \overline{u_m'^2} \sin^2 \gamma + \overline{v_m'^2} \cos^2 \gamma - \overline{u_m'v_m'} \sin 2\gamma \quad (23)$$

$$\overline{w_2'^2} = \sin^2 \alpha \left(\overline{u_m'^2} \cos^2 \gamma + \overline{v_m'^2} \sin^2 \gamma \right) + \overline{w_m'^2} \cos^2 \alpha + \overline{u_m'v_m'} \sin^2 \alpha \sin 2\gamma + \sin 2\alpha \left(\overline{u_m'w_m'} \cos \gamma + \overline{v_m'w_m'} \sin \gamma \right)$$

In Eq. (22), the extended forms of covariance terms in the matrix on the left-hand side are expressed in terms of the matrices on the right-hand side:

$$\begin{aligned}\overline{u'_2 v'_2} &= -\frac{1}{2}(\overline{u_m'^2} - \overline{v_m'^2}) \cos \alpha \sin 2\gamma + \overline{u'_m v'_m} \cos \alpha \cos 2\gamma + \sin \alpha (\overline{u'_m w'_m} \sin \gamma - \overline{v'_m w'_m} \cos \gamma) \\ \overline{u'_2 w'_2} &= \frac{1}{2} \sin 2\alpha \left[(\overline{u_m'^2} \cos^2 \gamma + \overline{v_m'^2} \sin^2 \gamma) - \overline{w_m'^2} + \overline{u'_m v'_m} \sin 2\gamma \right] + \cos 2\alpha (\overline{u'_m w'_m} \cos \gamma + \overline{v'_m w'_m} \sin \gamma) \\ \overline{v'_2 w'_2} &= -\sin \alpha \left[\frac{1}{2}(\overline{u_m'^2} - \overline{v_m'^2}) \sin 2\gamma - \overline{u'_m v'_m} \cos 2\gamma \right] - \cos \alpha (\overline{u'_m w'_m} \sin \gamma - \overline{v'_m w'_m} \cos \gamma)\end{aligned}\quad (24)$$

B.4 References

- Kaimal, J.C. and D.A. Haugen. 1969. "Some errors in the measurement of Reynolds stress." *Journal of Applied Meteorology* 8: 460–462.
- Kraus, E.B. 1968. "What we do not know about the sea-surface wind stress." *Bulletin of the American Meteorological Society* 49: 247–253.
- Tanner, C.B. and G.W. Thurtell. 1969. "Anemoclinometer measurements of Reynolds stress and heat transport in the atmospheric surface layer science lab." *US Army Electronics Command Atmospheric Sciences Laboratory TR ECOM 66-G22-F: R1–R10*.
- Wilczak, J.M., S.P. Oncley, and S.A. Stage. 2001. "Sonic Anemometer tilt correction algorithm." *Boundary-Layer Meteorology* 99: 127–150.

Appendix C. Coordinate rotations: Planar fit method

C.1 Planar fit

The planar fit method of coordinate rotations is based on Wilczak, Oncley, and Stage (2001). The method is used to transform the measured wind velocities in the right-handed measurement coordinate system of a sonic anemometer (u_m, v_m, w_m), where subscript m indicates the measurement coordinate system, to the natural wind coordinate system (u, v, w) if the three rotations are performed.

The first and second rotations in the planar fit are related to flux; that is, both rotations transform the measured wind velocities to a coordinate system with the horizontal coordinate plane parallel to the natural wind plane. The algorithm used for planar fit rotations mathematically describes two counterclockwise coordinate rotations, the first about the u_m -axis by an angle β , and the second about the intermediate v_1 -axis by an angle α , where subscript 1 indicates the variable after the first rotation. The expression of measured fluxes in this coordinate system avoids the errors in fluxes due to the tilt of the sonic anemometer vertical axis away from the vertical axis of the natural wind flow coordinate system.

The angle α is the angle between the instrument u_m -axis and the u - v plane of natural wind (that is, the tilt angle of the instrument vertical w_m -axis away from the natural wind vertical axis in the instrument u_m - w_m plane), where α increases clockwise in the 360° domain, which means a clockwise rotation for angle α is positive, and a counterclockwise rotation is negative.

The angle β is the angle between the instrument v_m -axis and the u - v plane of natural wind (that is, the tilt angle of the instrument vertical w_m -axis away from the natural wind vertical axis in the instrument v_m - w_m plane), where β increases counterclockwise in the 360° domain, which means a clockwise rotation for angle β is negative, and a counterclockwise rotation is positive.

Even if the sonic anemometer is well secured and leveled in the field, wind may force the mounting structure and sonic anemometer to tilt, especially if the tower is tall (greater than 3 m, for example). The degree of the inclination depends on the momentum load determined mainly by wind speed. Furthermore, the natural u - v plane relative to a fixed plane varies if the field undulates and has a slope that varies from different directions.

Therefore, in a given field station, the two coordinate rotation angles should be defined as a function of wind direction and wind speed. However, determining the angles for every possible wind direction and speed is impractical; instead, the angles are defined for certain sectors of wind direction using data averaged over a time interval (for example, 30 min), and the dependence on wind speed is not considered.

For the online planar fit algorithm, four sectors or ranges of wind direction *in the instrument coordinate system* are used. The boundaries of sectors match the boundaries of sectors in “horizontal orientation of the sonic anemometer” for data quality classification by Foken et al. (2012). Using statistically sufficient data (Wilczak, Oncley, and Stage 2001, Models 37 to 48) from the four direction sectors, the user can calculate the two angles for the four sectors, respectively. The four ranges are given below, along with the angle names used in the program:

Sector 1: [0, 60] and [300, 360]

α_{60_300}

β_{60_300}

Sector 2: (60, 170]

α_{60_170}

β_{60_170}

Sector 3: (170, 190]

α_{170_190}

β_{170_190}

Sector 4: (190, 300)

α_{190_300}

β_{190_300}

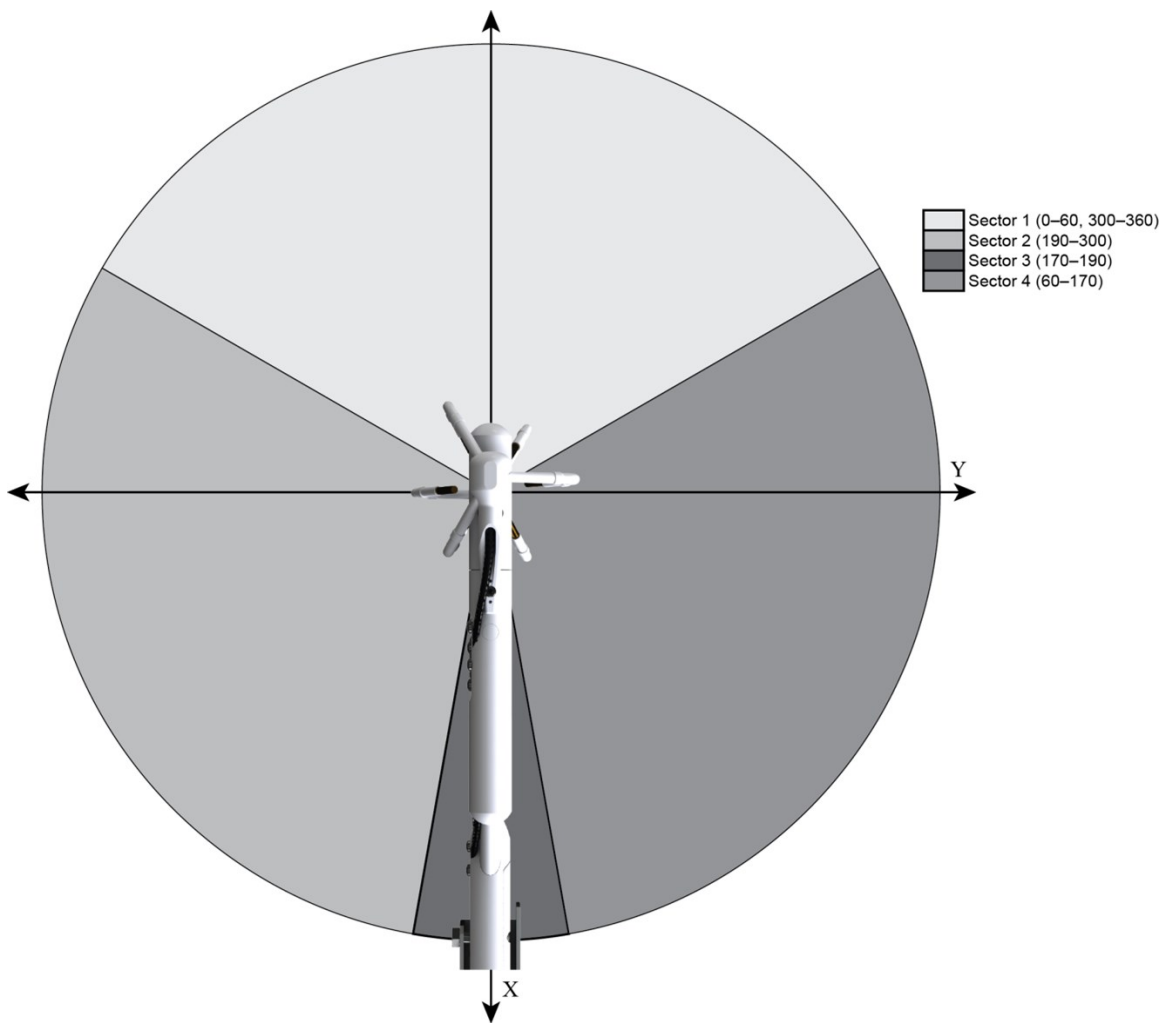


Figure C-1. Wind direction sectors for which planar fit angles are found by the user and entered into the program.

C.2 Algorithm

This section details the algorithms used for coordinate rotation corrections inside *EasyFlux DL CR6OP* or *CR1KXOP*.

C.2.1 Variables and model

To use the planar fit method, the user must independently (using post-processing software and time-series data for an appropriate length of time) determine the angles for each wind sector and enter these values with the data logger keypad (see [Enter site-specific variables with data logger keypad](#) or [LoggerNet](#) [p. 19]). The online flux program will then select the appropriate angles based on the mean wind direction during the averaging interval. The corresponding CRBasic code is as follows:

If (wind direction ≤ 60) OR (wind direction ≥ 300) then:

$$\alpha = \alpha_{60_300}$$

$$\beta = \beta_{60_300}$$

If ($60 < \text{wind direction} \leq 170$) then:

$$\alpha = \alpha_{60_170}$$

$$\beta = \beta_{60_170}$$

If ($170 < \text{wind direction} \leq 190$) then:

$$\alpha = \alpha_{170_190}$$

$$\beta = \beta_{170_190}$$

If ($190 < \text{wind direction} < 300$) then:

$$\alpha = \alpha_{190_300}$$

$$\beta = \beta_{190_300}$$

Given a pitch angle of α and a roll angle of β , the three orthogonal wind velocities (u, v, w) after the two rotations can be expressed in terms of the two angles (α, β) and three directly measured wind velocities (u_m, v_m, w_m) as:

$$\begin{bmatrix} u \\ v \\ w \end{bmatrix} = \begin{bmatrix} \cos \alpha & 0 & -\sin \alpha \\ 0 & 1 & 0 \\ \sin \alpha & 0 & \cos \alpha \end{bmatrix} \begin{bmatrix} 1 & 0 & 0 \\ 0 & \cos \beta & \sin \beta \\ 0 & -\sin \beta & \cos \beta \end{bmatrix} \begin{bmatrix} u_m \\ v_m \\ w_m \end{bmatrix} \quad (25)$$

Further:

$$\begin{bmatrix} u \\ v \\ w \end{bmatrix} = \begin{bmatrix} \cos \alpha & \sin \alpha \sin \beta & -\sin \alpha \cos \beta \\ 0 & \cos \beta & \sin \beta \\ \sin \alpha & -\cos \alpha \sin \beta & \cos \alpha \cos \beta \end{bmatrix} \begin{bmatrix} u_m \\ v_m \\ w_m \end{bmatrix} = \mathbf{R}_p \begin{bmatrix} u_m \\ v_m \\ w_m \end{bmatrix} \quad (26)$$

where \mathbf{R}_p is the 3×3 matrix in Eq. (26), and subscript p indicates the planar fit approach for the rotations.

C.2.2 Covariance of momentum variables after two coordinate rotations

Using matrix operations, the covariance of the momentum variables can be reasonably found as follows.

Using Eq. (26), we can express the mean terms as:

$$\begin{bmatrix} \overline{u} \\ \overline{v} \\ \overline{w} \end{bmatrix} = \mathbf{R}_p \begin{bmatrix} \overline{u}_m \\ \overline{v}_m \\ \overline{w}_m \end{bmatrix} = \begin{bmatrix} \overline{u}_m \cos \alpha + \sin \alpha (\overline{v}_m \sin \beta - \overline{w}_m \cos \beta) \\ \overline{v}_m \cos \beta + \overline{w}_m \sin \beta \\ \overline{u}_m \sin \alpha - \cos \alpha (\overline{v}_m \sin \beta - \overline{w}_m \cos \beta) \end{bmatrix} \quad (27)$$

and fluctuation terms as:

$$\begin{bmatrix} u' \\ v' \\ w' \end{bmatrix} = \mathbf{R}_p \begin{bmatrix} u'_m \\ v'_m \\ w'_m \end{bmatrix} \quad (28)$$

Self-multiplication generates:

$$\begin{bmatrix} u' \\ v' \\ w' \end{bmatrix} \begin{bmatrix} u' & v' & w' \end{bmatrix} = \mathbf{R}_p \begin{bmatrix} u'_m \\ v'_m \\ w'_m \end{bmatrix} \begin{bmatrix} u'_m & v'_m & w'_m \end{bmatrix} \mathbf{R}_p^T \quad (29)$$

Applying Reynolds averaging yields:

$$\begin{bmatrix} \overline{u'^2} & \overline{u'v'} & \overline{u'w'} \\ \overline{u'v'} & \overline{v'^2} & \overline{v'w'} \\ \overline{u'w'} & \overline{v'w'} & \overline{w'^2} \end{bmatrix} = \mathbf{R}_p \begin{bmatrix} \overline{u_m'^2} & \overline{u'_m v'_m} & \overline{u'_m w'_m} \\ \overline{u'_m v'_m} & \overline{v_m'^2} & \overline{v'_m w'_m} \\ \overline{u'_m w'_m} & \overline{v'_m w'_m} & \overline{w_m'^2} \end{bmatrix} \mathbf{R}_p^T \quad (30)$$

These matrix operations can then be expanded to be used in the online flux program. See [Extended equations](#) (p. 94) for the coding.

C.2.3 Covariance of a scalar variable with momentum variable after planar fit coordinate rotation

The covariance of a scalar variable (Q) and each rotated wind variable is found by multiplying the fluctuation of the scalar (Q') to Eq. (28):

$$Q' \begin{bmatrix} u' \\ v' \\ w' \end{bmatrix} = \mathbf{R}_p Q' \begin{bmatrix} u'_m \\ v'_m \\ w'_m \end{bmatrix} \quad (31)$$

Applying Reynolds averaging yields:

$$\begin{bmatrix} \overline{Q'u'} \\ \overline{Q'v'} \\ \overline{Q'w'} \end{bmatrix} = \mathbf{R}_p \begin{bmatrix} \overline{Q'u'_m} \\ \overline{Q'v'_m} \\ \overline{Q'w'_m} \end{bmatrix} = \begin{bmatrix} \overline{Q'u'_m} \cos \alpha + \sin \alpha \left(\overline{Q'v'_m} \sin \beta - \overline{Q'w'_m} \cos \beta \right) \\ \overline{Q'v'_m} \cos \beta + \overline{Q'w'_m} \sin \beta \\ \overline{Q'u'_m} \sin \alpha - \cos \alpha \left(\overline{Q'v'_m} \sin \beta - \overline{Q'w'_m} \cos \beta \right) \end{bmatrix} \quad (32)$$

C.3 Extended equations

The extended form of Eq. (30) is given by:

$$\begin{bmatrix} \overline{u'^2} & \overline{u'v'} & \overline{u'w'} \\ \overline{u'v'} & \overline{v'^2} & \overline{v'w'} \\ \overline{u'w'} & \overline{v'w'} & \overline{w'^2} \end{bmatrix} = \begin{bmatrix} \cos \alpha & \sin \alpha \sin \beta & -\sin \alpha \cos \beta \\ 0 & \cos \beta & \sin \beta \\ \sin \alpha & -\cos \alpha \sin \beta & \cos \alpha \cos \beta \end{bmatrix} \begin{bmatrix} \overline{u_m'^2} & \overline{u'_m v'_m} & \overline{u'_m w'_m} \\ \overline{u'_m v'_m} & \overline{v_m'^2} & \overline{v'_m w'_m} \\ \overline{u'_m w'_m} & \overline{v'_m w'_m} & \overline{w_m'^2} \end{bmatrix} \begin{bmatrix} \cos \alpha & 0 & \sin \alpha \\ \sin \alpha \sin \beta & \cos \beta & -\cos \alpha \sin \beta \\ -\sin \alpha \cos \beta & \sin \beta & \cos \alpha \cos \beta \end{bmatrix} \quad (33)$$

In Eq. (33), the extended forms of variance terms in the matrix on the left-hand side are expressed in terms of the matrices on the right-hand side:

$$\begin{aligned} \overline{u'^2} &= \overline{u_m'^2} \cos^2 \alpha + \sin^2 \alpha \left(\overline{v_m'^2} \sin^2 \beta - \overline{v'_m w'_m} \sin 2\beta + \overline{w_m'^2} \cos^2 \beta \right) + \sin 2\alpha \left(\overline{u'_m v'_m} \sin \beta - \overline{u'_m w'_m} \cos \beta \right) \\ \overline{v'^2} &= \overline{v_m'^2} \cos^2 \beta + \overline{v'_m w'_m} \sin 2\beta + \overline{w_m'^2} \sin^2 \beta \\ \overline{w'^2} &= \overline{u_m'^2} \sin^2 \alpha + \cos^2 \alpha \left(\overline{v_m'^2} \sin^2 \beta - \overline{v'_m w'_m} \sin 2\beta + \overline{w_m'^2} \cos^2 \beta \right) - \sin 2\alpha \left(\overline{u'_m v'_m} \sin \beta - \overline{u'_m w'_m} \cos \beta \right) \end{aligned} \quad (34)$$

In Eq. (33), the extended forms of covariance terms in the matrix on the left-hand side are expressed in terms of the matrices on the right-hand side:

$$\begin{aligned}\overline{u'v'} &= \sin \alpha \left[\frac{1}{2} (\overline{v_m'^2} - \overline{w_m'^2}) \sin 2\beta - \overline{v_m'w_m'} \cos 2\beta \right] + \cos \alpha (\overline{u_m'v_m'} \cos \beta + \overline{u_m'w_m'} \sin \beta) \\ \overline{u'w'} &= \frac{1}{2} \sin 2\alpha (\overline{u_m'^2} - \overline{v_m'^2} \sin^2 \beta - \overline{w_m'^2} \cos^2 \beta + \overline{v_m'w_m'} \sin 2\beta) - \cos 2\alpha (\overline{u_m'v_m'} \sin \beta - \overline{u_m'w_m'} \cos \beta) \\ \overline{v'w'} &= -\cos \alpha \left[\frac{1}{2} (\overline{v_m'^2} - \overline{w_m'^2}) \sin 2\beta - \overline{v_m'w_m'} \cos 2\beta \right] + \sin \alpha (\overline{u_m'v_m'} \cos \beta + \overline{u_m'w_m'} \sin \beta)\end{aligned}\quad (35)$$

C.4 References

- Foken, T., R. Leuning, S.R. Oncley, M. Mauder, and M. Aubinet. 2012. "Correction and Data Quality Control." In *Eddy Covariance: A Practical Guide to Measurement and Data Analysis*, edited by Aubinet, M., T. Vesala, and D. Papale, 85–131. New York: Springer.
- Wilczak, J.M., S.P. Oncley, and S.A. Stage. 2001. "Sonic Anemometer tilt correction algorithm." *Boundary-Layer Meteorology* 99: 127–150.

Appendix D. Frequency corrections

D.1 Introduction

The flux of any scalar (namely, heat, CO₂, or H₂O) or momentum is a summed amount of the scalar or momentum through a unit area per unit time (for example, g·m⁻²·s⁻¹ for H₂O) and transported by eddies of various frequencies (such as various sizes and velocities). The relative contribution of flux as a function of eddy frequency results in a cospectrum for covariance. The total, or net, flux is found by integrating over this cospectrum. To generate an accurate cospectrum, a measurement system must be able to measure and process fluctuations at all frequencies that contribute to the flux.

In practice, however, sensor measurements and digital processing methods cannot fully capture the instantaneous changes at all frequencies. The uncaptured changes related to larger eddies result in low frequency losses, and the uncaptured changes related to smaller eddies result in high frequency losses. Accounting for these frequency losses requires the corrections described below.

D.2 Frequency loss

D.2.1 High frequency loss

High frequency loss is caused by sensor response delay, signal averaging over the measurement path or volume (line/volume averaging), sensor separation, and low-pass filtering. A brief description of each of these causes is provided below.

Sensor response delay

A sensor requires a finite amount of time to measure a stimulus. When fluctuations of a scalar or wind occur faster than this time, high frequency losses occur. The response delay is described using a time constant defined as the time the sensor requires to respond to a 63.2 percent change in the input stimulus.

Line/volume averaging

Most sensors measure the change in a variable of interest over a linear measurement path (CSAT3) or measurement volume (KH20) and report its spatially averaged value over that path or volume at the measurement time. Such a sensor cannot accurately report a change in the

variable at a scale of eddies smaller than the dimension of the path or volume, which attenuates the signal at high frequencies.

Sensor separation

A covariance of wind velocity with CO₂ or H₂O concentration is measured using two sensors: a sonic anemometer and an infrared gas analyzer (IRGA). In most two-sensor combinations (except for the IRGASON, which integrates both sensors into a single head), the wind velocities and gas concentrations are measured separately in different measurement volumes. This means that a single eddy may be measured at different times by the two sensors when the eddy dimension is smaller than the separation, or when a large eddy boundary moves between the two sensors during measurement. This results in signal attenuation at high frequencies because the cross correlation of wind velocities to scalar variable decreases with increases in separation (Kaimal and Finnigan 1994, 289).

Another example of two separated sensors is the use of a sonic anemometer and a fine-wire thermocouple (for example, FW05, FW1, and FW3) for sensible heat flux to measure covariance of wind velocity with air temperature.

Low-pass filtering

A low-pass filter of Finite Impulse Response (FIR) improves the data quality for spectral analysis by removing the aliasing effect on the frequency passband due to signals at higher frequencies (namely, frequency stopband) but sharply attenuates the signal beyond the user-selected bandwidth (namely, frequency passband; Campbell Scientific 2014, 43). This attenuation helps reduce an unwanted aliasing effect on the frequency passband, but it may also result in the loss of high frequency fluxes depending on the sampling rate and frequency passband.

NOTE:

The EC100 electronics used with the IRGASON and the EC150/CSAT3A has four options for bandwidth (namely, passband): 5, 10, 12.5, or 20 Hz. For each option, the filter attenuates the signals at frequencies beyond the bandwidth.

D.2.2 Low frequency loss

Fluxes are typically calculated by taking a block average of the covariance and other related variables over an interval of 30 minutes or longer. The block averaging is a high-pass filter, which causes low frequency loss (Kaimal, Clifford, and Lataitis 1989).

D.3 Model for frequency loss corrections

The frequency loss of covariance is determined by the frequency losses of each variable from which the covariance is calculated. The correction for this loss is described using a general

correction model for covariance of any two variables.

Suppose the measured covariance is given by:

$$\overline{(\alpha' w')}_r \quad (36)$$

where α can represent T for temperature ($^{\circ}\text{C}$), ρ_{CO_2} for partial CO_2 density ($\text{mg}\cdot\text{m}^{-3}$), $\rho_{\text{H}_2\text{O}}$ for partial H_2O density ($\text{g}\cdot\text{m}^{-3}$), or u (or v) for horizontal wind speed ($\text{m}\cdot\text{s}^{-1}$); w is vertical wind speed ($\text{m}\cdot\text{s}^{-1}$); prime is the departure of a variable from its mean; over-bar denotes the block time average; and subscript r represents a variable after coordinate rotation correction. Then, the frequency-corrected covariance is given by:

$$\overline{(\alpha' w')}_{rf} \quad (37)$$

where subscript f indicates a variable after frequency correction and is defined as (Moore 1986, Eq. 1):

$$\overline{(\alpha' w')}_{rf} = \overline{(\alpha' w')}_r \left\{ \frac{\int_0^{\infty} C_{\alpha w}(f) df}{\int_0^{\infty} T_{\alpha w}(f) C_{\alpha w}(f) df} \right\} \quad (38)$$

where other variables are defined as follows:

f – cyclic frequency.

$C_{\alpha w}(f)$ – cospectrum of α with w , which is the distribution of covariance of α and w as a function of frequency.

$T_{\alpha w}(f)$ – transfer function, defined as the relative response to a measured signal of wind or scalar at f , ranging from 0 for no response to 1 for full response. The transfer function here is the total transfer function that is the combined system response of all sensors and digital processors to report the signals of covariance of α with w . It is a product of all sub-transfer functions. See [Sub-transfer functions](#) (p. 108).

The term in the braces is defined as a frequency correction factor. Evaluating this factor requires determination of the total transfer function and the cospectrum within the integration. The total transfer function is a multiplication of sub-transfer functions. See [Sub-transfer functions](#) (p. 108).

A sub-transfer function is covariance-specific, depending on flow aerodynamics, sensor configuration, and data processing method. The cospectrum is also covariance-specific, depending on aerodynamic height, wind speed, and atmospheric stability in the surface layer. See [Surface layer atmospheric stability](#) (p. 103).

D.4 Covariance variables requiring frequency corrections

This section lists the covariance variables that require frequency corrections.

D.4.1 Momentum covariance

Rotated wind components (for example, u , v , and w) are derived from the sonic anemometer. The covariance of the following variables requires frequency correction: $\overline{(v'w')}$ and $\overline{(u'w')}$.

Note that both covariances are used for calculating friction velocity (a scaling parameter in the surface layer).

D.4.2 Sonic temperature related covariance

The following covariances are from measurements from the sonic anemometer and IRGA and require frequency correction: $\overline{(T_s'w')}$ and $\overline{(T_c'w')}$, where T_s is sonic temperature and T_c is air temperature calculated from sonic temperature, water vapor density, and pressure. The data logger program calculates sonic buoyancy flux $[\overline{(T_s'w')}]$ each half hour and then applies the sonic sensible heat flux (SND) correction to convert the result to buoyancy flux. The SND correction requires inputs such as the mean water vapor as measured by the IRGA and air density, which requires mean air temperature. The mean air temperature may come from the EC100 temperature probe in the case of the EC150/CSAT3A, or from T_c in the case of the IRGASON since the collocated measurements allow for time series calculation of T_c from T_s and water vapor density.

NOTE:

T_c is considered the most accurate because it does not suffer from solar heating or radiative cooling; however, T_c can only be calculated using an IRGASON, since the sonic temperature and water vapor density measurements must be made in the exact same volume. Pressure in the sample volume is also required, but it is assumed that the difference between the pressure in the sample volume and the pressure measured by the EC100 barometer is negligible.

D.4.3 Air temperature related covariance

Similar to sonic temperature, covariances from measurements of air temperature from a fine-wire thermocouple such as FW05, FW1, or FW3 (hereafter referred to as FW) should also be

corrected, such as $\overline{(T_{FW} w')_r}$, where T_{FW} is air temperature and subscript FW indicates a fine-wire thermocouple measurement.

D.4.4 CO₂ and H₂O related covariances

Covariances of CO₂ and H₂O (measured by the IRGA) with vertical wind (measured by the sonic anemometer) must be corrected, such as $\overline{(\rho'_{CO_2} w')_r}$, $\overline{(\rho'_{H_2O} w')_r}$, where ρ_{CO_2} is the mass density of CO₂, and ρ_{H_2O} is the mass density of H₂O.

D.5 Sensor configuration and separation variables

Sensor configuration variables, which are required for determining frequency corrections used in sub-transfer functions that lead to the overall transfer function in Model (38), are described in this section and include descriptors such as the measurement path dimensions of the sonic anemometer and gas analyzer, sensor separation between the sonic anemometer and gas analyzer, and the diameter of the fine-wire thermocouple.

These configuration variables are all set inside the program. Some of the variables, such as those dealing with sensor separation, depend on how the sensors are installed at a site; following installation, the variables should be measured, recorded, and entered into the program through the data logger keypad. See [Enter site-specific variables with data logger keypad or LoggerNet](#) (p. 19).

D.5.1 Path length variables

For the CSAT3A or IRGASON sonic anemometer, the path length (l_{pt_CSAT}) is equal to 0.11547 m. The subscript pt indicates path.

For the EC150 or IRGASON gas analyzer, the path length (l_{pt_IRGA}) is equal to 0.1531 m.

D.5.2 Separation variables

In order to find the separation variables, which are entered into the program through the data logger keypad (see [Enter site-specific variables with data logger keypad or LoggerNet](#) [p. 19]), the center of the gas analyzer measurement path relative to the sonic coordinate system (see [Figure D-1](#) [p. 101] and [Figure D-2](#) [p. 102]) must be known. Determine each of these variables as described below:

IRGA Coord x (reported as the data field *separation_x_irga* in the *Flux_Notes* output table) is the abscissa (x-coordinate) of the center of the gas analyzer optical path in the sonic coordinate

system. It should be set to 0 m for the IRGASON and ranges from 0.041 to 0.091 m for the EC150 and CSAT3A, depending on the position of the EC150 in its standard mounting bracket. When an EC150 and CSAT3A are used, the program assumes a default value of 0.041 m, which corresponds to the furthest forward position of the EC150 in its standard mounting bracket.

IRGA Coord y (reported as the data field *separation_y_irga* in the *Flux_Notes* output table) is the ordinate (*y*-coordinate) of the center of the gas analyzer optical path in the sonic coordinate system. It should be set to 0 m for the IRGASON and ranges from 0.029 to 0.033 m for the configuration of EC150 and CSAT3A, depending on the position of the EC150 in its standard mounting bracket. When an EC150 and CSAT3A are used, the program assumes a default value of 0.029 m, which corresponds to the furthest forward position of the EC150 in its standard mounting bracket.

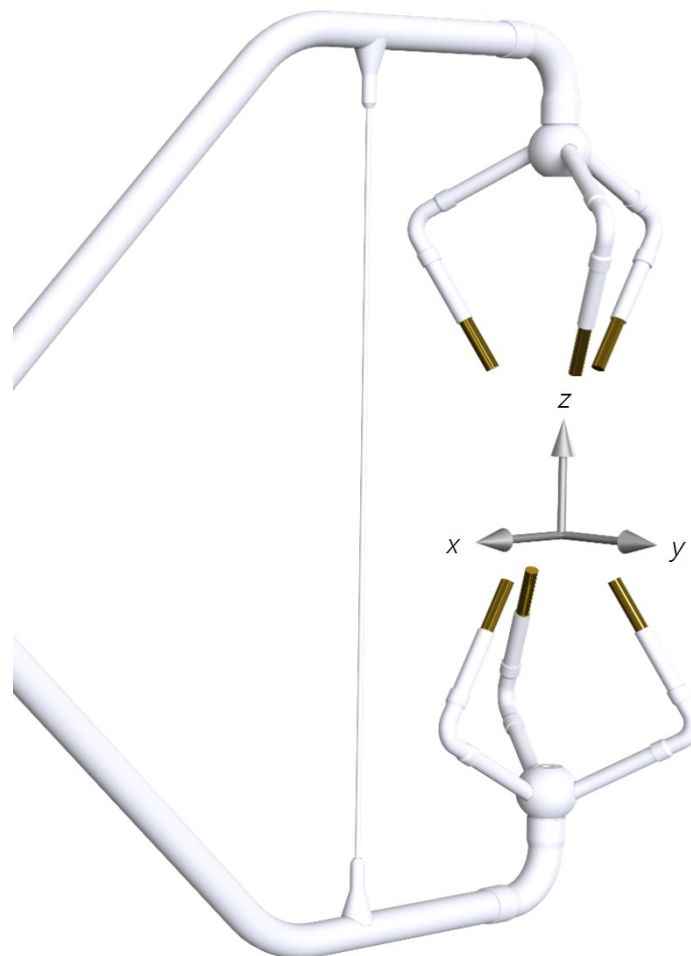


Figure D-1. The sonic coordinate system is shown with positive x-axis, y-axis, and z-axis. Note that the origin of the coordinate system should be exactly in the center of the sonic volume; as shown, the origin has been moved slightly downward for convenience in displaying the positive z-axis.

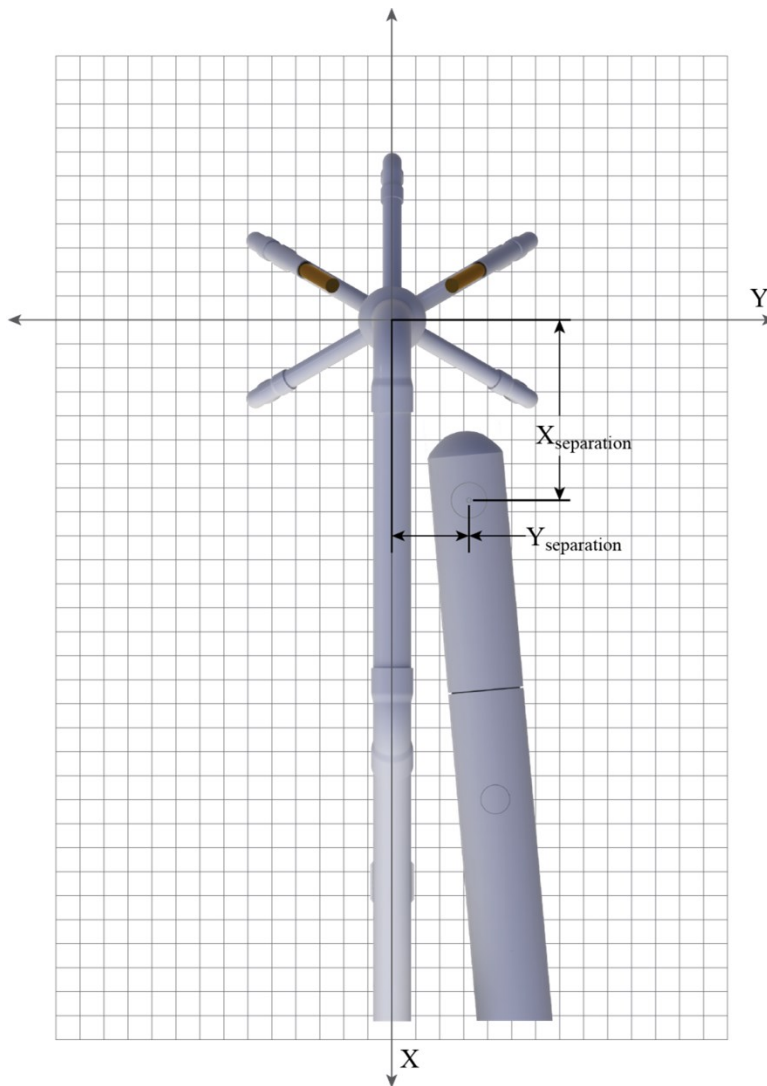


Figure D-2. The x and y spatial separations between a CSAT3A and EC150.

D.5.3 Fine-wire thermocouple

If a fine-wire thermocouple is used, additional configuration and separation variables must be entered into the program using the data logger keypad. See [Enter site-specific variables with data logger keypad or LoggerNet](#) (p. 19). These variables are described below.

Configuration variable FW Dim

Depending on the fine-wire thermocouple model being used, one of the following constants should be selected as the value for *FW Dim*, the configuration variable for dimension or diameter of the fine wire:

$FW05_DIA = 1.27 \times 10^{-5}$ m for the diameter of the FW05

$FW1_DIA = 2.54 \times 10^{-5}$ m for the diameter of the FW1

$FW3_DIA = 7.62 \times 10^{-5}$ m for the diameter of the FW3

Separation variables

FW Coord x (reported as the datafield *separation_x_FW* in the Flux_Notes output table) is the abscissa (*x*-coordinate) of the fine-wire thermocouple junction in the sonic coordinate system. See [Figure D-1](#) (p. 101) and [Figure D-2](#) (p. 102).

FW Coord y (reported as the datafield *separation_y_FW* in the Flux_Notes output table) is the ordinate (*y*-coordinate) of the fine-wire thermocouple junction in the sonic coordinate system.

The values for *FW Coord x* and *FW Coord y* are defaulted to 0.006 m and 0.03259 m, respectively, for the IRGASON and CSAT3A. These correspond to standard mounting and the lengths of the FW05, FW1, and FW3. These values may be easily edited at the site using the data logger keypad. See [Enter site-specific variables with data logger keypad or LoggerNet](#) (p. 19).

D.6 Surface layer atmospheric stability

The cospectrum in Model (38) depends on surface layer stability, which is defined as the ratio of aerodynamic height (*z*) to Monin-Obukhov length (*L*). This ratio is greater than 0 if the surface layer is stable, 0 if neutral, and less than 0 if unstable. The cospectrum has different model forms for neutral/unstable and stable conditions (Kaimal et al. 1972). Stability is used as a variable in the cospectrum model for stable conditions but not in the models for neutral or unstable conditions. The sub-sections below describe how the program calculates values for aerodynamic height and Monin-Obukhov length to determine stability. Stability during each averaging interval is reported in the *Flux_Notes* output table as *stability_zL*.

D.6.1 Aerodynamic height

Aerodynamic height is the measurement height (z_m) minus zero displacement height, given by:

$$z = z_m - d \quad (39)$$

where *d* is the zero displacement height.

1. *Measurement height* is the height of the center of the measurement volume of the eddy-covariance sensors above the surface of the ground. It is entered into the program as the variable *Meas Height* through the data logger keypad (see [Enter site-specific variables with data logger keypad or LoggerNet](#) [p. 19]) following installation and whenever the sensor height is adjusted. In the *Flux_Notes* output table, the last value to be entered is reported as *height_measurement*.
2. *Displacement height* is the mean height at which the momentum flux is balanced by the momentum absorption into rough surface elements (such as plants or ground surface). In the case of flat, bare land, the height of aerodynamic ground surface is effectively zero. Inside a canopy, the aerodynamic surface is elevated to some height above the ground surface. This elevated height is defined as the displacement height.

The displacement height (d) can be provided through three options:

- a. The user provides displacement height (d) and inputs it through the data logger keypad (see [Enter site-specific variables with data logger keypad or LoggerNet](#) [p. 19]); the last value to be entered is recorded as *displacement_user* in the *Flux_Notes* output table.
- b. For crop or grass canopy surface types, the user leaves displacement height variable (d) as zero; the displacement height is estimated in the program using Rosenberg, Blad, and Verma (1983, 138) Eq. 4.5 as follows:

$$d = 10^{0.979 \log_{10} h_c - 0.154} \quad (40)$$

where h_c is canopy height that is measured periodically by the user throughout the growing season and entered into the program with the data logger keypad (see [Enter site-specific variables with data logger keypad or LoggerNet](#) [p. 19]). It should be set to a constant in the non-growing season.

For surface types other than crop, grass, or forest, the 3/4 rule ($d = 3h_c / 4$) is an alternative (Kaimal and Finnigan 1994, 71).

- c. For a forest canopy surface type, eddy-covariance variables are measured using the 2/3 rule (Oke 1987, 116) in the program as:

$$d = 2h_c / 3 \quad (41)$$

In the program, whenever canopy height and surface type are re-entered (see [Enter site-specific variables with data logger keypad or LoggerNet](#) [p. 19]), the zero displacement height is recalculated (Eq. [40] and Eq. [41]) unless the user entered a specific value. Aerodynamic height (Eq. [39]) is also recalculated. In the *Flux_Notes* output table, the value for displacement height used during each averaging period is reported as d .

D.6.2 Monin-Obukhov length (L)

Monin-Obukhov length, as given by Rebmann et al. (2012), is an indication of surface layer depth, in which both shear and buoyancy drive the turbulent flows, generating turbulence kinetic energy. It is given by:

$$L = -\frac{u_*^3}{k \cdot (g_0 / \bar{T}_s) \cdot \left(\overline{w'T'_s} \right)_{rf}} \quad (42)$$

where:

k = von Karman constant (0.41)

g_0 = acceleration due to gravity at sea level (9.81 m·s⁻²)

\bar{T}_s = sonic temperature (K)

u_* = friction velocity (m·s⁻¹), given by (Stull 1988, 67; Wallace and Hobbs 2006, 384):

$$u_* = \left(\left(\overline{u'w'} \right)_{rf}^2 + \left(\overline{v'w'} \right)_{rf}^2 \right)^{\frac{1}{4}} \quad (43)$$

NOTE:

Recalculation of Monin-Obukhov length improves the accuracy of the frequency correction factor.

Monin-Obukhov length is used to determine the form of a cospectrum for a given covariance and as an independent variable in the cospectrum for stable conditions (see [Cospectra](#) [p. 106]; also see Kaimal et al. 1972). During initial operation of the program and in each calculation interval (for example, 30 min), the Monin-Obukhov length must be preliminarily estimated using uncorrected friction velocity and buoyancy flux. Based on this preliminary Monin-Obukhov length, the appropriate cospectra function [$C_{\alpha w}(f)$] (see Model [38]) can be identified and used for the calculation of correction factors to preliminarily correct the following three covariance variables: $\left(\overline{u'w'} \right)_r$, $\left(\overline{v'w'} \right)_r$, and $\left(\overline{w'T'} \right)_r$.

Thereafter, Monin-Obukhov length can be recalculated using these corrected covariance variables, which then requires the frequency correction factors to be recalculated, which can then be used to further correct the covariance values. This iterative calculation of Monin-Obukhov length, frequency correction factors, and covariance values is accomplished in the program using the [WhiTe\(\)](#)...[Wend\(\)](#) instructions and continues until the change in frequency correction factors is smaller than 0.0001 (Foken et al. 2012) or until ten iterations have completed. The final

Monin-Obukhov value is reported in the *Flux_Notes* output table as L , and the number of iterations performed is reported as *iteration_FreqFactor*.

NOTE:

For stable conditions, only the initial calculation of Monin-Obukhov length is required; recalculation is not needed because Monin-Obukhov length is not used in the equations for cospectra under stable conditions, and the sign of Monin-Obukhov does not change after recalculations of correction for covariance values used to calculate Monin-Obukhov length (see [Cospectra](#) [p. 106]).

D.7 Cospectra

This section contains mathematical descriptions of the cospectra functions used in Model (38) for various covariance variables in different stabilities.

D.7.1 Cospectra for $z/L > 0$ (stable surface layer)

For covariances $\overline{(u'w')}_r$ or $\overline{(v'w')}_r$, from Moore (1986, Eq. 21) and van Dijk (2002b, Eq. 2.80 and Table 2.1):

$$fS_{uw}(f) = \frac{\frac{z}{\bar{u}} f}{A_{uw} + B_{uw} \left(\frac{z}{\bar{u}} f \right)^{2.1}} \quad (44)$$

$$A_{uw} = 0.124 \left(1 + 7.9 \frac{z}{L} \right)^{0.75}$$

$$B_{uw} = 23.252 \left(1 + 7.9 \frac{z}{L} \right)^{-0.825}$$

where \bar{u} is the total mean velocity, or the mean horizontal velocity after rotation about the w -axis.

For covariances $\overline{(T'_s w')}_r$, $\overline{(T'_c w')}_r$, $\overline{(T'_{FW} w')}_r$, $\overline{(\rho'_{CO2} w')}_r$, and $\overline{(\rho'_{H2O} w')}_r$, from Moore (1986, Eq. 21), Moncrieff et al. (1997, Eqs. 12 and 13), and van Dijk (2002b, Eq. 2.80 and Table 2.1):

$$fS_{sw}(f) = \frac{\frac{z}{\bar{u}} f}{A_{sw} + B_{sw} \left(\frac{z}{\bar{u}} f \right)^{2.1}} \quad (45)$$

$$A_{sw} = 0.284 \left(1 + 6.4 \frac{z}{L} \right)^{0.75}$$

$$B_{sw} = 9.3447 \left(1 + 6.4 \frac{z}{L} \right)^{-0.825}$$

where subscript *s* is used to represent a scalar variable such as T_s , T_c , T_{fw} , ρ_{CO_2} , $\rho_{CO_2_LI}$, ρ_{H_2O} , $\rho_{H_2O_kh}$, or $\rho_{H_2O_LI}$.

D.7.2 Cospectra for $z/L \leq 0$ (neutral to unstable surface layer)

For covariances $\overline{(u'w')}_r$ or $\overline{(v'w')}_r$, from Moore (1986, Eq. 21) and van Dijk (2002b, Eq. 2.80 and Table 2.1):

$$fS_{uw}(f) = \begin{cases} \frac{20.78 \frac{z}{\bar{u}} f}{\left(1 + 31 \frac{z}{\bar{u}} f \right)^{1.575}} & \frac{z}{\bar{u}} f < 0.24 \\ \frac{12.66 \frac{z}{\bar{u}} f}{\left(1 + 9.6 \frac{z}{\bar{u}} f \right)^{2.4}} & \frac{z}{\bar{u}} f \geq 0.24 \end{cases} \quad (46)$$

For covariances $\overline{(T'_s w')}_r$, $\overline{(T'_c w')}_r$, $\overline{(T'_{FW} w')}_r$, $\overline{(\rho'_{CO_2} w')}_r$, and $\overline{(\rho'_{H_2O} w')}_r$, from Moore (1986, Eq. 25), Moncrieff et al. (1997, Eqs. 15 and 16), and van Dijk (2002b, Eq. 2.84 and Table 2.1):

$$fS_{sw}(f) = \begin{cases} \frac{12.92 \frac{z}{u} f}{\left(1 + 26.7 \frac{z}{u} f\right)^{1.375}} & \frac{z}{u} f < 0.54 \\ \frac{4.378 \frac{z}{u} f}{\left(1 + 3.78 \frac{z}{u} f\right)^{2.4}} & \frac{z}{u} f \geq 0.54 \end{cases} \quad (47)$$

As with stable surface layer conditions, the cospectrum of temperature with vertical velocity in neutral or unstable conditions presented above may be used as the cospectrum of other individual scalars with vertical velocity.

D.8 Sub-transfer functions

The total transfer function found in Model (38) consists of the products of all sub-transfer functions of each variable used to calculate a covariance. Sub-transfer functions account for block averaging, line averaging, sensor volume averaging (negligible in the cases of the IRGASON and EC150), electronic data filtering, sensor time response (for example, air temperature measured using FW sensors), and sensor separation (for example, the x and y separations of CSAT3A and EC150). These sub-transfer functions are described in the following sections.

D.8.1 Finite time block averaging

The sub-transfer function for finite time block averaging is derived from Kaimal, Clifford, and Lataitis (1989, Eq. 4) and Massman (2000, Eq. 3).

Every covariance is an average covariance over a finite block of time as defined by the user (for example, 30 or 60 min). Having a finite time block leads to attenuation of low frequencies; therefore, all covariance variables require a sub-transfer function to account for this. The sub-transfer function $[T_{sw_BA}(f, T_{ba})]$, due to a finite block averaging period (T_{ba}), is given by:

$$T_{sw_BA}(f, T_{ba}) = 1 - \frac{\sin^2(\pi T_{ba} f)}{(\pi T_{ba} f)^2} \quad (48)$$

where subscript *BA* or *ba* indicates **block averaging**, and $T_{ba} = 1,800$ seconds if a period of 30 minutes is used.

D.8.2 Line averaging

Sub-transfer functions for variances of individual variables: The attenuation of variance of vertical velocity (w) from the line average is described using Moore (1986, Eq. 9), Moncrieff (1997, 610), and Foken et al. (2012, Eq. 4.10).

The resulting sub-transfer function applied to vertical wind variance [$T_{ww_LA}(f, l_{pt_csat}, \bar{u})$] is as follows:

$$T_{ww_LA}(f, l_{pt_csat}, \bar{u}) = \frac{4}{(2\pi l_{pt_csat} / \bar{u}) f} \left(1 + \frac{\exp(-\frac{2\pi l_{pt_csat}}{\bar{u}} f)}{2} - \frac{1.5 \left[1 - \exp(-\frac{2\pi l_{pt_csat}}{\bar{u}} f) \right]}{(2\pi l_{pt_csat} / \bar{u}) f} \right) \quad (49)$$

The sub-transfer function for horizontal velocity variance [$T_{uu_LA}(f, l_{pt_csat}, \bar{u})$] has not been well defined for sonic anemometry (Moore 1986, 22; van Dijk 2002b, 46). Therefore, the sub-transfer function used by van Dijk (2002b, Eq. 2.70) for horizontal wind is adopted as an approximation:

$$T_{uu_LA}(f, l_{pt_csat}, \bar{u}) = \left[\frac{\sin\left(\frac{\pi l_{pt_csat}}{\bar{u}} f\right)}{\frac{\pi l_{pt_csat}}{\bar{u}} f} \right]^2 \quad (50)$$

For the variance of a scalar (s) measured by a gas analyzer, the sub-transfer function [$T_{ss_LA}(f, l_{pt_irga}, \bar{u})$] is given as follows, from Moore (1986, Eq. 7), van Dijk (2002b, Eq. 2.68), and Foken et al. (2012, Eq. 4.12):

$$T_{ss_LA}(f, l_{pt_irga}, \bar{u}) = \frac{1}{\frac{2\pi l_{pt_irga}}{\bar{u}} f} \left(3 + \exp(-\frac{2\pi l_{pt_irga}}{\bar{u}} f) - \frac{4 \left[1 - \exp(-\frac{2\pi l_{pt_irga}}{\bar{u}} f) \right]}{\frac{2\pi l_{pt_irga}}{\bar{u}} f} \right) \quad (51)$$

Sub-transfer functions for covariance due to line averaging: Sub-transfer functions for covariance of certain scalars with vertical wind are given below:

$$\overline{u'w'} \text{ or } \overline{v'w'}$$

$$T_{uw_LA}(f, l_{pt_csat}, \bar{u}) = \sqrt{T_{uu_LA}(f, l_{pt_csat}, \bar{u}) T_{ww_LA}(f, l_{pt_csat}, \bar{u})} \quad (52)$$

$$\overline{s'w'}$$

where s is a variable from the IRGA.

$$T_{sw_LA}(f, l_{pt_IRGA}, l_{pt_csat}, \bar{u}) = \sqrt{T_{ss_LA}(f, l_{pt_IRGA}, \bar{u}) T_{ww_LA}(f, l_{pt_csat}, \bar{u})} \quad (53)$$

$$\overline{T_s^i w^i}$$

from van Dijk (2002a, Eqs. 5 to 8).

In cylindrical coordinates, the sub-transfer function for line averaging of buoyancy flux measured using a Campbell Scientific sonic anemometer is as follows:

$$T_{T_s w^i LA}(f, l_{pt_csat}, \bar{u}) = \frac{91}{180\pi k^2} \int_0^\infty \int_0^{2\pi} K \sqrt{k^2 + K^2} \frac{k^2 + K^2 \sin^2 \theta}{k^2 + K^2} \sum_{i=1}^3 \sin c \frac{\mathbf{k} \cdot \mathbf{l}_i}{2} d\theta dK \quad (54)$$

where k is the wave number in the streamwise direction given by:

$$k = \frac{2\pi f}{\bar{u}} \quad (55)$$

and where k is the wave number vector in cylindrical coordinates given by:

$$\mathbf{k} = [k \quad K \sin \theta \quad K \cos \theta] \quad (56)$$

and where \mathbf{l}_i ($i = 1, 2,$ or 3) is a path vector that expresses a path length as three components in three dimensions, given by:

$$\mathbf{l}_1 = l_{pt_csat} \begin{bmatrix} -\sin 30^\circ \\ 0 \\ \cos 30^\circ \end{bmatrix}, \mathbf{l}_2 = \frac{l_{pt_csat}}{2} \begin{bmatrix} \sin 30^\circ \\ \sqrt{3} \sin 30^\circ \\ 2 \cos 30^\circ \end{bmatrix}, \text{ and } \mathbf{l}_3 = \frac{l_{pt_csat}}{2} \begin{bmatrix} \sin 30^\circ \\ -\sqrt{3} \sin 30^\circ \\ 2 \cos 30^\circ \end{bmatrix} \quad (57)$$

The integration of Eq. (54) requires much computation, so its numerical form in van Dijk (2002a, Table 1) is used (see Table D-1 [p. 110]).

Table D-1: Numerical form (transfer function values versus normalized frequencies) of sub-transfer function of buoyancy flux measured by a CSAT3								
Normalized frequency	<0.01	0.1	0.2	0.5	1.0	1.2	1.4	1.6
Sub-transfer function values	1.0000	0.9992	0.9976	0.9900	0.9670	0.9550	0.9417	0.9274

Table D-1: Numerical form (transfer function values versus normalized frequencies) of sub-transfer function of buoyancy flux measured by a CSAT3

Normalized frequency	1.8	2.0	2.2	2.4	2.6	2.8	3.0	4.0
Sub-transfer function values	0.9122	0.8962	0.8797	0.8626	0.8452	0.8274	0.8096	0.7201
Normalized frequency	5.0	6.0	7.0	8.0	9.0	10.0	14.0	20.0
Sub-transfer function values	0.6353	0.5588	0.4922	0.4355	0.3879	0.3481	0.2445	0.1700
Normalized frequency	30.0	40.0	50.0	60.0	70.0	80.0	90.0	100.0
Sub-transfer function values	0.1134	0.08503	0.06802	0.05668	0.04859	0.04251	0.03779	0.03401

For normalized frequencies between the values listed in [Table D-1](#) (p. 110), the sub-transfer function is linearly interpolated between two neighboring independent normalized frequencies. For normalized frequencies ≤ 0.01 Hz, the transfer function value is set to 1. For normalized frequencies > 100 Hz, trends from the first and second order numerical derivatives show that this sub-transfer function becomes nearly constant beyond 300 Hz at a value of 1.155511×10^{-4} . Therefore, for normalized frequencies from 300 to 10,000 Hz, the sub-transfer function is set to this value, and for frequencies falling between 100 and 300 Hz, the sub-transfer function is estimated by linear interpolation.

D.8.3 Volume averaging

Volume averaging is considered negligible in the cases of an IRGASON and EC150, due to the very small diameter-to-path length ratio; however, the sub-transfer function for volume averaging is briefly described here for completeness. A sensor such as a krypton hygrometer (KH20) has a much higher diameter-to-path length ratio, so the volume averaging must be considered. Its optical beam diameter is 8 mm, and its path length is 12 to 15 mm (see the calibration document for the unique path length for a particular KH20). Andreas (1981, Eq. 18) derived an exact transfer function for volume averaging. This transfer function includes a first-order Bessel function of the first kind, which makes the integration of the sub-transfer function over the frequency domain in need of significant computation time.

Later, Moene (2003) used a simpler function to approximate Eq. 18 of Andreas (1981) for Krypton hygrometers. His approximation was developed using the transfer function of Andreas (1981) for

a diameter-to-path length ratio between 0.5 and 1.0 when the ratio of the Kolmogorov microscale (1 mm in atmosphere) to the path length is 0.1 (Andreas 1981, Figure 2). The approximation equation (Moene 2003, 650) is given by:

$$T_{h2o_KH_VA}(f, p_{KH}, \bar{u}) = \exp\left[-2\left(\frac{p_{KH}}{\bar{u}} f\right)^2\right] \quad (58)$$

where p_{KH} is the path length of KH20.

D.8.4 FIR filtering

The sub-transfer function for the various data filters available on the EC100 electronics (the electronics module used with the EC150, CSAT3A, and IRGASON) has not yet been developed. However, it is assumed to be negligible compared to other sub-transfer functions, assuming the bandwidth has been appropriately selected for flux measurements.

D.8.5 Time constant

If a fine-wire thermocouple is used, a sub-transfer function describing the frequency response of the thermocouple should be used and is described by a simple first-order gain function (Moore 1986, square of Eq. 2):

$$T_{TT_TC}(f, \tau_{FW}) = \frac{1}{1 + (2\pi\tau_{FW}f)^2} \quad (59)$$

where τ_{FW} is the time constant of the FW.

The value of τ_{FW} depends on the physical properties of air, physical properties of the thermocouple, diameter of the thermocouple wire (D , entered by a user), and Nusselt number (**Nu**). It is given by (Moore 1986, Eq. 3; Shapland et al. 2014, Eq. 4):

$$\tau_{FW} = \gamma \frac{\rho_{FW} C_{FW}}{k_a \mathbf{Nu}} D^2 \quad (60)$$

where:

the γ is the shape coefficient; it is 0.25 for cylindrical and 0.167 for spherical sensors. For an FW, a cylindrical shape is assumed, since heat can be conducted through two paths around the junction, each having a cylindrical shape.

ρ_{FW} is the material density of the thermocouple {[8920 (constantan) + 8730 (chromel)] / 2 = 8825 kg·m³; Omega n.d.}.

C_{FW} is the specific heat of the thermocouple materials {[0.094 (constantan) + 0.107 (chromel)] / 2 = 0.1005 cal·g⁻¹·deg C⁻¹ = 420.7734 J·kg⁻¹·deg C⁻¹; Omega n.d.}.

k_a is the thermal conductivity of air [(7.038086×10⁻⁵ T + 2.42507×10⁻² in W·m⁻¹·deg C⁻¹), where T is air temperature in deg C], see Montgomery (1947, Table 1).

Nu is the Nusselt number. The Nusselt number for a sphere is used because the aerodynamics around the junction are influenced by its 3D dimensions (Moore 1986, Eq. 4). It is calculated as follows:

$$\mathbf{Nu} = 2.00 + 0.18\mathbf{Re}^{0.67} \quad (61)$$

where **Re** is the Reynolds number (Geankoplis 1993, Eqs. 3.1 and 3.2, 114–131, and Appendix).

$$\mathbf{Re} = \frac{2\rho_a D\bar{u}}{\mu} \quad (62)$$

where ρ_a is air density (calculated online by the data logger); \bar{u} is horizontal wind speed (use sonic data); and μ is viscosity of air (4.9821×10⁻⁸ T + 1.7168×10⁻⁵ in kg·m⁻¹·s⁻¹); see Montgomery (1947, Table 1).

D.8.6 Spatial separation

For eddy-covariance measurements that use two spatially separated sensors for measurements of wind velocity and a scalar, a passing eddy may be measured by the two sensors at different times if the sensors are mounted along the mean wind direction, creating a time lag in the measurements of the downstream sensor relative to the upstream one. Alternatively, it is possible that the eddy will be measured by only one of the two sensors if the sensors are mounted with a separation perpendicular to the mean wind direction (for example, a lateral separation with sensors mounted in a crosswind orientation) and the eddy is smaller than the separation distance. This can also happen if the boundary of the eddy passing through one sensor measurement volume does not reach the measurement volume of the other sensor. Accordingly, the separation along the wind direction is defined as lag distance and the separation in the crosswind direction as lateral distance.

The magnitude of covariance is decreased due to both the lag distance and the lateral distance (Horst and Lenschow 2009). In data processing, the loss of covariance due to the lag distance may be significantly or largely recovered by realigning the data with various time lags to maximize the covariance (such as lag maximization), and the loss of covariance due to lateral distance may be recovered using a frequency correction (Foken et al. 2012). For both corrections, the physical lag and lateral distances are needed.

In the installation of sensors, the horizontal coordinates of the center of the measurement volume of the scalar sensor relative to the sonic coordinate system (see [Figure D-1](#) [p. 101]) should be recorded. The coordinates can be expressed as a separation vector $[x, y]$.

When wind comes from a direction of zero degrees (for example, against the direction in which the sonic anemometer points), the x component of the vector is lag distance, and the y component of the vector is lateral distance. When the wind direction is not zero degrees, the separation vector may be projected onto the wind and crosswind axes by knowing the wind direction (θ_w) relative to the sonic coordinate system and using a coordinate rotation. The resulting projection along the wind direction is lag distance (d_{lag}), and the projection in the crosswind direction is lateral distance (d_{lat}).

These are given by:

$$\begin{bmatrix} d_{lag} \\ d_{lat} \end{bmatrix} = \begin{bmatrix} \cos \theta_w & \sin \theta_w \\ -\sin \theta_w & \cos \theta_w \end{bmatrix} \begin{bmatrix} x \\ y \end{bmatrix} \quad (63)$$

The lag distance (d_{lag}) along with wind speed will be used by the data logger for lag maximization by applying an appropriate lag to the measurement scans to align the sensors. The lateral distance is used in a sub-transfer function of frequency response due to sensor separation, $T_{sw_SP}(f, d_{lat}, \bar{u})$, which is given as follows (Foken et al. 2012, Eq. 4.8):

$$T_{sw_SP}(f, d_{lat}, \bar{u}) = \exp \left[-9.9 \left(\frac{fd_{lat}}{\bar{u}} \right)^{1.5} \right] \quad (64)$$

D.8.7 Total transfer function

A composite or total transfer function is given by the product of the appropriate sub-transfer functions for a particular covariance. The total transfer functions used by the data logger are given in this section (FIR correction is currently not included).

For $\overline{u'w'}$ or $\overline{v'w'}$:

$$T_{uw}(f, l_{pt_cscat}, T_{ba}, \bar{u}) = T_{uw_BA}(f, T_{ba}) T_{uw_LA}(f, l_{pt_cscat}, \bar{u}) \quad (65)$$

For $\overline{T_s'w'}$:

$$T_{T_s w}(f, l_{pt_cscat}, T_b, \bar{u}) = T_{T_s w_BA}(f, T_{ba}) T_{T_s w_LA}(f, l_{pt_cscat}, \bar{u}) \quad (66)$$

For $\overline{s'w'}$ (where s is a variable measured by the IRGA):

$$T_{sw}(f, l_{pt_cscat}, l_{pt_IRGA}, d_{lat}, T_{ba}, \bar{u}) = T_{sw_BA}(f, T_{ba}) T_{sw_LA}(f, l_{pt_cscat}, l_{pt_IRGA}, \bar{u}) T_{sw_SP}(f, d_{lat}, \bar{u}) \quad (67)$$

For $\overline{T'_{FW} w'}$:

$$T'_{T_{FW} w'}(f, l_{pt_csat}, d_{lat}, \tau_{FW}, T_{ba}, \bar{u}) = T'_{T_{FW} w'_{BA}}(f, T_{ba}) \sqrt{T'_{w'_{LA}}(f, l_{pt_csat}, \bar{u}) T'_{TT_TC}(f, \tau_{FW}) T'_{sw_SP}(f, d_{lat}, \bar{u})} \quad (68)$$

D.9 Working model

Evaluating the correction factor in Model (38) in the data logger program requires numerical integration. Because the cospectrum changes exponentially faster at low frequencies than at high frequencies, the interval of integration can be exponentially increased throughout the integration to save computation time without significantly reducing accuracy. Accordingly, $\ln f$ is used as an integration variable that increases at equal logarithmic intervals of frequency (f), which effectively increments the frequency interval exponentially for fast integration over the integration domain. This results in a working formula that is used to find the covariance:

$$\overline{(\alpha' w')_{rf}} = \overline{(\alpha' w')_r} \left\{ \frac{\int_0^{\infty} [f S_{\alpha w}(f)] d(\ln f)}{\int_0^{\infty} T_{\alpha w}(f) [f S_{\alpha w}(f)] d(\ln f)} \right\} \quad (69)$$

Recall that even though simple notation for $T_{\alpha w}(f)$ has been used, this is an overall transfer function that is comprised of the sub-transfer functions presented in the sections above and includes independent variables such as wind speed (\bar{u}), block average period, measurement path length, and/or sensor time constant and/or lateral separation distance. Accordingly, the components of the combined transfer function for different variables of vectors and scalars are unique due to sensor specifications and measurement installations.

D.10 Programmatic approach to computations for correction factors

The correction factor in Model (69) has a numerator and a denominator. Its numerator is found from a normalized spectrum, and its denominator is determined by numerical integration. For both normalized and non-normalized cospectra, we numerically integrate both the numerator and denominator. Moore (1986) used the composite Simpson's rule to estimate this denominator. In his estimation, 19 equal integration intervals at a scale of natural logarithm from 10^{-5} to 5 Hz were used, which resulted in an integration error of <1 percent. Currently, this can be further improved due to faster computational speeds in Campbell Scientific data loggers compared to microcomputers at that time. By increasing the integration range and decreasing the integration intervals, the data logger can more accurately account for frequency attenuation, particularly in the lower frequencies of the block averaging sub-transfer function. Specifically, we

extend the integration range from 10^{-6} to 10^4 Hz and divide the range into 100 frequency bins. It is believed that the integration error should be significantly smaller than Moore (1986) and the accuracy sufficient.

Because the cospectrum may change exponentially and dramatically in lower frequencies, the logarithm scale of cyclic frequency may be used for a numerical integration interval (bin width). For 100 bins from 10^{-6} to 10^4 Hz, the base frequency interval (Δf) is 1.258925, since $10^{-6} \times 1.258925^{100} = 10,000$. The lower frequency boundary of the j th interval is indexed as the $(j-1)$ th frequency, and the right boundary frequency is indexed as the j th frequency. The interval of integration (bin width) at natural logarithm scale $[\Delta \ln(f)]$ is given by:

$$\begin{aligned} \Delta \ln(f) &= \ln(10^{-6} \Delta f^j) - \ln(10^{-6} \times \Delta f^{j-1}) \\ &= \ln \frac{10^{-6} \Delta f^j}{10^{-6} \Delta f^{j-1}} = \ln \Delta f \end{aligned} \quad (70)$$

The composite Simpson's rule writes the integration for the numerator in Model 8.1 as (Burden and Faires 1993, 186):

$$\begin{aligned} \int_0^\infty [f S_{\alpha w}(f)] d(\ln f) &\approx \int_{10^{-6}}^{10000} [f S_{\alpha w}(f)] d(\ln f) \\ &= \frac{\ln(\Delta f)}{3} \left\{ [10^{-6} S_{\alpha w}(10^{-6})] + 4 \sum_{k=1}^{50} [10^{-6} \Delta f^{2k-1} S_{\alpha w}(10^{-6} \Delta f^{2k-1})] \right. \\ &\quad \left. + 2 \sum_{k=1}^{49} [10^{-6} \Delta f^{2k} S_{\alpha w}(10^{-6} \Delta f^{2k})] + [10^4 S_{\alpha w}(10^4)] \right\} \end{aligned} \quad (71)$$

with an error term as described in Burden and Faires (1993, 186):

$$\begin{aligned} Error &= \frac{10^4 - 10^{-6}}{180} \times (\ln \Delta f)^4 \frac{2}{100} \sum_{j=1}^{50} [\zeta_j S_{\alpha w}(\zeta_j)]^{(4)} \\ &\approx \frac{20}{18} \times (\ln \Delta f)^4 \sum_{j=1}^{50} [\zeta_j S_{\alpha w}(\zeta_j)]^{(4)} \end{aligned} \quad (72)$$

where ζ is a value of frequency that can maximize the value in the square bracket. The evaluation of this term requires more complicated calculations because the fourth order derivative of the integrated function is needed. We do not evaluate this term now, but Eq. (72) can show how the error can be reduced by adding the number of integration intervals and narrowing the width of the interval.

Similarly, the denominator with Simpson's rule applied becomes:

$$\begin{aligned} \int_0^{\infty} T_{\alpha w}(f) [f S_{\alpha w}(f)] d(\ln f) &\approx \int_{10^{-6}}^{10000} T_{\alpha w}(f) [f S_{\alpha w}(f)] d(\ln f) \\ &= \frac{\ln(\Delta f)}{3} \left\{ \left[T_{\alpha w}(10^{-6}) 10^{-6} S_{\alpha w}(10^{-6}) \right] + 4 \sum_{k=1}^{50} T_{\alpha w}(10^{-6} \Delta f^{2k-1}) \left[10^{-6} \Delta f^{2k-1} S_{\alpha w}(10^{-6} \Delta f^{2k-1}) \right] \right. \\ &\quad \left. + 2 \sum_{k=1}^{49} T_{\alpha w}(10^{-6} \Delta f^{2k}) \left[10^{-6} \Delta f^{2k} S_{\alpha w}(10^{-6} \Delta f^{2k}) \right] + T_{\alpha w}(10^4) \left[10^4 S_{\alpha w}(10^4) \right] \right\} \end{aligned} \quad (73)$$

The error term of this numerical integration can be calculated using Eq. (72) if the term $\xi_j S_{\alpha w}(\xi_j)$ is replaced with $T_{\alpha w}[\xi_j] \xi_j S_{\alpha w}(\xi_j)$.

The code in the program used to calculate the correction factor of one covariance (*Cor_factor*) is outlined below:

```
Cor_factor = 0
for j = 0 to 100      (100 steps)
  f = 10-6 × 1.258925j  (calculation of frequency)
  m = 2 + 4 × (j MOD 2) – ABS(j = 0) – ABS(j = 100)
```

NOTE:

$m = 1$ for $j = 0$ and $j = 100$; otherwise, $m = 4$ if j is odd, and $m = 2$ if j is even.

Numerator = Numerator + $m \times [f S_{\alpha\beta}(f)]$

Denominator = Denominator + $m \times T_{\alpha\beta}(f) [f S_{\alpha\beta}(f)]$

Next j:

Cor_factor = Numerator / Denominator

D.11 References

- Andreas, E.L. 1981. "The effects of volume averaging on spectra measured with Lyman-Alpha hygrometer." *Journal of Applied Meteorology* 20: 467–475.
- Burden, R.L. and J.D. Faires. 1993. *Numerical Analysis*. Boston: PWS Publishing Company.
- Campbell Scientific Inc. 2014. *IRGASON Integrated CO2/H2O Open-Path Gas Analyzer and 3D Sonic Anemometer*. Logan, UT, USA.

- Foken, T., R. Leuning, S.R. Oncley, M. Mauder, and M. Aubinet. 2012. "Correction and Data Quality Control." In *Eddy Covariance: A Practical Guide to Measurement and Data Analysis*, edited by Aubinet, M., T. Vesala, and D. Papale, 85–131. New York: Springer.
- Geankoplis, C.J. 1993. *Transportation Processes and Unit Operation*, 3rd edition. New Jersey: PTR Prentice Hall.
- Horst, T.W. and D.H. Lenschow. 2009. "Attenuation of scalar fluxes measured with spatially-displaced sensors." *Boundary-Layer Meteorology* 130: 275–300.
<https://doi.org/10.1007/s10546-008-9348-0>.
- Kaimal, J.C., S.F. Clifford, and R.J. Latatits. 1989. "Effect of finite sampling on atmospheric spectra." *Boundary-Layer Meteorology* 7: 827–837.
- Kaimal, J.C. and J.J. Finnigan. 1994. *Atmospheric Boundary Layer Flows: Their Structure and Measurement*. Oxford: Oxford University Press.
- Kaimal, J.C., J.C. Wyngaard, Y. Izumi, and O.R. Cote. 1972. Deriving power spectra from a three-component sonic anemometer. *Journal of Applied Meteorology* 7: 827–837.
- Massman, W.J. 2000. A simple method for estimating frequency response corrections for eddy covariance systems. *Agricultural and Forest Meteorology* 104: 185–198.
- Moene, A.F. 2003. Effects of water vapor on the structure parameter of the refractive index for near-infrared radiation. *Boundary-Layer Meteorology* 107:635–653.
- Moncrieff, J.B., J.M. Massheder, H. de Bruin, J.A. Elbers, T. Friborg, B. Heusinkveld, P. Kabat, S. Scott, H. Soegaard, and A. Verhoef. 1997. "A system to measure surface fluxes of momentum, sensible heat, water vapour and carbon dioxide." *Journal of Hydrology* 188-189: 589–611.
- Montgomery, R.B. 1947. "Viscosity and thermal conductivity of air and diffusivity of water vapor in air." *Journal of the Atmospheric Sciences* 4: 193–196.
- Moore, C.J. 1986. "Frequency response corrections for eddy correlation systems." *Boundary-Layer Meteorology* 37: 17–35.
- Oke, T.R. 1987. *Boundary Layer Climates, 2nd edition*. New York: Routledge Taylor & Francis Group.
- Omega. n.d. "Physical Properties of Thermoelement Materials." Accessed March 10, 2022.
<https://www.omega.co.uk/temperature/z/pdf/z016.pdf>.
- Rebmann, C., O. Kolle, B. Heinesch, R. Queck, A. Ibrom, and M. Aubinet. 2012. "Data acquisition and flux calculations." In *Eddy covariance: a practical guide to measurement and data analysis*, edited by Aubinet, M., T. Vesala, and D. Papale, 59–83. Dordrecht, Netherlands: Springer. https://doi.org/10.1007/978-94-007-2351-1_3, 2012.

- Rosenberg, N.J., B.B. Blad, and S.B. Verma. 1983. *Microclimate: The Biological Environment, 2nd ed.* New York: John Wiley & Son.
- Shapland, T.M., R.L. Snyder, K.T. Paw U, and A.J. McElrone. 2014. "Thermocouple frequency response compensation leads to convergence of the surface renewal alpha calibration." *Agricultural and Forest Meteorology* 189-190: 36–47.
- Stull, R.B. 1988. *An Introduction to Boundary Layer Meteorology.* Netherlands: Kluwer Academic Publishers.
- Tanner, C.B. and W.L. Pelton. 1960. "Potential evapotranspiration estimates by the approximate energy balance method of Penman." *Journal of Geophysical Research* 65: 3391.
- van Dijk, A. 2002a. "Extension of 3D of 'The effect of linear averaging on scalar flux measurements with a sonic anemometer near the surface' by Kristensen and Fitzjarrald." *Journal of Atmospheric and Oceanic Technology* 19: 80–82.
- van Dijk, A. 2002b. "The Principle of Surface Flux Physics." Research Group of the Royal Netherlands Meteorological Institute and Department of Meteorology and Air Quality with Agricultural University Wageningen.
- Wallace, J.M. and P.V. Hobbs. 2006. *Atmospheric Science: An Introductory Survey.* Amsterdam: Academic Press.

Appendix E. WPL corrections

Due to the vertical gradient of air temperature in the atmospheric surface layer, rising air parcels have different temperatures and densities than descending ones. For example, in the case of upward (positive) heat flux when the air closest to the ground is warmest, rising air parcels on average will be warmer and less dense than descending ones. In this same case, supposing the CO₂ or H₂O fluxes are zero (rising and descending parcels carry the same amount of CO₂ and H₂O), the measurements from an open-path eddy-covariance system will still report negative (downward) fluxes simply because of the correlation between rising air parcels and lower air density. This is explained by mass conservation or air continuity: the decrease in air density that is due to the increase in air temperature while the total pressure in the surface layer changes very little, which forces air to expand upward in the atmospheric surface layer. This expansion generates an upward (positive) flux of air at the measurement point and leads to a slightly positive mean vertical velocity. Thus, the downward CO₂ or H₂O flux measured by an open-path eddy-covariance system may be explained by the upward flux of air from a net upward vertical velocity.

Depending on whether the temperature profile increases or decreases with height, the mean vertical velocity may be negative or positive. Typically, it ranges from -0.75 to +1.5 mm/s when sensible heat flux is between -200 and +600 W/m² (Webb, Pearman, and Leuning 1980, Fig. 1). This change in vertical velocity that is due to change in air density is too small to be measured by a 3D sonic anemometer with sufficient accuracy.

Since typical applications of the open-path eddy-covariance method do not account for fluxes associated with non-zero mean flows ($\bar{w} \neq 0$), an appropriate correction for the vertical velocity due to heat and water vapor transfer is needed.

E.1 Basic considerations

Air density (ρ_a) is a sum of partial densities: dry air density (ρ_d), water vapor density (ρ_v), and CO₂ density (ρ_{CO_2}), given by:

$$\rho_a = \rho_d + \rho_v + \rho_{CO_2} \quad (74)$$

The contribution of ρ_{CO_2} relative to ρ_d and ρ_v is very small and, thus, can be considered negligible to the total air density. The equation therefore becomes:

$$\rho_a = \rho_d + \rho_v \quad (75)$$

The individual gas laws give the partial pressures of dry air (p_d), water vapor (p_v), and CO₂ density (p_{CO_2}) as follows:

$$\begin{aligned}
 p_d &= \frac{R^*}{m_d} \rho_d T \\
 p_v &= \frac{R^*}{m_v} \rho_v T \\
 p_{CO_2} &= \frac{R^*}{m_{CO_2}} \rho_{CO_2} T
 \end{aligned}
 \tag{76}$$

where subscripts d , v , and CO_2 denote dry air, water vapor, and carbon dioxide, respectively, and are used throughout; m is molecular mass; R^* is the universal gas constant (8.3143 J·K⁻¹·mol⁻¹; Wallace and Hobbs 2006, 467), and T is absolute temperature.

The total air pressure (p_a) is given by:

$$p_a = p_d + p_v + p_{CO_2} \tag{77}$$

The air pressure, dry air density, water vapor density, and CO₂ density are measured and calculated in an eddy-covariance system. Although the partial pressures of the different gas components are normally not measured, the other measured variables may be used to derive the partial pressures. Submitting Eq. (76) into Eq. (77) yields:

$$\frac{p_a}{R^* T} = \frac{\rho_d}{m_d} + \frac{\rho_v}{m_v} + \frac{\rho_{CO_2}}{m_{CO_2}} \approx \frac{\rho_d}{m_d} + \frac{\rho_v}{m_v} \tag{78}$$

Equation (78) describes the basic relationship of air and water vapor densities to temperature and atmospheric pressure. If the following term:

$$\frac{1}{T} = \frac{1}{(\bar{T} + T')} = \frac{1}{\bar{T} \left(1 + \frac{T'}{\bar{T}} \right)} \tag{79}$$

is expended in a power series of T' / \bar{T} , then the partial densities in Eq. (78) can be written in forms of instantaneous, mean, and fluctuation variables as follows:

$$\frac{\rho_d}{m_d} + \frac{\rho_v}{m_v} = \frac{p_a}{R^* \bar{T}} \left\{ 1 - \frac{T'}{\bar{T}} + \left(\frac{T'}{\bar{T}} \right)^2 - \left(\frac{T'}{\bar{T}} \right)^3 + \dots \right\} \tag{80}$$

$$\frac{\bar{\rho}_d}{m_d} + \frac{\bar{\rho}_v}{m_v} = \frac{p_a}{R^* \bar{T}} \left\{ 1 + \frac{\bar{T}'^2}{\bar{T}^2} - \frac{\bar{T}'^3}{\bar{T}^3} + \dots \right\} \quad (81)$$

$$\frac{\rho'_d}{m_d} + \frac{\rho'_v}{m_v} = \frac{p_a}{R^* \bar{T}} \left\{ -\frac{T'}{\bar{T}} + \frac{T'^2 - \bar{T}'^2}{\bar{T}^2} - \frac{T'^3 - \bar{T}'^3}{\bar{T}^3} + \dots \right\} \quad (82)$$

Equation (80) can further be expressed as:

$$\frac{p_a}{R^* \bar{T}} = \left(\frac{\bar{\rho}_d}{m_d} + \frac{\bar{\rho}_v}{m_v} \right) \left\{ 1 + \frac{\bar{T}'^2}{\bar{T}^2} - \frac{\bar{T}'^3}{\bar{T}^3} + \dots \right\}^{-1} \quad (83)$$

Substituting Eq. (83) into Eq. (82) yields:

$$\begin{aligned} \frac{\rho'_d}{m_d} + \frac{\rho'_v}{m_v} = & \left(\frac{\bar{\rho}_d}{m_d} + \frac{\bar{\rho}_v}{m_v} \right) \left\{ -\frac{T'}{\bar{T}} + \frac{T'^2 - \bar{T}'^2}{\bar{T}^2} - \frac{T'^3 - \bar{T}'^3}{\bar{T}^3} + \dots \right\} \left\{ 1 + \frac{\bar{T}'^2}{\bar{T}^2} - \frac{\bar{T}'^3}{\bar{T}^3} + \dots \right\}^{-1} \end{aligned} \quad (84)$$

By dropping the second order term ($<10^{-4}$) of absolute temperature, the fluctuation of dry air density can be expressed as:

$$\begin{aligned} \rho'_d &= -\frac{m_d}{m_v} \rho'_v - \bar{\rho}_d \left(1 + \frac{m_d}{m_v} \frac{\bar{\rho}_v}{\bar{\rho}_d} \right) \frac{T'}{\bar{T}} \\ &= -\mu \rho'_v - \bar{\rho}_d (1 + \mu \sigma) \frac{T'}{\bar{T}} \end{aligned} \quad (85)$$

where μ is the molecular weight ratio of dry air to water vapor, and σ is the mean water vapor mixing ratio.

E.2 Governing constraint and mean vertical velocity

The governing constraint that the mean vertical flux of dry air constituent should be zero is given by:

$$\overline{w \rho_d} = 0 \quad (86)$$

Equation (86) is equivalent to:

$$\overline{w\rho_d} = \overline{(\bar{w} + w')(\bar{\rho}_d + \rho'_d)} = \overline{\bar{w}\bar{\rho}_d + \bar{w}\rho'_d + w'\bar{\rho}_d + w'\rho'_d} = \bar{w}\bar{\rho}_d + \overline{w'\rho'_d} \quad (87)$$

Equations (86) and (87) give:

$$\bar{w} = -\frac{\overline{w'\rho'_d}}{\bar{\rho}_d} \quad (88)$$

Submitting Eq. (85) into this equation yields:

$$\bar{w} = \mu \frac{\overline{w'\rho'_v}}{\bar{\rho}_d} + (1 + \mu\sigma) \frac{\overline{w'T'}}{\bar{T}} \quad (89)$$

E.3 Eddy-covariance measurements

E.3.1 CO₂

The flux of CO₂ can be written as:

$$F_{CO_2} = \overline{w\rho_{CO_2}} = \overline{w'\rho'_{CO_2}} + \bar{w}\bar{\rho}_{CO_2} \quad (90)$$

Replacing the mean vertical velocity (\bar{w}) in Eq. (90) with Eq. (89) yields:

$$F_{CO_2} = \overline{w'\rho'_{CO_2}} + \left[\mu \frac{\overline{\rho_{CO_2}}}{\bar{\rho}_d} \overline{w'\rho'_v} + (1 + \mu\sigma) \frac{\overline{\rho_{CO_2}}}{\bar{T}} \overline{w'T'} \right] \quad (91)$$

The term in the rectangle bracket is the WPL correction. The first term is due to water flux, and the second term is due to heat flux.

$\bar{\rho}_{CO_2}$ is the mean CO₂ density measured by an IRGA.

$\bar{\rho}_d$ is the mean dry air density calculated from air temperature, pressure, and water vapor density.

\bar{T} is the mean air temperature in Kelvin.

μ is 1.60802 (the ratio of dry air molecular weight [md = 28.97 kg·kmol⁻¹] to water molecular weight [mv = 18.016 kg·kmol⁻¹]; Wallace and Hobbs 2006, 466).

σ is the mean water vapor mixing ratio (ratio of mean water vapor density [$\overline{\rho_v}$] to mean dry air density [$\overline{\rho_d}$]).

$\overline{w'\rho_v}$ is the water vapor flux measured using a sonic anemometer and IRGA.

$\overline{w'T'}$ is the heat flux (after rotations, frequency, and SND corrections) calculated from a sonic anemometer and optionally with a fine-wire thermocouple.

E.3.2 H₂O

The flux of water vapor is written as:

$$E = \overline{w\rho_v} = \overline{w'\rho_v} + \overline{w}\overline{\rho_v} \quad (92)$$

Replacing the mean vertical velocity (\overline{w}) in Eq. (92) with Eq. (89) yields:

$$E = \overline{w'\rho_v} + \left[\mu\sigma\overline{w'\rho_v} + (1 + \mu\sigma)\frac{\overline{\rho_v}}{\overline{T}}\overline{w'T'} \right] \quad (93)$$

The term in the bracket is the WPL correction. The first term is due to water flux itself, and the second term is due to heat flux.

$\overline{\rho_v}$ is the mean water vapor density measured by an IRGA.

$\overline{w'\rho_v}$ is the water vapor flux (after rotation and frequency corrections) measured using sonic anemometer and an IRGA.

E.4 References

Wallace, J.M. and P.V. Hobbs. 2006. *Atmospheric Science: An Introductory Survey*. Amsterdam: Academic Press.

Webb, E.K., G.I. Pearman, and R. Leuning. 1980. "Correction of flux measurements for density effects due to heat and water transfer." *Quarterly Journal of the Royal Meteorological Society* 106: 85–100.

Appendix F. Data quality grading

Data quality assurance (QA) and quality control (QC) are recommended for eddy-covariance measurements because of complex calculation procedures (Foken et al. 2012). A number of publications on QA and QC for eddy-covariance measurements are available (for example, Foken and Wichura 1996; Vickers and Mahurt 1997; Shearman 1992; Moncrieff et al. 1997; Aubinet et al. 2001; Foken et al. 2004 and 2012).

In the case of this data logger program, QA is accomplished using diagnostic outputs from the measurement system sonic anemometer and infrared gas analyzer. Specifically, the data logger only uses raw data for flux calculations when the diagnostic values from both sensors are zero (that is, when sensors work normally and measurements are in their reasonable ranges), when the measurements are within the calibrated range of the sensors, and when the signal strengths are adequate (that is, when nothing is blocking the optical path). Even when raw data is not used for flux calculations, it is still stored in the time series data table. More details on diagnostics are found in the manual of the specific sensor.

Regarding QC, the data logger program follows the method presented in Foken et al. (2012) to grade the relative quality of CO₂, latent heat, sensible heat, and momentum fluxes. Specifically, the following three variables are calculated and used to grade the quality of the data:

- *Relative Non-stationarity* (RN_{cov}) to describe the steady state
- *Relative Integral Turbulence Characteristics* (ITC) to define the developed turbulence condition
- Horizontal wind angle in the sonic anemometer coordinate system (wnd_dir_sonic)

[Relative non-stationarity \(RNcov\) for steady state](#) (p. 126) through [Wind direction in the sonic instrument coordinate system \(wnd_dir_sonic\)](#) (p. 130) give more information on each of these variables and how a quality grade for each is assigned. [Overall quality grade system](#) (p. 131) describes how an overall quality grade is found, and [Programmatic procedure to grade data quality](#) (p. 131) describes how this is implemented into the data logger program.

NOTE:

Due to differences in sonic anemometer models and geometries used in the AmeriFlux network, AmeriFlux prescribes the usage of only the steady-state and integral turbulence

characteristics tests as presented in Foken et al. (2004) for its standard QC results. Accordingly, the QC outputs in the *Flux_AmeriFluxFormat* output table (for example, FC_SSITC_TEST) ignore the wind direction and apply the tests as presented in the paper (see <http://ameriflux.lbl.gov/data/aboutdata/data-variables/> )

F.1 Relative non-stationarity (RN_{cov}) for steady state

Turbulence flux measurement theory is valid under the steady state conditions of turbulent flows. In such conditions, the surface layer turbulent flow structure is independent of time within an averaging interval (such as 30 min). The extent to which conditions conform to a steady state may be described using a variable called relative non-stationarity (RN_{cov}), which is defined as the relative difference between the averaged 5-min and 30-min covariance values, given by Foken et al. (2012, Eqs. 4.36 to 4.38):

$$RN_{cov} = 100 \times \left| \frac{\frac{1}{6} \sum_{i=1}^6 (\overline{s'w'})_{ri} - (\overline{s'w'})_r}{(\overline{s'w'})_r} \right| \quad (94)$$

where s can be T_s for sonic temperature, T_c for corrected temperature, ρ_{CO_2} for CO_2 density, ρ_{H_2O} for H_2O density, or u or v for horizontal wind speed; w represents vertical wind velocity; subscript r indicates the variable after coordinate rotation; subscript i (for example, 1, 2, ..., or 6 if a 30-min averaging period is used) indicates the covariance of the i^{th} 5-min interval within an averaging period; and the numerical number of 100 converts the relative non-stationarity into percentage. Based on the calculated value of RN_{cov} , the steady state is classified into nine grades. Grade 1 is most steady and indicates highest data quality, whereas grade 9 is least steady and indicates relatively lower data quality (see [Table F-1](#) [p. 127]).

Table F-1: Grades of relative non-stationarity, relative integral turbulence characteristics, and wind direction in the sonic instrument coordinate system

RN_{cov}		ITC_{sw} and ITC_{tau}		wnd_dir_sonic	
Relative non-stationarity (Foken et al. 2012, Model 2.3)		Relative integral turbulence characteristics (Foken et al. 2012, Model 2.5)		Wind direction	
Grade	Range (%)	Grade	Range (%)	Grade	Range (°)
1 (highest)	[0 , 15)	1 (highest)	[0 , 15)	1 (highest)	[0 , 150) and [210 , 360]
2	[15 , 30)	2	[15 , 30)	2	[150 , 170) and [190 , 210)
3	[30 , 50)	3	[30 , 50)	3 (lowest)	[170 , 190)
4	[50 , 75)	4	[50 , 75)		
5	[75 , 100)	5	[75 , 100)		
6	[100 , 250)	6	[100 , 250)		
7	[250 , 500)	7	[250 , 500)		
8	[500 , 1,000)	8	[500 , 1,000)		
9 (lowest)	≥1,000	9 (lowest)	≥1,000		

F.2 Turbulence conditions

Turbulence conditions are characterized using a term called integral turbulence characteristics (ITC), which is defined as a standard deviation of a fluctuating variable (for example, momentum variance or temperature variance) normalized by a scaling factor (for example, friction velocity or scaling temperature; Tillmann 1972). In a surface layer with fully developed turbulence, a given ITC term is a constant or at least follows a universal function of the scaling factor.

The most common scaling factor used is stability, defined as the ratio of aerodynamic height (z ; sensor sensing height minus zero displacement height) to the Monin-Obukhov length (L ; Stull 1988, 666; Kaimal and Finnigan 1994, 289), or z/L . The other scaling factor used is (Thomas and Foken 2002, 129–132):

$$\frac{z_+ f}{u_*} \tag{95}$$

where f is the Coriolis parameter in s^{-1} , u_* is friction velocity in $m \cdot s^{-1}$, and z_+ is a constant in m that was introduced and set to 1 to make the scaling factor dimensionless. For a given site, the Coriolis parameter can be calculated using:

$$f = 2\Omega \sin \phi \quad (96)$$

where Ω is angular velocity ($7.292 \times 10^{-5} \cdot s^{-1}$) and ϕ is latitude (positive in the northern hemisphere, negative in the southern hemisphere).

ITC values have been accurately simulated using a well-known model (for example, a function of the scaling factor) in conditions of fully developed turbulence. ITC may also be measured and then compared to the modeled ITC to show the degree to which turbulence has developed at that moment in time. The relative difference in percentage between the modeled and measured values are noted by ITC_{α} , where subscript α indicates the variable of interest. When α is vertical velocity (w) or horizontal wind speed (u), ITC_{α} is defined as follows:

$$ITC_{\alpha} = 100 \times \frac{\left| ITC_{\alpha_model} - \left(\frac{\sqrt{(\alpha'^2)_r}}{u_*} \right)_{measured} \right|}{ITC_{\alpha_model}} \quad (97)$$

where the ITC_{α_model} term is evaluated using:

$$ITC_{\alpha_model} = \begin{cases} c_{\alpha 1} \ln \frac{z+f}{u_*} + c_{\alpha 2} & \frac{z}{L} > 0 \\ c_{\alpha 1} \left(\frac{z}{|L|} \right)^{c_{\alpha 2}} & \frac{z}{L} \leq 0 \end{cases} \quad (98)$$

where $c_{\alpha 1}$ and $c_{\alpha 2}$ are parameters that depend on surface-layer stability (see [Table F-2](#) [p. 129]).

The relative difference in measured and theoretical ITC for temperature (T) is noted by ITC_T and is given by Foken et al. (2012, Eq. 4.41):

$$ITC_T = 100 \times \frac{\left| ITC_{T_model} - \left(\frac{\sqrt{(T'^2)_r}}{|T^*|} \right)_{measured} \right|}{ITC_{T_model}} \quad (99)$$

where T^* is scaling temperature, given by Kaimal and Finnigan (1994, Eq. 1.25b):

$$T^* = -\frac{\overline{T'w'}}{u_*} \quad (100)$$

and the ITC_{T_model} term is evaluated using:

$$ITC_{T_model} = c_{T1} \left(\frac{z}{|L|} \right)^{c_{T2}} \quad (101)$$

where c_{T1} and c_{T2} are parameters also depending on surface layer stability (see Table F-2 [p. 129]).

Variable in variance	$c_{\alpha 1}$	$c_{\alpha 2}$	z/L
Vertical velocity $a = W$	0.21	3.1	$0 < z/L < 0.4$
	1.3	0	$-0.032 < z/L \leq 0$
	2.0	1/8	$z/L \leq -0.032$
Horizontal wind speed $a = U$	0.44	6.3	$0 < z/L < 0.4$
	2.7	0	$-0.032 < z/L \leq 0$
	4.15	1/8	$z/L \leq -0.032$
Air temperature $a = T$	1.4	-1/4	$0.02 < z/L < 1$
	0.5	-1/2	$0.02 > z/L > -0.062$
	1.0	-1/4	$-0.062 > z/L > -1$
	1.0	-1/3	$-1 > z/L$

^{1/}Summarized from Foken et al. (2012, Tables 4.2 and 4.3).

Similarly, ITC_{sw} is used to describe the turbulent conditions when measuring the covariance of a scalar (s) and vertical wind (w). However, instead of an explicit equation for ITC_{sw} , its value is conservatively estimated by setting it equal to ITC_T or ITC_w , whichever is greater; that is:

$$ITC_{sw} = \max(ITC_T, ITC_w) \quad (102)$$

ITC_{sw} for fully developed turbulence conditions should be close to zero. The greater the ITC_{sw} value becomes, the less developed the turbulence. Foken et al. (2012) suggested classifying the

resulting value into nine grades, where grade 1 indicates conditions of fully developed turbulence, and grade 9 indicates conditions of undeveloped turbulence (see [Table F-1](#) [p. 127]).

Similarly, for momentum flux, a conservative approach is used:

$$ITC_{tau} = \begin{cases} \max(I TC_u, I TC_w) & \text{double rotations used} \\ I TC_w & \text{planar fit rotations used} \end{cases} \quad (103)$$

It should be noted that the variable u used in calculating ITC_u and ITC_{tau} in Foken et al. (2012, Table 4.2) is streamwise wind speed, although the authors did not explicitly specify this. Accordingly, the raw variable U_x from a sonic anemometer, which is rarely a streamwise wind speed, must undergo coordinate rotations. It becomes the streamwise wind speed only after the first rotation of Tanner and Thurtell (1969) or the third rotation of Wilczak, Oncley, and Stage (2001).

The data logger program uses either method of coordinate rotations, depending on the selection of the user; however, only the first two rotations of each method are done in order to reduce unnecessary computation time on the third rotation. Accordingly, u and, subsequently, ITC_u are only available to find ITC_{tau} if the method of Tanner and Thurtell (1969) is selected. If the planar fit method (Wilczak, Oncley, and Stage 2001) is used, ITC_{tau} is simply found from ITC_w as an approximation (see Eq. [103]).

Similar to the other relative turbulence characteristics, the greater the value of ITC_{tau} , the less developed the turbulence. The resulting value is classified into nine grades, where grade 1 indicates fully developed conditions of turbulence, and grade 9 indicates the least developed conditions of turbulence (see [Table F-1](#) [p. 127]).

Further, for stable surface layer conditions beyond the ranges where parameters are defined in [Table F-2](#) (p. 129), the quality grades for ITC_{α} , ITC_T , and ITC_{tau} are conservatively assigned as grade 9.

F.3 Wind direction in the sonic instrument coordinate system (wnd_dir_sonic)

The sonic anemometer has a boom-mount design that may affect the wind flow when the wind is blowing from behind the boom toward the sonic transducers. Accordingly, Foken et al. (2012) assigned a poorer data quality grade of 3 to wind coming from angles $180^\circ \pm 10^\circ$ relative to the sonic coordinate system, a medium grade of 2 to winds outside this range but within 29° of 180° , and a good grade of 1 for all other angles (see [Table F-1](#) [p. 127]).

F.4 Overall quality grade system

Each covariance variable over the averaging period is assigned an overall quality grade from 1 to 9 based on the individual grades of RN_{cov} , ITC_{sw} , and wnd_dir_sonic (see Table F-3 [p. 131]). Grade 1 is the highest overall quality, and grade 9 is the poorest.

Table F-3: Overall grades for each flux variable by the grades of relative non-stationarity, relative integral turbulence characteristics, and wind direction in the sonic instrument coordinate system^{1/}

Overall quality grade	RN_{cov}	ITC_{sw}	wnd_dir_sonic
	Relative non-stationarity	Relative integral turbulence characteristics	Wind direction
1 (best)	1	1–2	1
2	2	1–2	1
3	1–2	3–4	1
4	3–4	1–2	1
5	1–4	3–5	1
6	5	5	2
7	6	6	2
8	7–8	7–8	2
9 (worst)	9	9	3

^{1/}Simplified, from Foken et al. (2012, Table 4.5).

F.5 Programmatic procedure to grade data quality

The data logger program determines an overall quality grade using the following steps:

1. Calculate quality variables:

RN_{cov} for $\overline{u'w'}$, $\overline{v'w'}$, $\overline{T_s'w'}$, $\overline{\rho_{co2}'w'}$, and $\overline{\rho_{h2o}'w'}$

ITC_{tau} for momentum flux

$ITCT_{sw}$ for sensible heat, CO₂, and H₂O fluxes

2. Use RN_{cov} to grade stationarity, ITC_{tau} and ITC_{TSW} to grade the integral turbulence characteristics, and wind angle in the sonic coordinate system to grade wind direction (see [Table F-2](#) [p. 129]).
3. Define an array with three elements:

The first element records the best possible quality grade in the overall grade system for a given grade of relative non-stationarity. For example, a grade 2 for RN_{cov} can be assigned as grade 2 or 3 in the overall grade system. In this case, the data logger will store the value of **2** as the first element in the array.

Similarly, the second element in the array is the best possible quality grade in the overall grade system for a given grade of the integral turbulence characteristics.

The third element in the array is the best possible quality grade in the overall grade system for a given grade of wind direction.
4. The maximum value of the three elements is the overall quality grade for the variable being evaluated (for example, flux of CO_2 , H_2O , sensible heat, or momentum).

F.6 References

- AmeriFlux. n.d. "Data Variables." Accessed January 6, 2017.
<http://ameriflux.lbl.gov/data/aboutdata/data-variables/>.
- Aubinet M., B. Chermanne, M. Vandenhaute, B. Longdoz, M. Yernaux, and E. Laitat. 2001. "Long term carbon dioxide exchange above a mixed forest in the Belgian Ardennes." *Agricultural and Forest Meteorology* 108: 293–315.
- Foken, T., R.M. Göckede, M. Mauder, L. Mahrt, B.D. Amiro, and J.W. Munger. 2004. "Post-field data quality control." In *Handbook of Micrometeorology: A guide for surface flux measurement and analysis*, edited by Lee, X., W. Massman, and B. Law, 181–208. Kluwer, Dordrecht: Springer.
- Foken, T., R. Leuning, S.R. Oncley, M. Mauder, and M. Aubinet. 2012. "Corrections and data quality control." In *Eddy Covariance: A Practice Guide to Measurement and Data Analysis*, edited by Aubinet, M., T. Vesala, and D. Papale, 85–131. New York: Springer.
- Foken, T. and B. Wichura. 1996. "Tools for quality assessment of surface-based flux measurements." *Agricultural and Forest Meteorology* 78: 83–105.
- Kaimal, J.C. and J.J. Finnigan. 1994. *Atmospheric Boundary Layer Flows: Their Structure and Measurement*. Oxford: Oxford University Press.

- Moncrieff, J.B., J.M. Massheder, H. de Bruin, J.A. Elbers, T. Friborg, B. Heusinkveld, P. Kabat, S. Scott, H. Soegaard, and A. Verhoef. 1997. "A system to measure surface fluxes of momentum, sensible heat, water vapour and carbon dioxide." *Journal of Hydrology* 188-189: 589–611.
- Shearman, R.J. 1992. "Quality assurance in the observation area of the Meteorological Office." *Meteorological Magazine* 121: 212–216.
- Stull, R.B. 1988. *An introduction to Boundary Layer Meteorology*. Boston: Kluwer Academic Publisher.
- Tanner, C.B. and G.W. Thurtell. 1969. "Anemoclinometer measurements of Reynolds stress and heat transport in the atmospheric surface layer science lab." *US Army Electronics Command Atmospheric Sciences Laboratory TR ECOM 66-G22-F: R1–R10*.
- Thomas, C. and T. Foken. 2002. "Re-evaluation of integral turbulence characteristics and their parameterizations." American Meteorological Society 15th Conference on turbulence and boundary layer, Wageningen, Netherlands, July 15–19, 2002.
- Tillmann, J.E. 1972. "The indirect determination of stability, heat and momentum fluxes in the atmospheric boundary layer from simple scalar variables during dry unstable conditions." *Journal of Applied Meteorology* 11: 783–792.
- Vickers, D. and L. Mahurt. 1997. "Quality control and flux sampling problems for tower and aircraft data." *Journal of Atmospheric and Oceanic Technology* 14: 512–526.
- Wilczak, J.M., S.P. Oncley, and S.A. Stage. 2001. "Sonic Anemometer tilt correction algorithm." *Boundary-Layer Meteorology* 99: 127–150.

Appendix G. Footprint

The percentage of measured scalar flux from an area of interest is a major indicator of appropriate site selection and station design. The upwind range within which the sources/sinks contribute a given percent of total fluxes (for example, 40, 55, and 90 percent) is typically desired by an investigator. Additionally, the location of sources/sinks that contributes most to the measured fluxes is often of interest (Kljun et al. 2004). These footprint characteristics can be calculated using a footprint function of the measured scalar flux.

A footprint function of measured scalar flux, given by $f(x, y, z_m)$ where x and y are horizontal spatial variables with a positive x -axis pointing into the streamwise direction and z_m is measurement height, is a probability spatial distribution of the relative contribution to the fluxes measured at the point $(0, 0, z_m)$, assuming that surface sources/sinks in the x - y domain as described by $F(x, y, 0)$ are horizontally homogenous, or in other words $F(x, y, 0)$ is a constant. The footprint $[f(x, y, z_m)]$ can be implicitly defined using the measured flux $[F(0, 0, z_m)]$ and the flux spatial function at the surface $[F(x, y, 0)]$, given by:

$$F(0, 0, z_m) = \int_{-\infty}^{\infty} \int_0^{\infty} F(x, y, 0) f(x, y, z_m) dx dy \quad (104)$$

The two functions inside the double integration describe the amount of contribution to the measured flux from sources/sinks across the integrated area. Given the two functions, the proportion of the measured flux from a smaller defined area can also be calculated. For a general case, this equation may be simplified by the assumption that $F(x, y, 0)$ is a constant (for example, when sources/sinks of flux are horizontally homogenous). The CRBasic online calculations are designed for this general case. Therefore, $F(x, y, 0)$ is treated as a constant, and only the footprint $[f(x, y, z_m)]$ requires greater characterization.

To calculate the footprint in the CRBasic flux program, an analytical equation $[f(x, y, z_m)]$ is needed. Several studies (Gash 1986; Schuepp et al. 1990; Schmid 1994; Hsieh, Katul, and Chi 2000; Kormann and Meixner 2001; Kljun et al. 2004) provide analytical footprint equations. Because the equations of Kljun et al. (2004) were developed more recently than the others, they are used in the CRBasic program. Their application, however, is limited to the following ranges of atmospheric stability, friction velocity, and measurement height:

1. $-200 \leq (z_m - d) / L \leq 1$
 2. $u_* \geq 0.2$
 3. $z_m - d \geq 1 \text{ m}$
- (105)

where d is zero displacement height and L is Monin-Obukhov length. For cases outside the ranges above, the analytical footprint equation of Kormann and Meixner (2001) is used.

G.1 Kljun et al. (2004) analytical footprint equations

G.1.1 Models and parameters

By applying dimensional analysis (Buckingham Π method; see Stull 1988, 666) and analyzing numerical simulations, Kljun et al. (2004) summarized footprints in field scale for a given roughness length (z_0) and ratio of aerodynamic height to planetary boundary-layer (PBL) height as a dimensionless footprint (F_*) in terms of dimensionless length (X_*) for the range of conditions presented in Eq. (105). The summarized footprint is represented by the model:

$$F_*(X_*) = k_1 \left(\frac{X_* + k_4}{k_3} \right)^{k_2} \exp \left[k_2 \left(1 - \frac{X_* + k_4}{k_3} \right) \right] \quad (106)$$

where k_i (subscript $i = 1, 2, 3,$ and 4) is a parameter. If the parameters in the model are given, the dimensionless footprint can be calculated for different dimensionless lengths. These parameters can be statistically estimated using the sampled values of X_* and F_* . The dimensionless length is a combination of vertical wind standard deviation (σ_w), friction velocity (u_*), measurement aerodynamic height (z), and streamwise distance to measurement location (x), given by:

$$X_* = \left(\frac{\sigma_w}{u_*} \right)^{a_1} \frac{x}{z} \quad (107)$$

where a_1 is a parameter that was found to be 0.8 by numerical simulations using the software *LPDM-B* (Kljun et al. 2004). To consider the zero displacement height (d) over different surface types, the variable z should be interpreted as the measurement aerodynamic height ($z = z_m - d$), which was confirmed by Dr. Kljun per email on November 14, 2014. The dimensionless footprint of F_* is a combination of vertical wind standard deviation, friction velocity, planetary boundary-layer height (h), measurement aerodynamic height, and streamwise footprint integrated over crosswind (namely, marginal streamwise footprint) at a field scale [$f_y(x, z)$ in m^{-1}], given by:

$$F_* = \left(\frac{\sigma_w}{u_*} \right)^{a_2} \left(1 - \frac{z}{h} \right)^{-1} z f_y(x, z) \quad (108)$$

where a_2 is a parameter that was found to be -0.8 by simulation using the software *LPDM-B*.

For a given case, the values of σ_w , u_* , h , and z are known, and the value of $f_y(x, z)$ can be numerically simulated (Horst and Weil 1992). Given these values, X_* and F_* can be calculated using Eq. (107) and Eq. (108). Kljun et al. (2004) then used calculated values of dimensionless footprint and dimensionless length as samples to statistically estimate the parameters of k_1 to k_4 in Model (106) for four roughness lengths and four ratios of aerodynamic height to PBL height as shown in Table G-1 (p. 136).

Table G-1: Estimated parameters in dimensionless footprint model (106)								
z/h	k_1	k_2	k_3	k_4	k_1	k_2	k_3	k_4
	$z_0 = 0.01 \text{ m}$				$z_0 = 0.1 \text{ m}$			
0.005	0.024	3.84	31.0	18.0	0.028	2.47	22.0	12.0
0.075	0.024	4.11	33.0	15.0	0.027	2.87	24.0	10.0
0.250	0.021	3.61	35.0	12.0	0.026	3.40	27.0	10.0
0.500	0.025	4.23	33.0	9.0	0.028	5.06	32.0	12.0
	$z_0 = 0.30 \text{ m}$				$z_0 = 1.0 \text{ m}$			
0.075	0.042	4.06	19.0	7.00	0.052	2.40	11.0	5.00
0.250	0.038	4.24	21.0	7.00	0.050	3.19	14.0	4.00
0.500	0.042	6.02	23.0	6.00	0.051	3.93	15.0	3.00

Even without the PBL height, it is possible to use these parameters. From Kljun et al. (2004, Figure 7), it is evident that k_1 can be well described using a function of the natural logarithm of z_0 , which is independent of z/h . This function, per Kljun et al. (2004, Figure 7 left top panel) and email from Dr. Kljun on February 10, 2015, is given by:

$$k_1 \approx \frac{0.175}{3.418 - \ln z_0} \quad (109)$$

Parameters k_3 and k_4 are both linear functions of $\ln z_0$. Parameter k_3 , per Kljun et al. (2004, Figure 7 left bottom panel), is given by:

$$k_3 \approx 4.277 \times (3.418 - \ln z_0) \quad (110)$$

and parameter k_4 , per Kljun et al. (2004, Eq. 16 and Figure 7 right bottom panel), is given by:

$$k_4 \approx 1.685 \times (3.418 - \ln z_0) \quad (111)$$

NOTE:

Although the parameters published in Kljun et al. (2004) had fewer significant digits, email correspondence with Dr. Kljun dated February 10, 2015 led to the adoption of three digits after the decimal for parameters in Eqs. (109) through (111).

Parameter k_2 is independent of z_0 and is a constant. Determining its value requires taking the integral of $\hat{F}_*(\hat{X}_*)$ (the circumflex, or over-hat, indicates they are equations with statistically estimated parameters) over the entire domain of \hat{X}_* and setting it equal to one (Kljun et al. 2004, Appendix), as shown here:

$$\int_{k_4}^{\infty} \hat{F}_*(\hat{X}_*) d\hat{X}_* = k_1 k_3 \exp(k_2) k_2^{-k_2} \Gamma(k_2) = 1 \quad (112)$$

Substituting Eq. (109) and Eq. (110) into Eq. (112) leads to:

$$\exp(k_2) k_2^{-k_2} \Gamma(k_2) = 1.336050 \quad (113)$$

A numerical solution then generates k_2 :

$$k_2 = 3.682540 \quad (114)$$

G.1.2 Application of analytical footprint

The marginal streamwise footprint $[f_y(x, z)]$ in Eq. (108) is required to calculate the needed footprint characteristics. However, for many years its analytical form and the resulting cumulative footprint were unavailable for a wide range of stabilities and wind velocity profiles. This motivated several studies to conduct numerical simulations (Hsieh, Katul, and Chi 2000; Kljun et al. 2004), which could then be used to develop analytical footprint equations (for example, Model [106] and Table G-1 [p. 136]).

Given an analytical form of $f_y(x, z)$, the calculation of footprint characteristics is straightforward. The sections below present equations for footprint characteristics such as the percentage of flux from a defined upwind range of interest and the point of maximum source/sink contribution to the measured flux. These equations relate $f_y(x, z)$, $F_*(X_*)$, and footprint characteristics.

Percentage of measured scalar flux from the upwind range of interest

Given the marginal streamwise footprint $f_y(x, z)$, the percentage of contribution from the sources/sinks within the upwind range of R $[P_F(R)]$ can be calculated using:

$$P_F(R) = 100 \int_{-R_{k4}}^R f_y(x, z) dx \quad (115)$$

where $-R_{k4}$ is the downwind location of the starting contribution of sources/sinks to measured fluxes.

Since:

$$\int_{-R_{k4}}^R f_y(x, z) dx = \frac{\left(\frac{\sigma_w}{u_*}\right)^{a_2} \left(1 - \frac{z}{h}\right)^{-1} z \int_{-R_{k4}}^R f_y(x, z) dx}{\left(\frac{\sigma_w}{u_*}\right)^{a_2} \left(1 - \frac{z}{h}\right)^{-1} z} \quad (116)$$

$$= \left(\frac{\sigma_w}{u_*}\right)^{-a_2} \frac{1}{z} \left(1 - \frac{z}{h}\right) \int_{-R_{k4}}^R \hat{F}_*(\hat{X}_*) dx$$

and because $F_*(X_*)$ is defined in the domain of $X_* > -k_4$, this low limit of integration is the value of x at $X_*(x) = -k_4$. Thus, R_{k4} is given by:

$$R_{k4} = k_4 z \left(\frac{u_*}{\sigma_w}\right)^{a_1} \quad (117)$$

Submitting Eq. (116) into Eq. (115) generates:

$$p_F(R) = 100 \left(\frac{\sigma_w}{u_*}\right)^{-a_2} \frac{1}{z} \left(1 - \frac{z}{h}\right) \int_{-R_{k4}}^R F_*[X_*(x)] dx \quad (118)$$

Calculation for this is possible using numerical integration of the dimensionless footprint $F_*[X_*(x)]$ at discrete, incremental values of x , starting at a low value given by $-R_{k4}$ and increasing until the value for R is reached. Specifically, the value for dimensionless footprint at each value of x is found by using Model (106) and Eq. (107) with measured variables (σ_w and u_*), known variables (z), and estimated parameters (k_i , given by Eqs. [109] through [111] and Eq. [114]), as shown here:

$$F_*[X_*(x)] = k_1 \left[\frac{\left(\frac{\sigma_w}{u_*}\right)^{0.8} \frac{x}{z} + k_4}{k_3} \right]^{k_2} \exp \left\{ k_2 \left[1 - \frac{\left(\frac{\sigma_w}{u_*}\right)^{0.8} \frac{x}{z} + k_4}{k_3} \right] \right\} \quad (119)$$

The values for dimensionless footprint at every interval of x may then be summed to estimate the value of the integral term in Eq. (118) for the calculation of $p_F(R)$.

Upwind location of source/sink that contributes most to the measured flux

Differentiating both sides of Eq. (108) with respect to x generates:

$$\frac{df_y(x, z)}{dx} = \left(\frac{\sigma_w}{u_*} \right)^{-a_2} \left(1 - \frac{z}{h} \right) z^{-1} \frac{dF_*}{dX_*} \frac{dX_*}{dx} \quad (120)$$

The marginal streamwise footprint $[f_y(x, z)]$ is a bell-shaped function with respect to x , with a maximum occurring at x_{max} , which follows that:

$$\left. \frac{df_y(x, z)}{dx} \right|_{x=x_{max}} = 0 \quad (121)$$

For real-world cases in the field, the terms of measured variables on the right-hand side of Eq. (120) will never equal zero; therefore, Eq. (121) can only be true when the last two derivative terms are evaluated as zero at x_{max} . That is:

$$\left. \frac{dF_*}{dX_*} \frac{dX_*}{dx} \right|_{x=x_{max}} = 0 \quad (122)$$

This can be expanded to the following equation:

$$\begin{aligned} \left. \frac{dF_*}{dX_*} \frac{dX_*}{dx} \right|_{x=x_{max}} &= \frac{k_1 k_2}{k_3 z} \left(\frac{\sigma_w}{u_*} \right)^{a_1} \left[\frac{X_*(x_{max}) + k_4}{k_3} \right]^{k_2 - 1} \\ &\exp \left[k_2 \left(1 - \frac{X_*(x_{max}) + k_4}{k_3} \right) \right] \left[1 - \frac{X_*(x_{max}) + k_4}{k_3} \right] = 0 \end{aligned} \quad (123)$$

This equation is then solved for $X_*(x_{max}) > -k_4$, resulting in the upwind distance from the measurement station to the location that contributes most to the measured flux being expressed as:

$$x_{max} = (k_3 - k_4) z \left(\frac{u_*}{\sigma_w} \right)^{0.8} \quad (124)$$

According to Eq. (115) and Eq. (118), the percentage of contribution to the measured flux within an upwind range of x_p , where subscript p indicates percent and can have a value of 0 to 100, such as in $P_F(x_{10}) = 10$ and $P_F(x_{90}) = 90$, can be expressed as:

$$P_F(x_p) = 100 \left(\frac{\sigma_w}{u_*} \right)^{0.8} \frac{1}{z} \left(1 - \frac{z}{h} \right) \int_{-R_{k4}}^{x_p} F_* [X_*(x)] dx \quad (125)$$

This is an increasing monotonic function of x_p . Given this, for a value of $p_F(x_p)$, only one value of x_p can be found. The value of x_p may be estimated by performing a numerical integration of $p_F(R)$ as described in the section above. Using a subscript i for x indicates the sequential number of numerical integration steps, the two neighbor values of $p_F(x_i)$ (less than the target value of p [for example, $p = 10$]), and (greater than the target value) can then be used to interpolate a more precise value of x_p , where $P_F(x_p) = p$.

G.1.3 Programmatic approach to determining footprint characteristics

Roughness length

Applying Model (106), the roughness length is required to calculate the parameters in Eqs. (109) to (111). The roughness length depends on surface type and is approximately $0.13h_c$ for crops and grasses, where h_c represents canopy height (Tanner and Pelton 1960; Stanhill 1969), $0.06h_c$ for forests and shrubs (Jarvis, James, and Landsberg 1976; Raupach, Antonia, and Rajagopalan 1991), and $0.033h_r$, where h_r represents roughness element height for bare land and water surface (for example, sand) (Raupach, Antonia, and Rajagopalan 1991).

A more accurate value of roughness length depends not only on the surface type but also on surface roughness texture (for a canopy, this texture can be described using vegetative surface area per unit volume). However, this texture, the canopy height, and the resulting roughness length may change quickly during certain periods of the growing season. This makes it impractical to input a single roughness length and expect it to be valid for long time periods. Accordingly, the roughness length should be updated periodically, which is possible using the well-known equation of a wind profile under neutral conditions (Rosenberg, Blad, and Verma 1983, Eq. 4.2):

$$z_0 = (z_m - d) \exp \left(- \frac{k \sqrt{\bar{u}^2 + \bar{v}^2}}{u_*} \right) \quad (126)$$

where k is the von Karman constant (0.41) and \bar{u} and \bar{v} are the two orthogonal components of mean horizontal wind speeds, respectively. The roughness length is automatically updated by the data logger at the end of each averaging interval if the surface layer stability is under neutral

conditions, as defined by the strict criterion of $|z/L| < 0.02$ (Hsieh, Katul, and Chi 2000). The updated roughness length will then be used for the calculation of parameters k_1 , k_3 , and k_4 using Eqs. (109) to (111).

Until an averaging period occurs with neutral stability, an initial value for roughness length must be estimated and used. Accordingly, our programmatic approach is to require that the user select from among the menu options the land type that most closely matches the area around their eddy-covariance station. The program then uses this input to calculate an initial roughness length as follows:

$$z_0 = 10^{0.997 \log_{10} h_c - 0.883} \quad (127)$$

for crops and grasses (Szeicz, Endrodi, and Tajchman 1969), $0.06h_c$ for forests and shrubs, and 0.01 m for bare land and water surfaces, which corresponds with the parameters for lowest roughness length in Table G-1 (p. 136). As soon as measured half-hourly data is available and stability is under neutral conditions, this initial roughness length will be updated using Eq. (126).

Calculation for parameters of k_1 to k_4

$$k_1 \approx \frac{0.175}{3.418 - \ln z_0}$$

$$k_2 \approx 3.682540$$

$$k_3 \approx 4.277(3.418 - \ln z_0)$$

$$k_4 \approx 1.685(3.418 - \ln z_0)$$

(128)

Calculation of planetary boundary-layer height

The Monin-Obukhov length is calculated in eddy-covariance flux measurements, and then it is used to find the PBL height using the data points in Table G-2 (p. 141) and linear interpolation.

Table G-2: Relationship of Monin-Obukhov length (L) to planetary boundary-layer height (h)							
L (m)	-5	-30	-650	∞	1,000	130	84
h (m)	2,000	1,500	1,200	1,000	800	250	200

Upwind location of source/sink that contributes most to the measured flux (maximum location)

The following equation is used in the data logger:

$$x_{\max} = (k_3 - k_4) z \left(\frac{u_*}{\sigma_w} \right)^{0.8} \quad (129)$$

Upwind inflection points of footprint

The footprint is a bell-shaped function with one maximum point (turning point) and two inflection points. Because the footprint changes most in the segments from the left inflection point (x_{IL}) to x_{\max} and from x_{\max} to the right inflection point (x_{IR}), these inflection points may be used as boundaries for special numerical integration segments where the integration intervals are smaller to provide greater accuracy. Outside these special segments, the integration intervals may be larger and thereby decrease the computation required. Specifically, the inflection point located at the left side of x_{\max} (x_{IL}) is given as:

$$x_{IL} = \frac{x_{\max}}{k_3 - k_4} \left[k_3 \left(\frac{\sqrt{k_2} - 1}{\sqrt{k_2}} \right) - k_4 \right] \quad (130)$$

and the other is at the right side of x_{\max} (x_{IR}):

$$x_{IR} = \frac{x_{\max}}{k_3 - k_4} \left[k_3 \left(\frac{\sqrt{k_2} + 1}{\sqrt{k_2}} \right) - k_4 \right] \quad (131)$$

See the derivation of the inflection points in [Derivation of equations for upwind locations at inflection points of footprint in Kljun et al. \(2004\) \(KCRS\) \(p. 144\)](#).

Percentage of measured scalar flux from the upwind rand of interest to measurements

As explained previously, the percentage of measured flux coming from an area of interest may be calculated with the data logger using the following equation:

$$p_F(R) = 100 k_1 \left(\frac{\sigma_w}{u_*} \right)^{0.8} \frac{1}{z} \left(1 - \frac{z}{h} \right) \int_{-R_{x1}}^R \left[\frac{\left(\frac{\sigma_w}{u_*} \right)^{0.8} \frac{x}{z} + k_4}{k_3} \right]^{k_2} \exp \left\{ k_2 \left[1 - \frac{\left(\frac{\sigma_w}{u_*} \right)^{0.8} \frac{x}{z} + k_4}{k_3} \right] \right\} dx \quad (132)$$

where the integral is evaluated using numerical integration.

Within the first integration segment (from R_{k4} to x_{IL}), the trapezoidal rule for numerical integration is used with the segment divided into q intervals, where q is an integer selected such that the resolution of the numerical integration yields reasonable accuracy without a large burden in computation (for example, $q = 20$).

Within the second integration segment (x_{IL} to x_{max}), the trapezoidal rule is still used with an integration interval of $(x_{max} - x_{IL}) / q$.

The third integration segment also uses the trapezoidal rule and extends from x_{max} to $x_{IR} + (x_{IR} - x_{max})$ with an integration interval of $(x_{IR} - x_{max}) / q$.

The fourth and final integration segment begins at the end of the third segment. The fourth segment uses integration intervals of size $4z$. Although these intervals may be significantly larger than the intervals used in the other segments, the integration accuracy should still be acceptable since Boole's rule, rather than the trapezoidal rule, is used within this segment, and the slope of the footprint should be changing very slowly throughout the segment.

The fourth segment initially extends to $200z$ beyond the segment starting point or until the cumulative flux reaches 90 percent. If the distance of interest is not reached at the end of the fourth segment but is reached within another $100z$, an additional 25 integration intervals are added to the segment, with the endpoint being the distance of interest. If the distance of interest is beyond another $100z$, it is assumed that the cumulative footprint would be wholly contained within the distance of interest; thus, 99 percent is reported as the cumulative flux within the distance of interest. If the cumulative flux never reaches 90 percent, which is possible under certain conditions where the numerical integration is inadequate or the model does not truly reflect the real footprint distribution, the distance for 90 percent flux will be reported as **NAN** (not a number).

Scaling the integration intervals within each segment provides a way to have higher integration resolution when the slope of footprint changes more dramatically while still limiting the size of the integration interval when the slope is not changing as much. This approach is successful in converging the percentage flux to a value of one if numerically integrated over the entire domain. An additional advantage of this approach is that because x_{max} must be used as a segment boundary, the peak value of the function is never missed, which contributes to greater accuracy of the overall numerical integration.

Upwind range within which the sources/sinks contribute a given percent to measured flux

If this upwind range is denoted using x_p , where subscript p indicates the given percent, it can be implicitly expressed in an equation as:

$$p = 100k_1 \left(\frac{\sigma_w}{u_*} \right)^{0.8} \frac{1}{z} \left(1 - \frac{z}{h} \right) \int_{-R_{x4}}^{x_p} \left[\frac{\left(\frac{\sigma_w}{u_*} \right)^{0.8} \frac{x}{z} + k_4}{k_3} \right]^{k_2} \exp \left\{ k_2 \left[1 - \frac{\left(\frac{\sigma_w}{u_*} \right)^{0.8} \frac{x}{z} + k_4}{k_3} \right] \right\} dx \quad (133)$$

Among the values of $p_F(x_p)$ that were found in the process of numerical integration described above, if the value in current iteration is just greater than the target percentage (for example, $p = 40$), a more precise value of x_{40} , such as $p_F(x_{40}) = 40$, can be interpolated using this value along with the value in previous iterations. In this way, x_{40} , x_{55} , and x_{90} are found.

G.2 Derivation of equations for upwind locations at inflection points of footprint in Kljun et al. (2004) (KCRS)

As described above, integration segment boundaries should be determined by the upwind inflection points of the footprint. Since the footprint is known to be a bell-shaped function, one maximum point (x_{max}) is flanked by two inflection points (x_{IL} and x_{IR}). Accordingly, x_{max} may be found by setting the first order derivative of the footprint function to zero. Similarly, x_{IL} and x_{IR} may be found by setting the second order derivative to zero. The following section shows this derivation for these points.

G.2.1 KCRS footprint model

The footprint in Kljun et al. (2004) is given in the form of a dimensionless footprint [$F_*(X_*)$]:

$$F_*(X_*) = k_1 \left(\frac{X_* + k_4}{k_3} \right)^{k_2} \exp \left[k_2 \left(1 - \frac{X_* + k_4}{k_3} \right) \right] \quad (134)$$

where k_i (subscript $i = 1, 2, 3$, and 4) is a parameter and X_* is the dimensionless length. It is a combination of vertical wind standard deviation (σ_w), friction velocity (u_*), measurement aerodynamic height ($z = z_m - d$), and the upwind distance (x) from the measurement location, given by:

$$X_* = \left(\frac{\sigma_w}{u_*} \right)^{a_1} \frac{x}{z} \quad (135)$$

where a_1 is a parameter. The dimensionless footprint of F_* is a combination of vertical wind standard deviation, friction velocity, planetary boundary-layer height (h), measurement aerodynamic height, and streamwise footprint integrated over crosswind (that is, marginal streamwise footprint) at a field scale [$f_y(x, z)$ in m^{-1}], given by:

$$F_* = \left(\frac{\sigma_w}{u_*} \right)^{a_2} \left(1 - \frac{z}{h} \right)^{-1} z f_y(x, z) \quad (136)$$

where a_2 is a parameter.

G.2.2 Upwind location of maximum footprint

Differentiating both sides of Eq. (136) with respect to x generates:

$$\frac{df_y(x, z)}{dx} = \left(\frac{\sigma_w}{u_*} \right)^{-a_2} \left(1 - \frac{z}{h} \right)^{-1} \frac{dF_*}{dX_*} \frac{dX_*}{dx} \quad (137)$$

The derivative of dimensionless length with respect to x is greater than zero and is independent of x ; therefore:

$$\frac{df_y(x, z)}{dx} = 0 \text{ at } \frac{dF_*}{dX_*} = 0 \quad (138)$$

which indicates $f_y(x, z)$ and F_* reach maximum at the same upwind location (x_{max}). Therefore, the location of maximum footprint satisfies the following equation:

$$\left. \frac{dF_*}{dX_*} \right|_{x=x_{max}} = \frac{k_1 k_2}{k_3} \left[\frac{X_*(x_{max}) + k_4}{k_3} \right]^{k_2 - 1} \exp \left[k_2 \left(1 - \frac{X_*(x_{max}) + k_4}{k_3} \right) \right] \left[1 - \frac{X_*(x_{max}) + k_4}{k_3} \right] = 0 \quad (139)$$

Solving this equation for $X_*(x_{max}) > -k_4$ generates:

$$x_{max} = (k_3 - k_4) z \left(\frac{u_*}{\sigma_w} \right)^{0.8} \quad (140)$$

G.2.3 Upwind locations of inflection points

Differentiating both sides of Eq. (137) with respect to x generates:

$$\frac{d^2 f_y(x, z)}{dx^2} = \left(\frac{\sigma_w}{u_*} \right)^{-a_2} \left(1 - \frac{z}{h} \right) z^{-1} \frac{d^2 F_*}{dX_*^2} \left(\frac{dX_*}{dx} \right)^2 \quad (141)$$

The derivative of dimensionless length with respect to x is greater than zero and is independent of x ; therefore:

$$\frac{d^2 f_y(x, z)}{dx^2} = 0 \text{ at } \frac{d^2 F_*}{dX_*^2} = 0 \quad (142)$$

which indicates $f_y(x, z)$ and F_* have inflection points at the same upwind locations; therefore:

$$\frac{d^2 F_*}{dX_*^2} = 0 \quad (143)$$

This can be used to find the upwind locations of the inflection points in the footprint curve.

Referencing Eq. (139), the first order derivative of dimensionless footprint can be written as:

$$\frac{dF_*}{dX_*} = \frac{k_2}{k_3} \left[\left(\frac{X_* + k_4}{k_3} \right)^{-1} - 1 \right] F_* \quad (144)$$

Using this equation, the derivative at the second order can be derived as:

$$\begin{aligned} \frac{d^2 F_*}{dX_*^2} &= \frac{k_2}{k_3} \left[-\frac{1}{k_3} \left(\frac{X_* + k_4}{k_3} \right)^{-2} F_* + \left(\frac{X_* + k_4}{k_3} \right)^{-1} \frac{dF_*}{dX_*} - \frac{dF_*}{dX_*} \right] \\ &= -\frac{k_2}{k_3^2} \left(\frac{X_* + k_4}{k_3} \right)^{-2} F_* + \frac{k_2^2}{k_3^2} \left[\left(\frac{X_* + k_4}{k_3} \right)^{-1} - 1 \right]^2 F_* \\ &= -\frac{k_2}{k_3^2} F_* \left\{ \left(\frac{X_* + k_4}{k_3} \right)^{-2} + k_2 \left[\left(\frac{X_* + k_4}{k_3} \right)^{-1} - 1 \right]^2 \right\} \end{aligned} \quad (145)$$

In this equation, the term ahead of the braces is not zero. Therefore, to satisfy Eq. (143), the term inside the braces must be zero. If assuming:

$$X = \left(\frac{X_* + k_4}{k_3} \right)^{-1} \quad (146)$$

then the term inside the braces satisfies Eq. (143) in the following form:

$$X^2 + k_2 [X - 1]^2 = 0 \quad (147)$$

Solving this equation, substituting Eq. (135) into X , and referencing Eq. (140) leads to an equation for the left inflection point:

$$x_{IL} = \frac{x_{\max}}{k_3 - k_4} \left[k_3 \left(\frac{\sqrt{k_2} - 1}{\sqrt{k_2}} \right) - k_4 \right] \quad (148)$$

Similarly, the equation for the right inflection point is obtained by:

$$x_{IR} = \frac{x_{\max}}{k_3 - k_4} \left[k_3 \left(\frac{\sqrt{k_2} + 1}{\sqrt{k_2}} \right) - k_4 \right] \quad (149)$$

G.3 Kormann and Meixner (2001) (KM) analytical footprint equations

G.3.1 KM footprint model

As an alternative to the analytical approach used by Kljun et al. (2004), which is limited by the conditions presented in Eq. (105), the footprint was derived by Kormann and Meixner (2001) based on van Ulden (1978) as (see the detailed derivations in [Derivation of analytical footprint in Kormann and Meixner \(2001\)](#) [p. 154]) a two-dimensional (2D) marginal streamwise footprint:

$$f_y(x, z) = \frac{1}{\Gamma(\mu)} \xi^\mu \left(\frac{z^{m+1}}{x^{\mu+1}} \right) \exp\left(-\xi \frac{z^r}{x} \right) \quad (150)$$

where r , μ , and ξ are composites of other variables that have been combined for succinctness in the expression. Each of these variables is defined below.

r (shape factor):

$$r = 2 + m - n \quad (151)$$

where m is the exponent in a vertical profile of horizontal wind (see Eq. [198] in [Derivation of analytical footprint in Kormann and Meixner \(2001\)](#) [p. 154]), and n is the exponent in a vertical profile of eddy diffusivity (see Eq. [187] in [Derivation of analytical footprint in Kormann and Meixner \(2001\)](#) [p. 154]).

μ :

$$\mu = \frac{m + 1}{r} \quad (152)$$

ξ :

$$\xi = \frac{U}{\mathbf{K}r^2} \quad (153)$$

where U is the wind constant in a vertical profile of horizontal wind (see Eq. [198] in [Derivation of analytical footprint in Kormann and Meixner \(2001\)](#) [p. 154]), and \mathbf{K} is the constant in power-law profile of the eddy diffusivity.

$$\mathbf{K} = \frac{ku_*z^{1-n}}{\varphi_c(z/L)} \quad (154)$$

The calculations for the variables m , n , U , and \mathbf{K} will be given in the following sections.

G.3.2 Programmatic approach

The 3D footprint $[f(x, y, z)]$ can be expressed in terms of a marginal streamwise footprint and a downwind probability distribution of scalar concentrations from upwind sources in a domain of x and y $[c(x, y)]$ (see Horst and Weil 1992, Model 9; Kormann and Meixner 2001, Model 8), given by:

$$f(x, y, z) = c(x, y)f_y(x, z) \quad (155)$$

where:

$$c(x, y) = \frac{\bar{u}(x)}{\sqrt{2\pi x\sigma_y}} \exp\left[-\frac{1}{2}\left(\frac{y\bar{u}(x)}{x\sigma_y}\right)^2\right] \quad (156)$$

where the constant σ_y is the standard deviation of crosswind scalar concentration, and $\bar{u}(x)$ is the effective velocity of the scalar plume. This equation is derived from Model 10 in Horst and Weil (1992) and Model 9 in Kormann and Meixner (2001) after the simple scalar dispersion (σ) in the model is replaced with a detailed descriptive dispersion $[\sigma_y x / \bar{u}(x)]$, which depends on distance from the station (x) and effective velocity of the scalar plume $[\bar{u}(x)]$. Substituting Eq. (150) and Eq. (156) into Eq. (155) leads to the three-dimensional footprint:

$$f(x, y, z) = \frac{\bar{u}(x)}{\sqrt{2\pi}\sigma_y\Gamma(\mu)} \xi^\mu \left(\frac{z^{m+1}}{x^{\mu+2}} \right) \exp \left[-\frac{1}{x^2} \left(\xi x z^r + \frac{1}{2} \left(\frac{y\bar{u}(x)}{\sigma_y} \right)^2 \right) \right] \quad (157)$$

where:

$$\bar{u}(x) = U \frac{\Gamma(\mu)}{\Gamma\left(\frac{1}{r}\right)} \left(\frac{\kappa r^2}{U} x \right)^{\frac{m}{r}} \quad (158)$$

See Eqs. (206) through (216) in [Derivation of analytical footprint in Kormann and Meixner \(2001\)](#) (p. 154) for associated derivations.

G.3.3 Application of analytical footprint

Unlike the dimensionless footprint in Kljun et al. 2004, the footprint developed by Kormann and Meixner (2001) explicitly gives the analytical marginal (crosswind integrated) streamwise footprint (Eq. [150]) and three-dimensional footprint (Eq. [157] and Eq. [158]). Both can be directly used to calculate footprint characteristics.

Percentage of measured scalar flux from the upwind range of interest

The percentage of contribution from these sources/sinks, within the upwind range of interest, to the measured flux [$p_F(R)$] is given by:

$$\begin{aligned} p_F(R) &= 100 \int_0^R f_y(x, z) dx \\ &= 100 \frac{\xi^\mu z^{m+1}}{\Gamma(\mu)} \lim_{\Delta x \rightarrow 0} \int_{0+\Delta x}^R \frac{1}{x^{\mu+1}} \exp\left(-\xi \frac{z^r}{x}\right) dx \end{aligned} \quad (159)$$

where the Gamma function of μ can be accurately approximated using Nemes (2010):

$$\Gamma(\mu) \approx \sqrt{\frac{2\pi}{\mu}} \left[\frac{1}{e} \left(\mu + \frac{1}{12\mu - \frac{1}{10\mu}} \right) \right]^\mu \quad (160)$$

Location of source/sink that contributes most to the measured flux

1. Approach using 2D marginal streamwise footprint $[f_y(x, z)]$:

Differentiating Eq. (150) with respect to x generates:

$$\begin{aligned} \frac{df_y(x, z)}{dx} &= \frac{\xi^\mu z^{m+1}}{\Gamma(\mu)} \frac{d}{dx} \left[\frac{1}{x^{\mu+1}} \exp\left(-\xi \frac{z^r}{x}\right) \right] \\ &= \frac{\xi^\mu z^{m+1}}{\Gamma(\xi)} \exp\left(-\xi \frac{z^r}{x}\right) \left\{ \frac{-(\mu+1)}{x^{\mu+2}} + \frac{\xi z^r}{x^{\mu+3}} \right\} \\ &= \frac{\xi^\mu z^{m+1}}{\Gamma(\mu)} \exp\left(-\xi \frac{z^r}{x}\right) \left[\frac{\xi z^r - x(\mu+1)}{x^{\mu+3}} \right] \end{aligned} \quad (161)$$

The marginal streamwise footprint $[f_y(x, z)]$ is a bell-shaped function with respect to x , with the maximum found at x_{max} which follows that:

$$\left. \frac{df_y(x, z)}{dx} \right|_{x=x_{max}} = 0 \quad (162)$$

All terms except for the term in the brackets in Eq. (160) are greater than zero for any real-world case in the field; therefore, setting that term equal to zero results in the solution for x_{max} :

$$x_{max} = \frac{\xi z^r}{\mu + 1} \quad (163)$$

2. Approach using 3D footprint $[f(x, y, z)]$:

Differentiating Eq. (157) with respect to x at $y = 0$:

$$\begin{aligned} \frac{df(x, 0, z)}{dx} &= \frac{\xi^\mu z^{m+1}}{\sqrt{2\pi\sigma_y} \Gamma(\mu)} \frac{d}{dx} \left[\frac{\bar{u}(x)}{x^{\mu+2}} \exp\left(-\xi \frac{z^r}{x}\right) \right] \\ &= \frac{\xi^\mu z^{m+1}}{\sqrt{2\pi\sigma_y} \Gamma(\mu)} \exp\left(-\xi \frac{z^r}{x}\right) \left\{ \frac{1}{x^{\mu+2}} \frac{d\bar{u}(x)}{dx} - \frac{(\mu+2)\bar{u}(x)}{x^{\mu+3}} + \frac{\xi z^r \bar{u}(x)}{x^{\mu+4}} \right\} \end{aligned} \quad (164)$$

The footprint $[f(x, 0, z)]$ is a bell-shaped function along x , with the maximum found at x_{max} , which follows that:

$$\left. \frac{df(x, 0, z)}{dx} \right|_{x=x_{max}} = 0 \quad (165)$$

To satisfy this equation, the term inside the braces in Eq. (164) must be zero, or:

$$\left[\frac{1}{x^{\mu+2}} \frac{d\bar{u}(x)}{dx} - \frac{(\mu+2)\bar{u}(x)}{x^{\mu+3}} + \frac{\xi z^r \bar{u}(x)}{x^{\mu+4}} \right]_{x=x_{max}} = 0 \quad (166)$$

Using Eq. (158), the derivative term is expressed as:

$$\frac{d\bar{u}(x)}{dx} = U \frac{m\Gamma(\mu)}{r\Gamma\left(\frac{1}{r}\right)} \left(\frac{\kappa r^2}{U} \right)^{\frac{m}{r}} x^{\frac{m}{r}-1} \quad (167)$$

Substituting this equation along with Eq. (158) into Eq. (166) leads to:

$$\left[\frac{mx^{\frac{m}{r}-1}}{rx^{\mu+2}} - \frac{(\mu+2)x^{\frac{m}{r}}}{x^{\mu+3}} + \frac{\xi z^r x^{\frac{m}{r}}}{x^{\mu+4}} \right]_{x=x_{max}} = 0 \quad (168)$$

Because $x \neq 0$, it can be simplified as:

$$\left[mx - r(\mu+2)x + r\xi z^r \right]_{x=x_{max}} = 0 \quad (169)$$

The solution of this equation is the location of source/sink that contributes most to the measured flux and is given as:

$$x_{max} = \frac{r\xi z^r}{2r+1} \quad (170)$$

For practical purposes of handling the computation required for numerical integration, we use x_{max} from the 2D footprint approach, although, admittedly, in some cases the solution from the 3D footprint may be preferable since the 3D footprint uses the detailed descriptive dispersion (Kormann and Meixner 2001, 215).

Equation (159) can be used to estimate upwind range within which the sources/sinks contribute 10 percent or 90 percent to measured flux. The percentage of contribution to the measured flux from the upwind range of x_p , where subscript p indicates percent of 0 to 100, can be expressed as:

$$p_F(x_p) = 100 \frac{\xi^\mu z^{m+1}}{\Gamma(\mu)} \lim_{\Delta x \rightarrow 0} \int_{0+\Delta x}^{x_p} \frac{1}{x^{\mu+1}} \exp\left(-\xi \frac{z^r}{x}\right) dx \quad (171)$$

This is an increasing monotonic function of x_p ; therefore, for a given value of $p_F(x_p)$, a unique value of x_p can be found. Similar to the method described for applying the Kljun et al. (2004) model, the value of x_p may be estimated by performing a numerical integration for intervals of x and then interpolating values of $P_F(x_p)$ to find the corresponding value of x_p for $p_F(x_p)$, where $p = 40, 55, \text{ or } 90$.

G.3.4 Programmable algorithms

Calculate the individual variables

Find the exponent of vertical profile of eddy diffusivity (see Eq. [189] in [Derivation of analytical footprint in Kormann and Meixner \(2001\)](#) [p. 154]):

$$n = \begin{cases} \frac{1}{1 + 5z/L} & z/L > 0 \\ \frac{1 - 24z/L}{1 - 16z/L} & z/L \leq 0 \end{cases} \quad (172)$$

Find the exponent of vertical profile of horizontal wind (see Eq. [200] in [Derivation of analytical footprint in Kormann and Meixner \(2001\)](#) [p. 154]):

$$m = \frac{u_*}{k \sqrt{\bar{u}^2(z) + \bar{v}^2(z)}} \phi_m\left(\frac{z}{L}\right) \quad (173)$$

where $\phi_m(z/L)$ is wind shear, given by:

$$\phi_m\left(\frac{z}{L}\right) = \begin{cases} 1 + 5z/L & z/L > 0 \\ (1 - 16z/L)^{-\frac{1}{4}} & z/L \leq 0 \end{cases} \quad (174)$$

Find the wind constant (see Eq. [198] in [Derivation of analytical footprint in Kormann and Meixner \(2001\)](#) [p. 154]):

$$U = \frac{\sqrt{\overline{u^2}(z) + \overline{v^2}(z)}}{z^m} \quad (175)$$

Composite variables

Calculate the shape factor and other composite variables:

$$r = 2 + m - n \quad (176)$$

μ :

$$\mu = \frac{m+1}{r} \quad (177)$$

ξ :

$$\xi = \frac{U}{\kappa r^2} \quad (178)$$

Calculate the gamma function of μ (see Nemes 2010, verified as accurate)

$$\Gamma(\mu) \approx \sqrt{\frac{2\pi}{\mu}} \left[\frac{1}{e} \left(\mu + \frac{1}{12\mu - \frac{1}{10\mu}} \right) \right]^\mu \quad (179)$$

Footprint characteristics

Percent of measured scalar flux from upwind range of interest to measurements:

$$p_F(R) = 100 \frac{\xi^\mu z^{m+1}}{\Gamma(\mu)} \lim_{\Delta x \rightarrow 0} \int_{0+\Delta x}^R \frac{1}{x^{\mu+1}} \exp\left(-\xi \frac{z^r}{x}\right) dx \quad (180)$$

Similar to the description of applying the Kljun et al. (2004) model, the integral is evaluated by the data logger using four integration segments, each containing scaled integration intervals to increase resolution when the slope of the function is changing more and to decrease computation when the slope is changing less. The segment boundaries and interval sizes are the same as described previously, except that when applying the Kormann and Mexiner (2001) model, zero instead of R_{k4} is used as the first segment lower boundary.

Location of source/sink that contributes most to the measured flux:

$$x_{\max} = \frac{\xi z^r}{\mu + 1} \quad (181)$$

Upwind inflection location of footprint, where the Kormann and Meixner (2001) model is a bell-shaped function, includes one maximum point (turning point) and two inflection points. As described previously, these points should be used as boundaries for the numerical integration segments. One of the inflection points (x_{IL}) is located at the left side of the maximum point and given by:

$$x_{IL} = x_{\max} \left(1 - \frac{1}{\sqrt{\mu + 2}} \right) \quad (182)$$

and the other is at the right side (x_{IR}) and given by:

$$x_{IR} = x_{\max} \left(1 + \frac{1}{\sqrt{\mu + 2}} \right) \quad (183)$$

See the derivation of these inflection points in [Upwind locations at inflection points of footprint in Kormann and Meixner \(2001\)](#) (p. 164).

Upwind range within which the sources/sinks contribute a given percent to measured flux:

$$p = 100 \frac{\xi^\mu z^{m+1}}{\Gamma(\mu)} \lim_{\Delta x \rightarrow 0} \int_{0+\Delta x}^{x_p} \frac{1}{x^{\mu+1}} \exp\left(-\xi \frac{z^r}{x}\right) dx \quad (184)$$

Because an analytical solution for x_p is not available, the value of x_p can be interpolated in the process of numerical integration of Eq. (180) when p is between two consecutive integrated values. In this way, x_{40} , x_{55} , and x_{90} are found.

G.4 Derivation of analytical footprint in Kormann and Meixner (2001)

G.4.1 Model derivation

Following Horst and Weil (1992), the probability distribution of a scalar concentration downwind of a sink/source in three dimensions may be described using a function $c(x, y, z)$, where x and y are horizontal spatial variables with the x -axis following mean wind direction, and z is a vertical

spatial variable. The function is approximated using two independent probability distributions of downwind scalar concentration in two dimensions and the vertical profile of horizontal wind speed $[u(z)]$, given by:

$$c(x, y, z) = \frac{c(x, y)c(x, z)}{\int_0^\infty u(z)c(x, z) dz} = \frac{c(x, y)c(x, z)}{\bar{u}(x)} \quad (185)$$

where $\bar{u}(x)$ is termed as a plume effective velocity. In probability theory, integration of $c(x, y, z)$ over the entire domain of y is the marginal (crosswind integrated) probability distribution of the downwind scalar concentration in x and z [$c_y(x, z)$]. Applying this integration to both sides of Eq. (185) generates:

$$c_y(x, z) = \frac{c(x, z)}{\bar{u}(x)} \quad (186)$$

According to K-theory, the product of the vertical profile of eddy diffusivity $[K(z)]$ and the vertical scalar concentration gradient is the scalar flux. Therefore, the crosswind integrated footprint [$f_y(x, z)$, that is to say, the crosswind integrated probability distribution of flux] is given as:

$$f_y(x, z) = -K(z) \frac{dc_y(x, z)}{dz} \quad (187)$$

To analytically express $f_y(x, z)$ for real-world applications, $K(z)$ and $c_y(x, z)$ must be analytically expressed in terms of measured variables.

G.4.2 Analytical expression: Vertical profile of eddy diffusivity

The vertical profile of eddy diffusivity can be described as:

$$K(z) = kz^n \quad (188)$$

where k is the von Karman constant (0.41) and n is the power exponent depending on the surface layer stability, given by (Huang 1979):

$$n = \frac{z}{K(z)} \frac{dK(z)}{dz} = \begin{cases} \frac{1}{1+5z/L} & z/L > 0 \\ \frac{1-24z/L}{1-16z/L} & z/L \leq 0 \end{cases} \quad (189)$$

Equations (188) and (189) express the vertical profile of eddy diffusivity in terms of measured variables.

G.4.3 Analytical expression: Crosswind integrated scalar concentration distribution

The most common analytical expression for the crosswind integrated scalar concentration distribution $[c_y(x, z)]$ is a Gaussian plume model (van Ulden 1978; Horst and Weil 1992), given by:

$$c_y(x, z) = \frac{A}{\bar{u}(x)\bar{z}(x)} \exp\left[-\left(\frac{Bz}{\bar{z}(x)}\right)^r\right] \quad (190)$$

where A , B , and r are parameters. $\bar{u}(x)$ is the effective speed of plume advection along the streamwise wind vector, implicitly defined in Eq. (185), given explicitly by:

$$\bar{u}(x) = \frac{\int_0^\infty u(z)c_y(x, z) dz}{\int_0^\infty c_y(x, z) dz} \quad (191)$$

and $\bar{z}(x)$ is the effective height of plume advection along the wind stream, defined by:

$$\bar{z}(x) = \frac{\int_0^\infty zc_y(x, z) dz}{\int_0^\infty c_y(x, z) dz} \quad (192)$$

The remaining work is to find parameters A , B , and r and analytically express $\bar{u}(x)$ and $\bar{z}(x)$ in terms of measured variables.

Parameter estimation: A and B

Examination of Eq. (186) reveals that because $c(x, z)$ is the probability distribution of scalar concentration in two dimensions, we effectively have:

$$\int_0^\infty c_y(x, z) dz = \frac{1}{\bar{u}(x)} \quad (193)$$

which means:

$$A = \frac{\bar{z}(x)}{\int_0^\infty \exp\left[-\left(\frac{Bz}{\bar{z}(x)}\right)^r\right] dz} = \frac{B}{\int_0^\infty \exp\left[-\left(\frac{Bz}{\bar{z}(x)}\right)^r\right] d\left(\frac{Bz}{\bar{z}(x)}\right)} = \frac{B}{\frac{1}{r}\Gamma\left(\frac{1}{r}\right)} \quad (194)$$

The solution to parameter B is needed. Submitting Eq. (190) into Eq. (192) generates:

$$\bar{z}(x) = \frac{\int_0^\infty z \exp \left[- \left(\frac{Bz}{\bar{z}(x)} \right)^r \right] d \left(\frac{Bz}{\bar{z}(x)} \right)}{\int_0^\infty \exp \left[- \left(\frac{Bz}{\bar{z}(x)} \right)^r \right] d \left(\frac{Bz}{\bar{z}(x)} \right)} \quad (195)$$

Multiplying $B / \bar{z}(x)$ to both sides of this equation leads to:

$$B = \frac{\int_0^\infty \frac{Bz}{\bar{z}(x)} \exp \left[- \left(\frac{Bz}{\bar{z}(x)} \right)^r \right] d \left(\frac{Bz}{\bar{z}(x)} \right)}{\int_0^\infty \exp \left[- \left(\frac{Bz}{\bar{z}(x)} \right)^r \right] d \left(\frac{Bz}{\bar{z}(x)} \right)} = \frac{\Gamma \left(\frac{2}{r} \right)}{\Gamma \left(\frac{1}{r} \right)} \quad (196)$$

Equation (194) and Eq. (196) give:

$$A = \frac{r \Gamma(2/r)}{[\Gamma(1/r)]^2} \quad (197)$$

$$B = \frac{\Gamma(2/r)}{\Gamma(1/r)}$$

Parameter estimation: r

This parameter is a shape factor of the plume, given by van Ulden (1978):

$$r = 2 + m - n \quad (198)$$

where n is the power exponent of the vertical profile of eddy diffusivity (see Eq. [188] and Eq. [189]) and m is the exponent of the vertical profile of horizontal wind, given by:

$$u(z) = Uz^m \quad (199)$$

which depends on the surface layer stability, given by (Kaimal and Finnigan 1994, 16):

$$m = \frac{z}{u(z)} \frac{du(z)}{dz} = \frac{u_*}{ku(z)} \phi_m \left(\frac{z}{L} \right) \quad (200)$$

where $\phi_m(z/L)$ is wind shear and given by:

$$\phi_m\left(\frac{z}{L}\right) = \begin{cases} 1 + 5z/L & z/L > 0 \\ (1 - 16z/L)^{-\frac{1}{4}} & z/L \leq 0 \end{cases} \quad (201)$$

The other parameter U in Eq. (199) is a wind constant and can be calculated using measured $\bar{u}(z)$ and calculated m :

$$U = \frac{u(z)}{z^m} = \frac{\sqrt{\bar{u}_x(z) + \bar{u}_y(z)}}{z^m} \quad (202)$$

Analytical expression: Effective height of plume advection [$\bar{z}(x)$]

Examining Eq. (195) reveals that the numerator can be analytically evaluated only if the term $B/\bar{z}(x)$ is multiplied to both sides of the equation. As a result, it becomes a Gamma function; therefore, the effective speed of plume advection cannot be analytically expressed in terms of measured variables using its definition in Eq. (192). Alternatively, differentiating both sides of Eq. (192) with respect to x generates:

$$\begin{aligned} \frac{d\bar{z}(x)}{dx} &= \frac{\int_0^\infty z \frac{\partial c_y(x,z)}{\partial x} dz}{\int_0^\infty c_y(x,z) dz} - \frac{\int_0^\infty z c_y(x,z) dz}{\int_0^\infty c_y(x,z) dz} \frac{\int_0^\infty \frac{\partial c_y(x,z)}{\partial x} dz}{\int_0^\infty c_y(x,z) dz} \\ &= \frac{\int_0^\infty [z - \bar{z}(x)] \frac{\partial c_y(x,z)}{\partial x} dz}{\int_0^\infty c_y(x,z) dz} \end{aligned} \quad (203)$$

Neglecting the streamwise eddy diffusion, the change in concentration along the wind direction (derivative term) must cause a change in flux due to the continuity in air mass (van Ulden 1978; Horst and Weil 1992), given by:

$$u(z) \frac{\partial c_y(x,z)}{\partial x} = -\frac{\partial}{\partial z} \left[-K(z) \frac{\partial c_y(x,z)}{\partial z} \right] \quad (204)$$

Submitting Eq. (188) and Eq. (199) into this equation generates:

$$\frac{\partial c_y(x,z)}{\partial x} = \frac{k}{U} z^{-m} \frac{\partial}{\partial z} \left[z^n \frac{\partial c_y(x,z)}{\partial z} \right] \quad (205)$$

Submitting this equation into Eq. (203) generates:

$$\frac{d\bar{z}(x)}{dx} = \frac{k}{U} \frac{1}{\int_0^\infty c_y(x,z) dz} \left[\int_0^\infty z^{1-m} \frac{\partial}{\partial z} z^n \frac{\partial c_y(x,z)}{\partial z} dz - \bar{z}(x) \int_0^\infty z^{-m} \frac{\partial}{\partial z} z^n \frac{\partial c_y(x,z)}{\partial z} dz \right] \quad (206)$$

The equation can then be evaluated by substituting Eq. (190) into the three integration terms on the right-hand side. Performing these three substitutions at once becomes overly complex, so substitution and simplification of each integral term is presented separately below.

Integration term in the denominator

$$\int_0^\infty c_y(x,z) dz = \frac{A}{\bar{z}(x)\bar{u}(x)} \int_0^\infty \exp\left[-\left(\frac{Bz}{\bar{z}(x)}\right)^r\right] dz = \frac{A}{Br\bar{u}(x)} \Gamma\left(\frac{1}{r}\right) \quad (207)$$

The first integration term in the numerator

Assuming the gradient of scalar concentration at the surface ($z = 0$) and beyond the top of the boundary layer ($z \rightarrow \infty$) is zero and the concentration beyond the top of the boundary layer is zero, this integration can be evaluated as follows:

$$\begin{aligned} \int_0^\infty z^{1-m} \frac{\partial}{\partial z} z^n \frac{\partial c_y(x,z)}{\partial z} dz &= z^{1-m+n} \frac{\partial c_y(x,z)}{\partial z} \Big|_0^\infty - \int_0^\infty z^n \frac{\partial c_y(x,z)}{\partial z} dz z^{1-m} \\ &= -(1-m) \left[z^{n-m} c_y(x,z) \Big|_0^\infty - \int_0^\infty c_y(x,z) dz z^{n-m} \right] \\ &= (1-m)(n-m) \int_0^\infty z^{n-m-1} \frac{A}{\bar{z}(x)\bar{u}(x)} \exp\left[-\left(\frac{Bz}{\bar{z}(x)}\right)^r\right] dz \\ &= \frac{A(1-m)(n-m)\bar{z}^{n-m-1}(x)}{B^{n-m}\bar{u}(x)} \int_0^\infty \left(\frac{Bz}{\bar{z}(x)}\right)^{n-m-1} \exp\left[-\left(\frac{Bz}{\bar{z}(x)}\right)^r\right] d\left(\frac{Bz}{\bar{z}(x)}\right) \\ &= \frac{A(1-m)(n-m)\bar{z}^{n-m-1}(x)}{rB^{n-m}\bar{u}(x)} \Gamma\left(\frac{n-m}{r}\right) \\ &= \frac{A(1-m)\bar{z}^{n-m-1}(x)}{B^{n-m}\bar{u}(x)} \Gamma\left(\frac{2}{r}\right) \end{aligned} \quad (208)$$

The second integration term in the numerator

Using the same derivation approach, the second integration term in the numerator can be evaluated as:

$$\begin{aligned}
 \int_0^{\infty} z^{-m} \frac{\partial}{\partial z} z^n \frac{\partial c_y(x, z)}{\partial z} dz &= z^{-m+n} \frac{\partial c_y(x, z)}{\partial z} \Big|_0^{\infty} - \int_0^{\infty} z^n \frac{\partial c_y(x, z)}{\partial z} dz z^{-m} \\
 &= m \left[z^{n-m-1} c_y(x, z) \Big|_0^{\infty} - \int_0^{\infty} c_y(x, z) dz^{n-m-1} \right] \\
 &= -m(n-m-1) \int_0^{\infty} z^{n-m-2} \frac{A}{\bar{z}(x) \bar{u}(x)} \exp \left[- \left(\frac{Bz}{\bar{z}(x)} \right)^r \right] dz \\
 &= - \frac{Am(n-m-1) \bar{z}^{n-m-2}(x)}{B^{n-m-1} \bar{u}(x)} \int_0^{\infty} \left(\frac{Bz}{\bar{z}(x)} \right)^{n-m-2} \exp \left[- \left(\frac{Bz}{\bar{z}(x)} \right)^r \right] d \left(\frac{Bz}{\bar{z}(x)} \right) \quad (209) \\
 &= - \frac{Am(n-m-1) \bar{z}^{n-m-2}(x)}{r B^{n-m-1} \bar{u}(x)} \Gamma \left(\frac{n-m-1}{r} \right) \\
 &= - \frac{Am \bar{z}^{n-m-2}(x)}{B^{n-m} \bar{u}(x)} B \Gamma \left(\frac{1}{r} \right) \\
 &= - \frac{Am \bar{z}^{n-m-2}(x)}{B^{n-m} \bar{u}(x)} \Gamma \left(\frac{2}{r} \right)
 \end{aligned}$$

Substituting the evaluated terms in Eqs. (207) to (209) into Eq. (206) expresses the derivative of the effective height with respect to x as a fundamental differential equation:

$$\begin{aligned}
 \frac{d\bar{z}(x)}{dx} &= \frac{\kappa}{U} \frac{1}{\frac{A}{Br\bar{u}(x)} \Gamma\left(\frac{1}{r}\right)} \left\{ \frac{A(1-m)\bar{z}^{n-m-1}(x)}{B^{n-m}\bar{u}(x)} \Gamma\left(\frac{2}{r}\right) - \bar{z}(x) \left[-\frac{Am\bar{z}^{n-m-2}(x)}{B^{n-m}\bar{u}(x)} \Gamma\left(\frac{2}{r}\right) \right] \right\} \\
 &= \frac{\kappa}{U} rB \frac{\Gamma\left(\frac{2}{r}\right) \bar{z}^{n-m-1}(x)}{\Gamma\left(\frac{1}{r}\right) B^{n-m}} \\
 &= \frac{\kappa}{U} rB^2 \frac{\bar{z}^{n-m-1}(x)}{B^{n-m}} \\
 &= \frac{\kappa}{U} rB^{2+m-n} \bar{z}^{1-(2+m-n)}(x) \\
 &= \frac{\kappa}{U} rB^r \bar{z}^{1-r}(x)
 \end{aligned} \tag{210}$$

This fundamental equation can be written as:

$$\int r\bar{z}^{r-1}(x) d\bar{z}(x) = \frac{\kappa}{U} r^2 B^r \int dx \tag{211}$$

Therefore:

$$\bar{z}(x) = B \left(\frac{\kappa r^2}{U} x \right)^{\frac{1}{r}} \tag{212}$$

Analytical expression: Effective speed of plume advection $[\bar{u}(x)]$

Substituting Eq. (198) into Eq. (190) gives:

$$\bar{u}(x) = \frac{U \int_0^\infty z^m c_y(x, z) dz}{\int_0^\infty c_y(x, z) dz} \tag{213}$$

The denominator was evaluated in Eq. (207), and the integration term in the numerator can be evaluated as:

$$\begin{aligned}
 \int_0^{\infty} z^m c_y(x, z) dz &= \int_0^{\infty} z^m \frac{A}{\bar{z}(x) \bar{u}(x)} \exp \left[- \left(\frac{Bz}{\bar{z}(x)} \right)^r \right] dz \\
 &= \frac{A \bar{z}^m(x)}{B^{m+1} \bar{u}(x)} \int_0^{\infty} \left(\frac{Bz}{\bar{z}(x)} \right)^m \exp \left[- \left(\frac{Bz}{\bar{z}(x)} \right)^r \right] d \left(\frac{Bz}{\bar{z}(x)} \right) \\
 &= \frac{A \bar{z}^m(x)}{r B^{m+1} \bar{u}(x)} \Gamma \left(\frac{m+1}{r} \right)
 \end{aligned} \tag{214}$$

Substituting this equation along with Eq. (207) into Eq. (213) generates:

$$\bar{u}(x) = \frac{U \frac{A \bar{z}^m(x)}{r B^{m+1} \bar{u}(x)} \Gamma \left(\frac{m+1}{r} \right)}{\frac{A}{r B \bar{u}(x)} \Gamma \left(\frac{1}{r} \right)} = U \frac{\bar{z}^m(x) \Gamma \left(\frac{m+1}{r} \right)}{B^m \Gamma \left(\frac{1}{r} \right)} \tag{215}$$

Substituting the analytical expression of effective height of plume advection $[\bar{z}(x)]$ into this equation generates:

$$\bar{u}(x) = U \frac{\Gamma \left(\frac{m+1}{r} \right)}{\Gamma \left(\frac{1}{r} \right)} \left(\frac{\kappa r^2}{U} x \right)^{\frac{m}{r}} \tag{216}$$

By substituting the solved parameters of A and B (see Eq. [197]), analytically expressed effective height of plume advection $[\bar{u}(x)$; see Eq. (212)], and analytical expressed effective speed of plume advection $[\bar{z}(x)$; see Eq. (216)] into Eq. (190), finally, the crosswind integrated scalar concentration distribution can be analytically expressed in terms of spatial variables (x and z), the constant in the power-law profile of the eddy diffusivity (\mathbf{K}), and calculated variables from measurements (m , n , and U).

That is:

$$c_y(x, z) = \frac{r \frac{\Gamma(2/r)}{\Gamma^2(1/r)}}{U \frac{\Gamma[(m+1)/r]}{\Gamma(1/r)} \left(\frac{\kappa r^2}{U} x\right)^{\frac{m}{r}} B \left(\frac{\kappa r^2}{U} x\right)^{\frac{1}{r}}} \exp \left[- \left(\frac{Bz}{B \left(\frac{\kappa r^2}{U} x\right)^{\frac{1}{r}}} \right)^r \right] \quad (217)$$

$$= \frac{r}{U \Gamma[(m+1)/r]} \left(\frac{U}{\kappa r^2 x}\right)^{\frac{m+1}{r}} \exp \left[- \frac{U z^r}{\kappa r^2 x} \right]$$

More succinctly, given that:

$$\xi = \frac{U}{\kappa r^2} \quad (218)$$

$$\mu = \frac{m+1}{r}$$

the crosswind integrated scalar concentration distribution, in an analytical form, can be presented as:

$$c_y(x, z) = \frac{r}{U \Gamma(\mu)} \left(\xi \frac{1}{x}\right)^\mu \exp \left[-\xi \frac{z^r}{x} \right] \quad (219)$$

Examining Eq. (186) reveals that the crosswind integrated footprint can be thus derived as:

$$f_y(x, z) = -K(z) \frac{dc_y(x, z)}{dz}$$

$$= -\kappa z^n \frac{r}{U \Gamma(\mu)} \left(\xi \frac{1}{x}\right)^\mu \exp \left(-\xi \frac{z^r}{x} \right) \left(-\xi \frac{r z^{r-1}}{x} \right) \quad (220)$$

$$= \frac{1}{\Gamma(\mu)} \xi^\mu \left(\frac{z^{m+1}}{x^{\mu+1}}\right) \exp \left(-\xi \frac{z^r}{x} \right)$$

G.5 Upwind locations at inflection points of footprint in Kormann and Meixner (2001)

As described previously, integration segment boundaries should be determined by the upwind inflection points of the footprint. Since the footprint is known to be a bell-shaped function, there is one maximum point (x_{max}) and two inflection points (x_{IL} and x_{IR}) on both sides of the maximum, respectively. Accordingly, x_{max} may be found by setting the first order derivative of the footprint function to zero. Similarly, x_{IL} and x_{IR} may be found by setting the second order derivative to zero. The following section shows derivations for these points.

G.5.1 KM footprint model

The crosswind integrated footprint [$f_y(x, z)$] in Kormann and Meixner (2001) is given by:

$$f_y(x, z) = \frac{1}{\Gamma(\mu)} \xi^\mu \left(\frac{z^{m+1}}{x^{\mu+1}} \right) \exp\left(-\xi \frac{z^r}{x} \right) \quad (221)$$

where x is the upwind distance to the measurement station; z is measurement aerodynamic height; m is the exponent of the vertical profile of horizontal wind velocity; and r , μ , and ξ are composite variables, given by:

Shape factor:

$$r = 2 + m - n \quad (222)$$

where n is the exponent of vertical profile of eddy diffusivity.

μ :

$$\mu = \frac{m+1}{r} \quad (223)$$

ξ :

$$\xi = \frac{U}{\kappa r^2} \quad (224)$$

where U is the wind constant.

G.5.2 Upwind location of maximum footprint

Differentiating Eq. (221) with respect to x generates:

$$\begin{aligned} \frac{df_y(x, z)}{dx} &= \frac{\xi^\mu z^{m+1}}{\Gamma(\mu)} \frac{d}{dx} \left[\frac{1}{x^{\mu+1}} \exp\left(-\xi \frac{z^r}{x}\right) \right] \\ &= \frac{\xi^\mu z^{m+1}}{\Gamma(\mu)} \exp\left(-\xi \frac{z^r}{x}\right) \left[\frac{\xi z^r - x(\mu+1)}{x^{\mu+3}} \right] \end{aligned} \quad (225)$$

The marginal streamwise footprint $[f_y(x, z)]$ is a bell-shaped function with respect to x , with the maximum found at x_{max} which follows that:

$$\left. \frac{df_y(x, z)}{dx} \right|_{x=x_{max}} = 0 \quad (226)$$

All terms except for the term in the brackets in Eq. (225) are greater than zero for any real-world case in the field; therefore, setting that term equal to zero results in the solution for x_{max} :

$$x_{max} = \frac{\xi z^r}{\mu + 1} \quad (227)$$

G.5.3 Upwind location of inflection points in footprint curve

Differentiating both sides of Eq. (225) with respect to x generates:

$$\begin{aligned} \frac{d^2 f_y(x, z)}{dx^2} &= \frac{\xi^\mu z^{m+1}}{\Gamma(\mu)} \frac{d}{dx} \left\{ \exp\left(-\xi \frac{z^r}{x}\right) \left[\frac{\xi z^r - x(\mu+1)}{x^{\mu+3}} \right] \right\} \\ &= \frac{\xi^\mu z^{m+1}}{\Gamma(\mu)} \exp\left(-\xi \frac{z^r}{x}\right) \left\{ \xi \frac{z^r}{x^2} \left[\frac{\xi z^r - x(\mu+1)}{x^{\mu+3}} \right] - \frac{(\mu+3)\xi z^r}{x^{\mu+4}} + \frac{(\mu+1)(\mu+2)}{x^{\mu+3}} \right\} \end{aligned} \quad (228)$$

Because the footprint is a bell-shaped function, it has two inflection points. One is to the left of x_{max} (x_{IL}), and the other is to the right of x_{max} (x_{IR}). Eq. (228) must equal zero at the inflection points. In this equation, the term ahead of the braces is never zero. Therefore, we can simply set the terms in the braces to zero to find the inflection points:

$$\xi \frac{z^r}{x^2} \left[\frac{\xi z^r - x(\mu + 1)}{x^{\mu+3}} \right] - \frac{(\mu + 3)\xi z^r}{x^{\mu+4}} + \frac{(\mu + 1)(\mu + 2)}{x^{\mu+3}} = 0 \quad (229)$$

Rearranging the terms in this equation yields:

$$\xi^2 z^{2r} - 2(\mu + 2)\xi z^r x + (\mu + 1)(\mu + 2)x^2 = 0 \quad (230)$$

Solving the quadratic equation results in:

$$x = \frac{\xi z^r (\mu + 2 \pm \sqrt{\mu + 2})}{(\mu + 1)(\mu + 2)} \quad (231)$$

Substituting x_{max} (Eq. [227]) into Eq. (231) and then taking the point to the left results in:

$$x_{IL} = x_{max} \left(1 - \frac{1}{\sqrt{\mu + 2}} \right) \quad (232)$$

and taking the point to the right gives:

$$x_{IR} = x_{max} \left(1 + \frac{1}{\sqrt{\mu + 2}} \right) \quad (233)$$

G.6 References

- Gash, J.H.K. 1986. "A note on estimating the effect of a limited fetch on microclimate evaporation measurements." *Boundary-Layer Meteorology* 35: 409–413.
- Hsieh, C.I., G. Katul, and T.W. Chi. 2000. "An approximation analytical model for footprint estimation of scalar fluxes in the thermal stratified atmospheric flows." *Advances in Water Resources* 23: 765–772.
- Horst, T.W. and J.C. Weil. 1992. "Footprint estimation for scalar flux measurements in the atmospheric surface layer." *Boundary-Layer Meteorology* 59: 279–296.
- Huang, C.H. 1979. "A theory of dispersion in turbulent shear flow." *Atmospheric Environment* 13: 453–463.

- Jarvis, P.G., G.B. James, and J.J. Landsberg. 1976. "Coniferous Forest." In *Vegetation and the Atmosphere*, Vol. 2, edited by J.L. Monteith, 171–240. London: Academic Press.
- Kaimal, J.C. and J.J. Finnigan. 1994. *Atmospheric Boundary Layer Flows: Their Structure and Measurement*. Oxford: Oxford University Press.
- Kljun, N., P. Calanca, M.W. Rotach, and H.P. Schmid. 2004. "A simple parameterization for flux footprint predictions." *Advances in Water Resources* 23: 765–772.
- Kormann, R. and F.X. Meixner. 2001. "Analytical footprint model for non-neutral stratification." *Boundary-Layer Meteorology* 99: 207–224.
- Nemes, G. 2010. "New asymptotic expansion for the Gamma function." *Archiv der Mathematik* 95: 161–169.
- Raupach, M.R., R.A. Antonia, and S. Rajagopalan. 1991. "Rough-wall turbulent boundary layers." *Applied Mechanics Review* 44: 1–25.
- Rosenberg, N.J., B.B. Blad, and S.B. Verma. 1983. *Microclimate: The Biological Environment*, 2nd ed. New York: John Wiley & Son.
- Schmid, P.H. 1994. "Source areas for scalar and scalar fluxes." *Boundary-Layer Meteorology* 67: 293–318.
- Schuepp, P.H., M.Y. Leclerc, J.I. MacPherson, and R.L. Desjardins. 1990. "Footprint prediction of scalar from analytical solution of diffusion equation." *Boundary-Layer Meteorology* 50: 355–373.
- Szeicz, G., G. Endrodi, and S. Tajchman. 1969. "Aerodynamic and surface factors in evaporation." *Water Resource Research* 5: 380–394.
- Stanhill, G. 1969. "A simple instrument for the field measurements of turbulent diffusion flux." *Journal of Applied Meteorology* 8: 509.
- Stull, R.B. 1988. *An Introduction to Boundary Layer Meteorology*. Netherlands: Kluwer Academic Publishers.
- Tanner, C.B. and W.L. Pelton. 1960. "Potential evapotranspiration estimates by the approximate energy balance method of Penman." *Journal of Geophysical Research* 65: 3391.
- van Ulden, A.P. 1978. "Simple estimates for vertical diffusion from sources near the ground." *Atmospheric Environment* 12: 2125–2129.

Appendix H. Surface energy flux

Calculation of the soil surface heat flux is done only if all necessary measurements are available, which include soil heat flux, soil temperature, and soil volumetric water content.

The soil surface heat flux (G), typically reported in units $W \cdot m^{-2}$, is found by summing the average soil heat flux measured at some depth and the change in heat storage in the layer of soil above that depth over some interval of time:

$$G = G_{Depth} + \Delta_{storage} \quad (234)$$

G_{Depth} in the program is found by averaging the heat flux measurements from soil heat flux plates over the averaging interval (such as 30 min). If there are multiple heat flux plates, an average of the temporal averages of each plate is used.

In the data logger program, calculation of the change in storage is done as follows:

$$\Delta_{storage} = \frac{[c_s \rho_s (T_{soil,f} - T_{soil,i}) + c_w \rho_w (T_{soil,f} q_{v,f} - T_{soil,i} q_{v,i})] D}{\Delta t} \quad (235)$$

where:

c_s = specific heat of dry mineral soil at the site in $J \cdot kg^{-1} \cdot K^{-1}$. This value is among the station configuration variables (see C_{dry_soil} in [Table 4-1](#) [p. 21]) entered by the user. If no value is entered, a default of 870 is used.

ρ_s = soil bulk density at the site in $kg \cdot m^{-3}$; entered by the user (see *Bulk Density* in [Table 4-1](#) [p. 21]). If no value is entered, a default of 1300 is used.

$T_{soil,f}$ = soil temperature averaged over the last minute of the current flux averaging interval.

$T_{soil,i}$ = soil temperature averaged over the last minute of the previous flux averaging interval.

c_w = specific heat of liquid water in $J \cdot kg^{-1} \cdot K^{-1}$; a value of 4210 is used, which is the specific heat of liquid water at 0 °C.

ρ_w = density of liquid water in $kg \cdot m^{-3}$; a value of 1000 is used.

$q_{v,f}$ = volumetric water content averaged over the last minute of the current flux averaging interval (for example, 30 min).

$q_{v,i}$ = volumetric water content averaged over the last minute of the previous flux averaging interval.

D = depth in m below the surface at which the soil heat flux plates are buried (see *HFP Depth* in [Table 4-1](#) [p. 21] and [Figure H-1](#) [p. 170]); entered by the user. If no value is entered, a default of 0.08 is used.

Δt = length of time of the flux averaging interval (for example, 30 min).

NOTE:

TCAV and CS65X sensors both make soil temperature measurements; however, if they are both being used, the TCAV measurements will be used preferentially for $T_{soil,f}$ and $T_{soil,i}$ as the TCAV provides a greater spatial average.

NOTE:

The program supports either CS650s or CS655s for measurements of soil water content; both types of sensors will not be supported at the same time.

NOTE:

If a CS655 is used, outputs for water content are corrected for temperature as detailed in the CS655 manual. The temperature measurement from the TCAV sensor assumed to be closest to the CS655 is used for this correction.

It is assumed that soil sensors are installed in a manner similar to that presented in [Figure H-1](#) (p. 170). In many applications, the setup shown in [Figure H-1](#) (p. 170) (one heat flux plate, one TCAV, and one CS655) is replicated for better spatial averaging at the site. Accordingly, the program supports up to three soil heat flux plates (for example, HFP01 or HFP01SC), three soil temperature sensors (for example, TCAV or CS65X where X can be 0 or 5), and three water content sensors (for example, CS650 or CS655).

All soil sensors must be completely inserted into the soil face before the hole is backfilled.

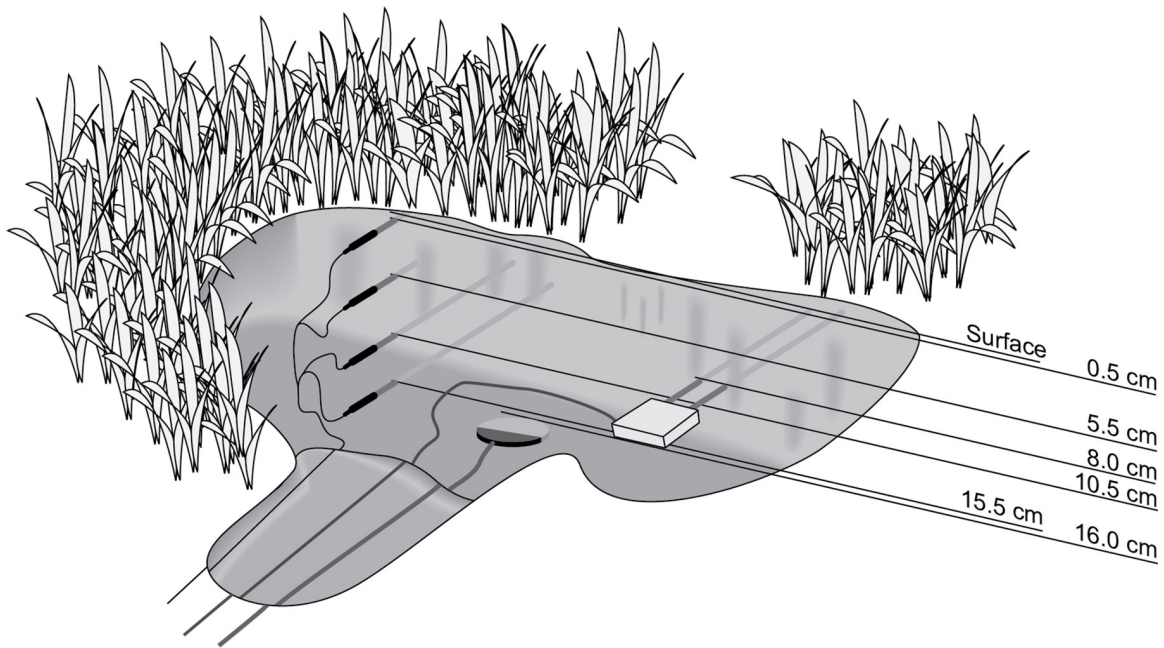


Figure H-1. Soil sensor setup example.

Finally, if a measurement of average net radiation over the flux averaging interval is available, energy closure may be calculated as follows:

$$E_{closure} = \frac{LE+H}{R_n-G}$$

where all variables are in $W \cdot m^{-2}$ and LE is latent heat flux, H is sensible heat flux, and R_n is net radiation.

Appendix I. *EasyFlux DL CR6OP* or *CR1KXOP* process flow diagram

I.1 Sequence of program functions

I.1.1 Every SCAN_INTERVAL (default 100 ms)

Collect raw data from gas analyzer, sonic anemometer, FW (if applicable), and panel temp.



Align data, accounting for electronic delays.



Parse out diagnostic flags from gas analyzer and sonic anemometer.



Calculate various variables (for example, e , ρ_d , ρ_a , T_d , CO₂ mixratio, H₂O mixratio, RH).



Store raw data in multiple arrays, the element in each array with a different lag applied to gas analyzer data relative to sonic analyzer data (to be used later in covariance maximization; lags from $-MAX_LAG$ to $+MAX_LAG$ are used; MAX_LAG default is 5).



If using FW, store raw data in multiple arrays, the elements in each array with a different lag applied to FW data relative to sonic data (to be used later in covariance maximization; lags from $-MAX_LAG$ to $+MAX_LAG$ are used; MAX_LAG default is 5).



The aligned data in each record is written to `ts_data` and diagnostic output tables.

I.1.2 Every SLOWSEQUENCE_SCAN_INTERVAL (default 5 sec)

Measure battery voltage.



Measure biomet and energy balance (slow response) sensors.



If any station variable has been changed, save new values to memory after validation.

I.1.3 Every 5 min

Do coordinate rotations and find the 5-minute covariances for u with w , v with w , T_s with w , CO_2 with w , and H_2O with w (used later for steady state test for quality grading). See [Data quality grading](#) (p. 125).

I.1.4 Every AVERAGING_INTERVAL (default 30 min)

Calculate all covariance values while filtering out data with diagnostic flags or signal strengths or measurements outside of acceptable ranges when the OPEC system is continuously running. The coordinate rotations (use double coordinate rotation method unless planar fit angles have been entered by user) are applied to mean, variance, and covariance for aerodynamic variables and to covariance of CO_2 , H_2O , or air temperature with three-dimensional wind speeds. See [Coordinate rotations: Double rotation method](#) (p. 83) and [Coordinate rotations: Planar fit method](#) (p. 89).



Use rotated wind and sonic temperature fluxes to find turbulent kinetic energy, friction velocity, and preliminary values of Monin-Obukhov length and stability.



Calculate frequency correction factors for WT_SONIC, UW, and VW to account for block averaging and line averaging. If conditions are stable, iteratively calculate Monin-Obukhov length, cospectral equations, and correction factors until factors change by <0.0001 or until 10 iterations

have completed. See [Frequency corrections](#) (p. 96).



Calculate the value for a steady state test using the 5-minute covariances for a 30-minute summary. See [Data quality grading](#) (p. 125).



Calculate the overall quality grade for momentum flux. See [Data quality grading](#) (p. 125).



Calculate and use a new roughness length if: (1) the user did not enter a fixed value, (2) there is neutral stability, and (3) wind speed is >3 m/s. See [Footprint](#) (p. 134).



Calculate footprint characteristics using the Kljun et al. (2004) model if conditions are appropriate; otherwise, use the Kormann and Meixner (2001) model. See [Footprint](#) (p. 134).



Find the effective lateral separation distance between gas analyzer and sonic (used in frequency correction) and the effective separation scan lag (used to constrain which lagged datasets are physically possible). See [Frequency corrections](#) (p. 96).



Find the dataset with the physically possible lag that maximizes the covariance of CO₂ and vertical wind. Use this dataset for the FLUX_AMERIFLUXFORMAT and FLUX_CSFORMAT output tables. If any results are invalid, continue with lag of zero. See [Frequency corrections](#) (p. 96).



Assume the lag found for CO₂ will also maximize covariance of H₂O and vertical wind. Calculate covariances of appropriately lagged H₂O and rotated wind components.



Calculate cospectra functions and frequency correction factors for covariances of CO₂, taking into account attenuation from block averaging, line averaging, and spatial separation. See [Frequency corrections](#) (p. 96).



Calculate cospectra functions and frequency correction factors for covariances of H₂O, taking into account attenuation from block averaging, line averaging, and spatial separation. See [Frequency corrections](#) (p. 96).



Calculate final momentum flux from rotated and frequency corrected covariances of u with w and v with w .



Apply SND correction to the rotated and frequency corrected covariance of w and T_s .



Calculate specific heat of ambient (moist) air and calculate final sensible heat flux.



Calculate scaling temperature (used for data quality grading). See [Data quality grading](#) (p. 125).



Apply WPL correction to rotated and frequency corrected covariance of CO₂ and vertical wind for final CO₂ flux. See [WPL corrections](#) (p. 120).



Apply WPL correction to rotated and frequency corrected covariance of H₂O and vertical wind. Then multiply result by calculated latent heat of vaporization for final latent heat flux. See [WPL corrections](#) (p. 120).



Calculate Bowen Ratio.



Calculate the overall quality grades for fluxes of sensible heat, latent heat, and CO₂. See [Data quality grading](#) (p. 125).



Calculate the covariance of FW temperature and rotated wind components from each element of array to hold lagged data.



Find the effective lateral separation distance between FW and sonic (used in frequency correction) and the effective separation scan lag (used to constrain which lagged element in the array are physically possible). See [Frequency corrections](#) (p. 96).



Find the dataset with the lag that maximizes the covariance of FW temperature and vertical wind. Use this set of covariance values for the FLUX_AMERIFLUXFORMAT and FLUX_CSFORMAT output tables. If any results are invalid, continue with lag of zero.

If FW05, FW1, or FW3 is used



Calculate the time constant for the FW (to be used in frequency corrections). See [Frequency corrections](#) (p. 96).



Calculate frequency correction factors for covariances of FW temperature and rotated wind components, taking into account attenuation from block averaging, line averaging, spatial separation, and the FW time constant. See [Frequency corrections](#) (p. 96).



Calculate the final FW sensible heat flux.

If energy
balance
sensors are
used



Calculate soil surface energy flux. See [Surface energy flux](#) (p. 168).



Calculate energy closure.



Write records to the Flux_AmeriFluxFormat, Flux_CSFormat, and Flux_Notes output tables.

Limited warranty

Products manufactured by Campbell Scientific are warranted by Campbell Scientific to be free from defects in materials and workmanship under normal use and service for twelve months from the date of shipment unless otherwise specified on the corresponding product webpage. See Product Details on the Ordering Information pages at www.campbellsci.com[↗]. Other manufacturer's products, that are resold by Campbell Scientific, are warranted only to the limits extended by the original manufacturer.

Refer to www.campbellsci.com/terms#warranty[↗] for more information.

CAMPBELL SCIENTIFIC EXPRESSLY DISCLAIMS AND EXCLUDES ANY IMPLIED WARRANTIES OF MERCHANTABILITY OR FITNESS FOR A PARTICULAR PURPOSE. Campbell Scientific hereby disclaims, to the fullest extent allowed by applicable law, any and all warranties and conditions with respect to the Products, whether express, implied or statutory, other than those expressly provided herein.

Assistance

Products may not be returned without prior authorization.

Products shipped to Campbell Scientific require a Returned Materials Authorization (RMA) or Repair Reference number and must be clean and uncontaminated by harmful substances, such as hazardous materials, chemicals, insects, and pests. Please complete the required forms prior to shipping equipment.

Campbell Scientific regional offices handle repairs for customers within their territories. Please see the back page for the Global Sales and Support Network or visit www.campbellsci.com/contact  to determine which Campbell Scientific office serves your country.

To obtain a Returned Materials Authorization or Repair Reference number, contact your CAMPBELL SCIENTIFIC regional office. Please write the issued number clearly on the outside of the shipping container and ship as directed.

For all returns, the customer must provide a "Statement of Product Cleanliness and Decontamination" or "Declaration of Hazardous Material and Decontamination" form and comply with the requirements specified in it. The form is available from your CAMPBELL SCIENTIFIC regional office. Campbell Scientific is unable to process any returns until we receive this statement. If the statement is not received within three days of product receipt or is incomplete, the product will be returned to the customer at the customer's expense. Campbell Scientific reserves the right to refuse service on products that were exposed to contaminants that may cause health or safety concerns for our employees.

Safety

DANGER — MANY HAZARDS ARE ASSOCIATED WITH INSTALLING, USING, MAINTAINING, AND WORKING ON OR AROUND TRIPODS, TOWERS, AND ANY ATTACHMENTS TO TRIPODS AND TOWERS SUCH AS SENSORS, CROSSARMS, ENCLOSURES, ANTENNAS, ETC. FAILURE TO PROPERLY AND COMPLETELY ASSEMBLE, INSTALL, OPERATE, USE, AND MAINTAIN TRIPODS, TOWERS, AND ATTACHMENTS, AND FAILURE TO HEED WARNINGS, INCREASES THE RISK OF DEATH, ACCIDENT, SERIOUS INJURY, PROPERTY DAMAGE, AND PRODUCT FAILURE. TAKE ALL REASONABLE PRECAUTIONS TO AVOID THESE HAZARDS. CHECK WITH YOUR ORGANIZATION'S SAFETY COORDINATOR (OR POLICY) FOR PROCEDURES AND REQUIRED PROTECTIVE EQUIPMENT PRIOR TO PERFORMING ANY WORK.

Use tripods, towers, and attachments to tripods and towers only for purposes for which they are designed. Do not exceed design limits. Be familiar and comply with all instructions provided in product manuals. Manuals are available at www.campbellsci.com. You are responsible for conformance with governing codes and regulations, including safety regulations, and the integrity and location of structures or land to which towers, tripods, and any attachments are attached. Installation sites should be evaluated and approved by a qualified engineer. If questions or concerns arise regarding installation, use, or maintenance of tripods, towers, attachments, or electrical connections, consult with a licensed and qualified engineer or electrician.

General

- Protect from over-voltage.
- Protect electrical equipment from water.
- Protect from electrostatic discharge (ESD).
- Protect from lightning.
- Prior to performing site or installation work, obtain required approvals and permits. Comply with all governing structure-height regulations.
- Use only qualified personnel for installation, use, and maintenance of tripods and towers, and any attachments to tripods and towers. The use of licensed and qualified contractors is highly recommended.
- Read all applicable instructions carefully and understand procedures thoroughly before beginning work.
- Wear a **hardhat** and **eye protection**, and take **other appropriate safety precautions** while working on or around tripods and towers.
- **Do not climb** tripods or towers at any time, and prohibit climbing by other persons. Take reasonable precautions to secure tripod and tower sites from trespassers.
- Use only manufacturer recommended parts, materials, and tools.

Utility and Electrical

- **You can be killed** or sustain serious bodily injury if the tripod, tower, or attachments you are installing, constructing, using, or maintaining, or a tool, stake, or anchor, come in **contact with overhead or underground utility lines**.
- Maintain a distance of at least one-and-one-half times structure height, 6 meters (20 feet), or the distance required by applicable law, **whichever is greater**, between overhead utility lines and the structure (tripod, tower, attachments, or tools).
- Prior to performing site or installation work, inform all utility companies and have all underground utilities marked.
- Comply with all electrical codes. Electrical equipment and related grounding devices should be installed by a licensed and qualified electrician.
- Only use power sources approved for use in the country of installation to power Campbell Scientific devices.

Elevated Work and Weather

- Exercise extreme caution when performing elevated work.
- Use appropriate equipment and safety practices.
- During installation and maintenance, keep tower and tripod sites clear of un-trained or non-essential personnel. Take precautions to prevent elevated tools and objects from dropping.
- Do not perform any work in inclement weather, including wind, rain, snow, lightning, etc.

Maintenance

- Periodically (at least yearly) check for wear and damage, including corrosion, stress cracks, frayed cables, loose cable clamps, cable tightness, etc. and take necessary corrective actions.
- Periodically (at least yearly) check electrical ground connections.

Internal Battery

- Be aware of fire, explosion, and severe-burn hazards.
- Misuse or improper installation of the internal lithium battery can cause severe injury.
- Do not recharge, disassemble, heat above 100 °C (212 °F), solder directly to the cell, incinerate, or expose contents to water. Dispose of spent batteries properly.

WHILE EVERY ATTEMPT IS MADE TO EMBODY THE HIGHEST DEGREE OF SAFETY IN ALL CAMPBELL SCIENTIFIC PRODUCTS, THE CUSTOMER ASSUMES ALL RISK FROM ANY INJURY RESULTING FROM IMPROPER INSTALLATION, USE, OR MAINTENANCE OF TRIPODS, TOWERS, OR ATTACHMENTS TO TRIPODS AND TOWERS SUCH AS SENSORS, CROSSARMS, ENCLOSURES, ANTENNAS, ETC.



Global Sales & Support Network

A worldwide network to help meet your needs



Campbell Scientific Regional Offices

Australia

Location: Garbutt, QLD Australia
Phone: 61.7.4401.7700
Email: info@campbellsci.com.au
Website: www.campbellsci.com.au

Brazil

Location: São Paulo, SP Brazil
Phone: 11.3732.3399
Email: vendas@campbellsci.com.br
Website: www.campbellsci.com.br

Canada

Location: Edmonton, AB Canada
Phone: 780.454.2505
Email: dataloggers@campbellsci.ca
Website: www.campbellsci.ca

China

Location: Beijing, P. R. China
Phone: 86.10.6561.0080
Email: info@campbellsci.com.cn
Website: www.campbellsci.com.cn

Costa Rica

Location: San Pedro, Costa Rica
Phone: 506.2280.1564
Email: info@campbellsci.com
Website: www.campbellsci.com

France

Location: Vincennes, France
Phone: 0033.0.1.56.45.15.20
Email: info@campbellsci.fr
Website: www.campbellsci.fr

Germany

Location: Bremen, Germany
Phone: 49.0.421.460974.0
Email: info@campbellsci.de
Website: www.campbellsci.de

India

Location: New Delhi, DL India
Phone: 91.11.46500481.482
Email: info@campbellsci.in
Website: www.campbellsci.in

South Africa

Location: Stellenbosch, South Africa
Phone: 27.21.8809960
Email: sales@campbellsci.co.za
Website: www.campbellsci.co.za

Spain

Location: Barcelona, Spain
Phone: 34.93.2323938
Email: info@campbellsci.es
Website: www.campbellsci.es

Thailand

Location: Bangkok, Thailand
Phone: 66.2.719.3399
Email: info@campbellsci.asia
Website: www.campbellsci.asia

UK

Location: Shepshed, Loughborough, UK
Phone: 44.0.1509.601141
Email: sales@campbellsci.co.uk
Website: www.campbellsci.co.uk

USA

Location: Logan, UT USA
Phone: 435.227.9120
Email: info@campbellsci.com
Website: www.campbellsci.com